

Research Article

Carbon Nanotubes—Based Intelligent Platform for Cancer Vaccine Co-delivery Nanocarriers Immunotherapy Achievements: Challenges In vitro and In vivo

Loutfy H. Madkour*

Professor of Physical chemistry, Nanoscience and Nanotechnology
Chemistry Department, Faculty of Science, Tanta University, 31527,
Tanta, Egypt.

Corresponding Author: Loutfy H. Madkour. Physical chemistry, Nanoscience and Nanotechnology Chemistry Department, Faculty of Science, Tanta University, 31527, Tanta, Egypt.

Received: 📅 2023 Sep 10

Accepted: 📅 2023 Oct 14

Published: 📅 2023 Nov 13

Abstract

Vaccine delivery can be achieved by linking antigen to CNT and by inducing antibody response. Use of CNTs can improve immune response. Tailoring the physical properties of MWNT-based vaccine delivery systems may increase their efficiency in inducing potent T cell immune responses against challenging infectious or cancer diseases. Tumour-specific, immune-based therapeutic interventions can be considered as safe and effective approaches for cancer therapy. Exploitation of nano-vaccinology to intensify the cancer vaccine potency may overcome the need for administration of high vaccine doses or additional adjuvants and therefore could be a more efficient approach. Carbon nanotubes (CNTs) have shown marked capabilities in enhancing antigen delivery to antigen presenting cells. However, proper understanding of how altering the physical properties of CNTs may influence antigen uptake by antigen presenting cells, such as dendritic cells (DCs), has not been established yet.

Although anti-cancer immuno-based combinatorial therapeutic approaches have shown promising results, efficient tumour eradication demands further intensification of anti-tumour immune response. With the emerging field of nanovaccinology, multi-walled carbon nanotubes (MWNTs) have manifested prominent potentials as tumour antigen nanocarriers. Nevertheless, the utilization of MWNTs in co-delivering antigen along with different types of immunoadjuvants to antigen presenting cells (APCs) has not been investigated yet.

Keywords: Carbon Nanotubes, Vaccine Delivery, Cancer Immunotherapy, Antigen Presenting Cells and Dendritic Cells.

1. Delivery of vaccines by CNTs

Carbon nanotube (CNT) can be described as carbon sheet(s) rolled up into a cylinder that is nanometers wide and nanometers to micrometers long. Stemming from the observed capacities of CNTs to enter various types of cells via diversified mechanisms utilizing energy-dependent and/or passive routes of cell uptake, the use of CNTs for the delivery of therapeutic agents has drawn increasing interests over the last decade.

Functionalized CNTs can be used in vaccination procedures. CNTs were shown to activate cells deriving from the innate immune system, such as monocytes, macrophages, and dendritic cells [1]. Microarray profiling of a monocytic cell line, THP-1, showed that CNTs, both functionalized and non-functionalized, activate several genes involved in monocyte response to infection or vaccination, such as nuclear factor kappa-light-chain-enhancer of activated B cells (NF- κ B), interleukin-1 β (IL-1 β), IL-6, tumor necrosis factor- α (TNF- α), among others [2].

CNTs activate the class II Major Immuno-compatibility Complex (MHC) in antigen presenting cells which can, in turn, promote an antibody-based response. The linkage of either a bacterial or viral antigen to CNTs allows the maintenance of antigen conformation integrity, thereby, inducing antibody response increasing both the specificity and the sensitivity [3].

It has also been suggested that SWNT conjugated with unmethylated CpG DNA motifs can be used as an adjuvant in vaccines. Functionalized CNTs have been demonstrated to be able to act as carriers for antimicrobial agents, such as the antifungal amphotericin B. CNTs covalently attached to amphotericin B reduced the undesired toxicity by about 40% as compared to the free drug [4].

Moreover, CNTs themselves might have antimicrobial activity through oxidation of the intracellular antioxidant glutathione, resulting in increased oxidative stress on the bacterial cells and eventual pathogen death [3].

Efforts are continuing to develop novel systems for the delivery of protective antigens. The basic idea of using CNTs in vaccine delivery entails linking an antigen to CNTs, without losing its conformation, thereby inducing an antibody response with the right specificity. However, it is equally important that the incorporated CNTs do not possess intrinsic immunogenicity and, hence, trigger an immune response. CNTs therefore act as templates, upon which chiral molecules are attached, which in turn act as centers for molecular recognition (Figure 1, A, pathway 2) [5- 9]. Reported the use of CNTs in eliciting an improved immune response. Peptides derived from VP1 protein of the foot-and-mouth-disease vi-

rus (FMDV) were coupled to SWNTs [07, 10]. Serum samples from inoculated (by injection with CNT conjugates) Balb/c mice were collected and analyzed by enzyme-linked immunosorbent assay for presence of anti-peptide antibodies. Peptide-CNT complexes were shown to elicit greater immune response against the peptides, with no detectable cross-reactivity to the CNTs, confirming the no immunogenicity of the carrier. It was also observed that the CNT-protein complex enhanced the immune response when attached to an antigen, which strengthens the possibility of incorporating CNTs in vaccines.

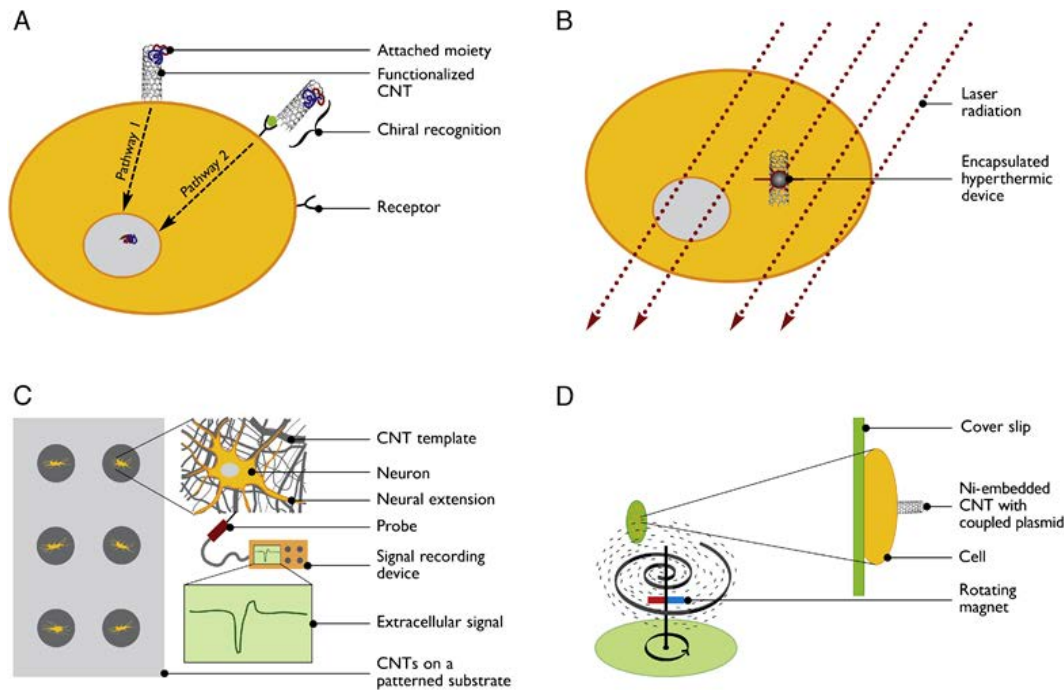


Figure 1: Conceptual diagrams of selected pharmaceutical and biomedical applications of CNTs. (A),

The two approaches for in vitro delivery of pharmaceutically active moieties into cells via endocytosis. Pathway 1 exploits the propensity of cationic f-CNTs to penetrate cells and their ability to bind these moieties as carriers for delivery. Pathway 2 uses f-CNTs for cell targeting by incorporating moieties that bind selectively to epitopes or receptors on cells. (B), The concept of hyperthermic cell destruction, either by irradiating “endocytosed” CNTs directly or by triggering a hyperthermic device within the endocytosed CNTs. (The latter example is shown.) In either case, specific cell destruction is achieved without harming surrounding cells. (C), The use of CNTs/aligned CNTs as templates, as signal transfer substrates, and as nonbiodegradable substrates for the growth and support of neurons. CNT templates have been demonstrated to promote the growth and extension of neural extensions, as illustrated by the extensive neurite branching that follows the contour of the CNT bundle. CNTs can conduct electricity, so a neural signal can be detected and recorded by placing a probe on a conducting CNT matrix. (D), Spearling of immobilized cells with nickel-embedded ferromagnetic CNTs under the influence of a rotating magnetic field. CNTs spear cells cultured on a coverslip.

Bianco et al [7] demonstrated that the presence of cationic f-CNTs in the delivery of synthetic oligodeoxynucleotides containing CpG motifs (ODN-CpGs) improve the immunostimulatory properties of ODN-CpGs in vitro [07, 10]. Synthetic oligonucleotides containing CpGs are reported to confer nonspecific protection against cellular pathogens and enhance antigen-specific immune responses. These properties have made them target candidates for incorporation in vaccines. To evaluate the immunostimulatory properties of CNTs, various ratios of CNT-ODN CpG complexes were incubated with splenocytes. The efficiency of the process was measured by the amount of interleukin-6 (IL-6), a proinflammatory cytokine whose production is stimulated by ODN-CpG secretion in the supernatant of the culture. The results showed higher levels of IL-6 when f-CNTs were in complex with ODN-CpGs than when only ODN-CpGs were incubated with splenocytes. From the foregoing, f-CNTs could potentially be used as nonreplicating vectors for proteins, peptide antigens, and CpGs.

2. Carbon Nanotubes in Cancer Vaccines

Conventional treatments for cancer include surgery, chemotherapy and radiotherapy. Surgical operations can be associ-

ated with complications arising from damaging the tissues surrounding the tumour site. Radiotherapy, which relies on the application of ionising radiation to the tumour sites, leading to DNA damage and inhibition of cancer cell proliferation, can also affect the division of normal cells such as blood forming cells in bone marrow [11,12]. In addition, cancer surgery and radiotherapy are only efficient in treating localised tumour. In cases where cancer cells have metastasised, i.e. gained access to sites distal to the primary tumour, chemotherapeutic drugs, e.g. cisplatin, are administered to slow down cancer cell proliferation and prolong patient survival [13]. Chemotherapeutic agents are typically non-specific and can also inhibit the proliferation of normal cells leading to serious side effects such as myelosuppression and immunosuppression, which can limit the administration of higher doses to achieve better efficacy [12,14].

The human body is equipped with a number of defensive mechanisms that can be harnessed to fight the cancer cells. In fact, it is hypothesised that the immune system is in a continuous state of cancer immune surveillance [15]. According to this concept, professional antigen presenting cells (APCs) such as the dendritic cells (DCs) sample all tissues for the presence of stress signals such as danger-associated molecular patterns which are upregulated in tumour tissues. The presence of such stress signals activates the innate immune system and the resulting immune response keeps tumour growth in check. Once the cancer cells acquire mutations that let them escape the control by the immune system they acquire the ability to establish tumours. Given this, the use of immunotherapy for cancer has attracted significant interests over the last decades culminating in numerous clinical trials [16].

Cancer vaccines are one such intervention. Like traditional vaccines against infectious disease, cancer vaccines are comprised of cancer cell-derived antigens formulated in such a fashion as to provoke a potent immune response. Typically, the antigenic payload of these vaccines is either mutated proteins arising as a direct result or as a byproduct of tumorigenesis (so called neo antigens), proteins which are overexpressed in tumours or proteins which are the result of aberrant expression of embryonic genes in tumours [17–19]. The anti-tumour immune responses elicited by the cancer vaccine are aimed to systemically target the cancer cells throughout the whole body; hence cancer immunotherapy can be used to treat metastatic tumours [20]. Moreover, immunisation with cancer vaccines can induce persistent T cell memory-specific against the tumour cells, providing long-lived protection and prolonged patient survival [21].

Unfortunately, while in preclinical model's cancer vaccine has proven efficacious there has been limited progress in the development of human cancer vaccines, with a number of high-profile candidates failing to meet their end points in clinical trials [22]. This is, in part due to the failure to overcome tumour-induced immunosuppression [23, 24]. However, there has been a surge of renewed interest in the field since the advent of checkpoint blockade and increased understanding of the immune suppressive tumour micro-environment [25].

It is likely that a successful cancer vaccine will be composed of three components: the antigen, the adjuvant and the delivery vehicle. This regime may or may not be supplemented with a checkpoint inhibitor. Speculating further it may be proposed that cancer vaccines will require novel formulations distinct from formulations previously used for infectious disease (such as alum absorbed antigen) as cancer immunity will primarily be driven by cell-mediated cytotoxic responses rather than antibody-mediated humoral responses [16]. This chapter discusses one such formulation; carbon nanotubes in the context of cancer vaccines. Here we review the previous studies that demonstrated the possible benefits of these cylindrical nano-vectors as cancer vaccine delivery systems as well as the obstacles their clinical application is facing.

3. Carbon Nanotubes (CNTs) as Nanocarriers

Nanotubes are a type of fullerene and are molecular-scale tubes of carbon arranged similarly to the layers in graphite. Carbon nanotubes have a very high melting point, as each carbon atom is joined to three other carbon atoms by strong covalent bonds. This also leaves each carbon atom with a spare electron, which forms a sea of delocalized electrons within the tube, meaning nanotubes can conduct electricity.

CNTs are synthetic allotropes of carbon. Allotropy is described as the chemical elements ability to exist in more than one form. Three allotropic forms have been identified for carbon. The natural carbon allotropes include diamond, graphite (several layers of graphene) and amorphous carbon (non-crystalline form of carbon) [26]. The synthetic carbon allotropes that have been discovered include fullerene (sphere of carbon atoms), graphene (single layer of graphite) and CNT (cylinder consisting of rolled graphene layer(s)) (Fig. 2) [27–29]. Morphologically, CNTs can be described as cylinders that are nanometers wide and nanometers to micrometers long, consisting of graphene rolled up in the form of single or multiple concentric layer(s) that are referred to as single-walled CNT (SWNT) or multi-walled CNT (MWNT), respectively [30].

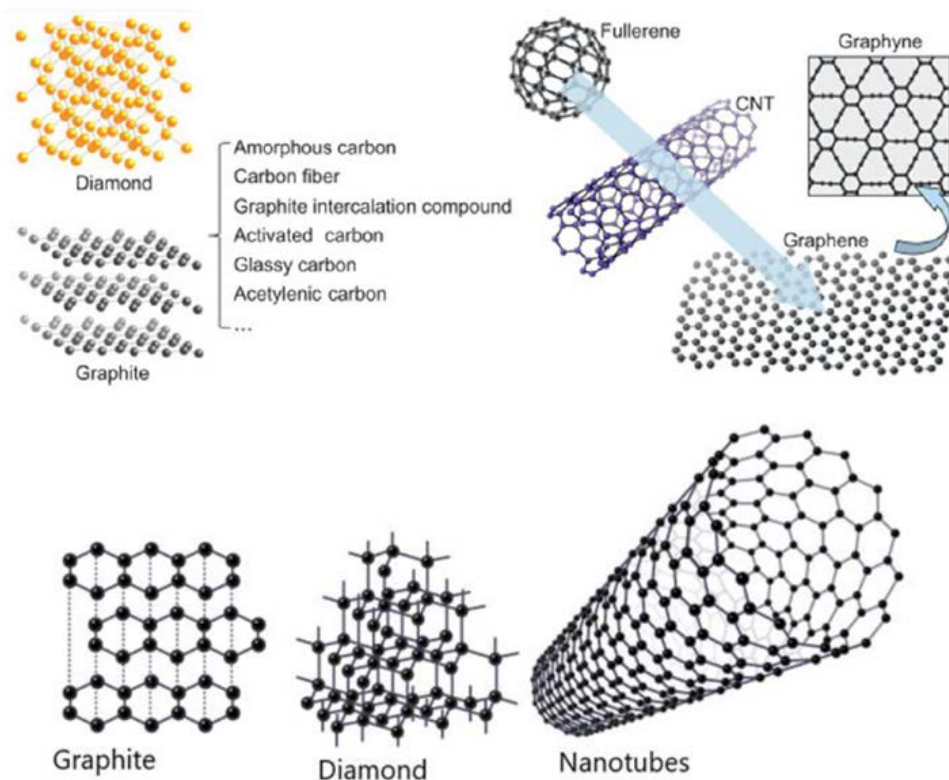


Figure 2: Carbon allotropes and related materials CNT.

3.1. Spheres vs. Tubes vs. Sheets as Nanocarriers

In terms of carbonaceous nanomaterials two carriers have been widely employed, namely CNT and the carbon nanosheet Graphene oxide (GO). Unlike most other materials there has been minimal work assessing the spherical form of carbon: fullerenes, as a carrier [31]. Therefore, it is difficult to attribute the observed effects to morphology or material composition when comparing CNT to other carriers. However, morphology dependent behaviour can be observed in other systems. For instance, Trewyn et al. compared the cellular uptake of silica nanoparticles that were either tube-shaped (100 nm wide and 600 nm long) or spherical shaped (115 nm in diameter) of comparable surface charges [32]. The tube-shaped silica nanoparticles demonstrated higher uptake by CHO cells or fibroblast cells, *in vitro*, compared to the spherical ones. Similarly, Huang et al. have reported that internalization of rod-shaped silica nanoparticles (100 nm wide and 450 nm long) by the epithelial A375 line *in vitro* was higher compared to the spherical nanoparticles (100 nm in diameter) [33]. Whether the carrier's morphology-dependent cellular uptake affects the biological response induced by the loaded cargo demands future investigations. In light of these findings and hypotheses, comparative studies need to be carried out to investigate the cellular uptake and immunogenicity of CNTs versus spherical nanoparticles, ideally fullerenes but also the extensively studied poly (lactic-co-glycolic acid) (PLGA) nanoparticles and liposomes. The findings of such studies will undoubtedly contribute to the nanovaccinology field and further searches for nano-carriers with optimal morphological properties capable of efficient vaccine delivery.

The other commonly used carbon allotrope is the carbon nanosheet; GO [34–37]. The use of GO, as a cancer vaccine carrier, has been assessed by several groups. Yue et al. demonstrated that a subcutaneous injection of GO–OVA in C57BL/6 mice showed significantly elevated OVA-specific CTL response in comparison to OVA alone [38]. Furthermore, in a thymoma model immunisation of the aforementioned mice with GO–OVA was more efficient than OVA alone in limiting the growth of E. G7–OVA lymphoma cells. Testing the ability to induce protective anti-tumour immunity, Sinha et al. have reported that compared to C57BL/6 mice immunised with OVA alone, mice vaccinated with dextran-functionalised GO–OVA showed smaller tumour sizes after challenging with subcutaneous injection of OVA-expressing melanoma B16 cells [39]. These findings presented GO as a competent vaccine nanocarrier.

Both CNTs and GO possess attractive properties of being able to incorporate the biomolecules of interest via simple surface adsorption. However, the proficiency of these carbon nanosheets (GO) compared to the CNTs in delivering vaccines remains in question. Zhang et al. have demonstrated that radiolabeled oxidized MWNTs were taken up in higher amounts compared to radiolabeled GO, by HeLa cells *in vitro* [40]. The degree of cellular uptake is a key, but is not the only, factor determining the intensity of elicited immune response. Proper comparative assessment of CNTs and GO uptake by the APCs and the subsequent impact on the induced immune response will assist future researches on further developing carbon nanocarriers suitable for vaccine delivery.

3.2. Mechanisms of CNTs' Cellular Uptake

Pristine (unmodified) CNTs are hydrophobic in nature and are thus characterised by their low dispersibility and high tendency to form aggregates in aqueous media. CNT bundle formation is attributed to the non-covalent interactions between the nanotubes such as the π - π stacking that occur between the aromatic rings of adjacent nanotubes. Therefore, it was essential to find chemical approaches that can improve the CNTs biocompatibility by enhancing the CNTs degree of individualization and dispersibility in physiological fluids. The chemical approaches that have been applied to functionalise CNTs can be classified into covalent and non-covalent functionalization [41,42]. For instance, utilizing covalent functionalization, pristine CNTs sonication in a mixture of acids (e.g., sulphuric and nitric acids) can incorporate carboxylic groups that can be activated using carbodiimide-based approach which can be further derivatised with amine-terminated linkers yielding functionalised CNT with improved hydrophilicity [42-44]. Relying on non-covalent interactions, Zheng et al. have shown that SWNT dispersibility in aqueous solution was improved by sonication with single stranded DNA (ssDNA) [45]. Wang et al. have also demonstrated that bovine serum albumin non-covalent conjugation with oxidised MWNTs led to an enhanced dispersibility in phosphate-buffered saline [46].

In order to assess the possible benefits that can be obtained from using CNTs as therapeutics delivery vector, it was important to study the mechanisms by which these nanoscopic scaffolds can enter the cells. CNTs have demonstrated high ability to enter various types of cells [47-49]. It has been previously reported that polymeric spherical nanoparticles, e.g. PLGA nanoparticles, mainly utilise energy-dependent mechanisms of cellular uptake rather than energy-independent ones [33, 50, 51]. However, there is good data to suggest the efficiency and uptake route of CNTs is highly dependent on morphology and surface chemistry.

For instance, Shi Kam et al. showed that the cellular uptake of fluorescent labelled streptavidin protein, by HL60 leukaemia cells, was improved by its conjugation to oxidized SWNTs [52, 53]. The uptake of the SWNT-streptavidin conjugate was reduced when cells were placed at 4 °C, suggesting that the internalisation of SWNT was carried out via endocytosis, which is an energy-dependent mechanism. In addition, staining the endosomes with a fluorescent marker followed by confocal microscopy revealed the presence of SWNT-streptavidin in the endocytic vesicles of these cells, which further supported the proposed endocytosis mechanism. Relying on the detection of SWNTs intrinsic near infra-red fluorescence to assess the cellular uptake, Cherukuri et al. have shown that the uptake of pristine SWNTs, dispersed in Pluronic surfactant, by mouse macrophage cells in vitro was dramatically reduced by incubating the cells at 27 °C rather than 37 °C [54]. This finding also suggested an endocytosis-dependent mechanism for SWNTs uptake.

On the other hand, other studies have suggested that the cellular uptake of CNTs is mainly achieved via passive diffusion through the cell membrane. Pantarotto et al. have

demonstrated that amine-functionalised SWNTs improved the internalisation of fluorescent labeled peptide by human 3 T6 fibroblasts incubated at 37 °C, as determined by epifluorescence microscopy that also revealed the presence of the SWNTs in the nucleus [55]. Inhibiting the metabolic functions of cell by incubation at 4 °C or treatment with sodium azide did not affect the cellular uptake of the SWNTs, which suggested an energy-independent mechanism of cell uptake. The CNT's ability to penetrate through the cell membrane, like nano-needles, could be explained by the nano-syringe mechanism theoretically simulated by Lopez et al. for nanotubes insertion into the lipid bilayer [56]. Molecular dynamics presented by Lopez et al. showed that hydrophobic nanotube with hydrophilic tips firstly adsorbs, in a horizontal plane, onto a model membrane [56]. Partial insertion of the nanotube into the model bilayer is then followed by spontaneous change in the nanotube orientation from the horizontal into the vertical alignment, forming a transmembrane pore-like orientation through the bilayer. Insertion into the membrane bilayer could be then followed by translocation to the intracellular compartments as reported by Pantarotto et al. In another study, further investigation of the energy-independent CNT uptake was carried out, and confocal microscopy images revealed the internalisation of fluorescent labelled and amine-functionalised MWNTs by fungal (*Saccharomyces cerevisiae*) and yeast cells.

(*Cryptococcus neoformans*) [57]. The functionalized MWNTs internalization by these prokaryotic cells (which normally lack the ability to carry out active processes such as endocytosis) highlighted the MWNTs' utilization of mechanisms other than endocytosis for cell entry. In addition, it was shown that Jurkat leukaemic T cells incubation with the functionalized MWNTs at 4 °C in the presence of sodium azide did not inhibit the cellular uptake of MWNTs, which confirmed the involvement of passive cellular uptake mechanism. The contradicting mechanisms of CNTs cellular uptake reported by different authors could be attributed to the properties of the CNTs used in these studies such as the CNTs' degree of individualization and dispersibility in the cell culture media, which is highly dependent on the CNTs' functionalization density.

Mu et al. have studied the uptake of functionalised MWNTs by HEK293 epithelial cells using TEM [58]. In this study, single MWNT were imaged penetrating the cell membrane, while MWNTs bundles were found intracellular surrounded by endosome membrane. Single MWNT released from the MWNTs bundle entrapped in endosomes were also imaged while penetrating the endosome membrane, to enter the cytosol.

Collectively, from these studies it could be concluded that CNTs can access the intracellular compartments via more than one mechanism of cell entry. This could be attributed to the length to width ratio of the CNTs that allows the, nanoneedle-shaped, CNTs to passively penetrate the cell membrane utilizing the hypothesized and experimentally demonstrated nanosyringe mechanism, in addition to the active endocytosis mechanism. The role of uptake cannot be

understated as the ultimate goal of cancer vaccines is to induce tumour-specific cytotoxic and memory CD8+ T cells responses, capable of eradicating the established tumours and providing long-term protection, respectively [22]. Promoting antigen translocation to the DC's cytosol, where proteasome processing occurs, could enhance antigen cross-presentation and, subsequently, the induction of antigen-specific CD8+ T cell response [59]. The fact that CNTs can passively diffuse through the cell membrane and reach the cytosol or leak through the endosomes into the cytosol following internalizations via endocytosis could suggest that CNTs are qualified, as delivery vector, to translocate their loaded antigen to the cytosolic compartments (Fig. 3) [55, 57, 58]. The CNTs ability to penetrate the cell membrane might be assigned to their nanoneedle-like structure which arises from their high aspect ratio (length to width ratio) [56]. Nevertheless, endosomal membrane disruption associated with CNTs endosomal escape could induce cell damage [60, 61]. Membrane disruption could activate NLRP3 inflammasome and consequently induce pyroptotic cell death, and is a concern that should not be overlooked on designing a CNT-based vaccine delivery system [60, 61], and is a concern that should not be overlooked on designing a CNT-based vaccine delivery system.

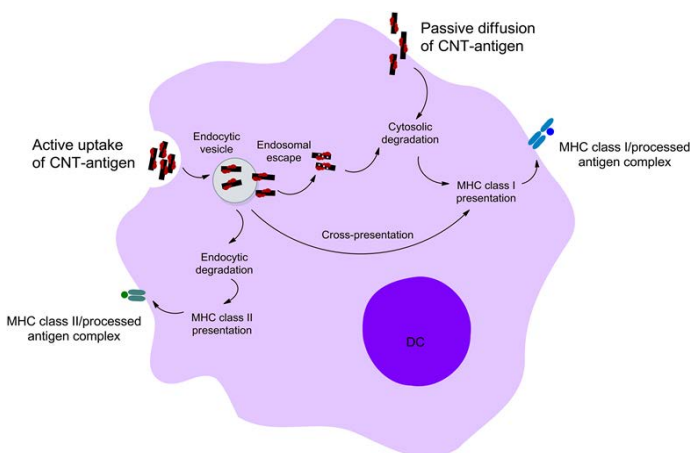


Figure 3: Proposed pathways for MHC presentation of CNTs-delivered antigens. CNTs could deliver the incorporated antigen to the cytosol of the DCs, via two proposed routes, where degradation by proteasome and subsequent MHC class I presentation occur. The ability of CNT-antigen conjugates to passively diffuse through the cell membrane could directly deliver the loaded antigen to the cytosol.

Alternatively, following the active uptake of CNT-antigen conjugates by DCs and the subsequent endosome escape; the incorporated antigen could gain entry into the cytosol. In addition, overcoming the need for endosomes escape, antigenic fragments yielded from antigens processed in the endosomes by endosome proteases could be loaded onto the MHC class I molecules recycled from the plasma membrane. Furthermore, professional cross-priming DCs could translocate endocytosis antigenic cargo to the MHC class I pathway via the utilization of cross-presentation mechanism. Lysosomal degradation of CNTs-delivered antigens that fail to escape the endosomes could be followed by MHC class II presentation.

3.3. CNTs' biocompatibility in Vitro

3.3.1. Effect of CNTs' chemical Functionalization

Residual transition metal catalysts such as iron, cobalt or nickel contained in the pristine CNTs can catalyze the intracellular formation of free radicals and oxidative stress leading to cytotoxic effects. For instance, treating HEK293 human kidney embryo cells with pristine SWNTs induced cell apoptosis and reduced cell proliferation, additionally incubating Calu-3 human epithelial cells with pristine MWNTs significantly reduced cell viability [62, 63]. However, chemically functionalized CNTs have shown better biocompatibility profiles compared to the pristine material. This could be attributed to the fact that exposing pristine CNTs to chemical reactions followed by successive washing in organic solvents with the aid of bath sonication help in removing metal catalysts adsorbed onto the CNTs wall. In addition, chemical reactions, such as bath sonication-assisted acid oxidation, that generate surface defects onto the CNTs help in removing trapped metal catalysts [64].

Coccini et al. have shown that acid-oxidised MWNTs possessed lower metal content and exerted minor effects on the cell viability compared to the pristine MWNTs following incubation with the epithelial A549 cells at 1 µg/ml [65]. However, increasing the oxidized MWNT concentration in the culture media was accompanied by dramatic decrease in the A549 cells viability. Vuković et al. have reported that treating fibroblast L929 cells with pristine MWNTs at concentrations ranging 3–12.5 µg/ml significantly reduced the cell proliferation, while incubation with carboxylic or amine-functionalised MWNTs did not show this effect [66]. Despite this, the proliferation of the L929 cells incubated with the functionalised MWNTs at higher concentrations (25–100 µg/ml) was significantly lower than the untreated cells. Incubating human epidermal keratinocytes with acid-functionalised SWNTs also showed a dose-dependent reduction in cell viability and increased production of the pro-inflammatory cytokine IL-8 [67]. This observation could be attributed to the rupture of CNT-contained endosomes that led to NLRP3 inflammasome activation and pyroptosis [60, 61].

It could be suggested that although chemical functionalization can improve the CNTs purity and biocompatibility, the associated increase in CNTs individualisation increased their cellular uptake thus the possibility of causing cytotoxic effects with increased dosage. In a similar fashion, Li et al. have demonstrated that as the positivity of chemically functionalized MWNTs was increased (by manipulating the surface chemistry), the cellular uptake by THP-1 cell (monocytic cell line) and BEAS-2B cells (bronchial epithelial cell line) was enhanced causing production of pro-inflammatory cytokines [68].

3.3.2. Biocompatibility with Immune Cells

Cytotoxic effects of CNTs on immune cells have been investigated in various studies. Using TEM imaging, it was demonstrated that carboxylated SWNTs formed less intracellular aggregates following incubation with human monocyte-derived macrophages and exerted lower effects on the cell viability than pristine SWNTs [69]. Treating murine RAW 264.7

macrophages with pristine SWNTs (26wt% of iron) led to significant depletion of glutathione (oxidative stress biomarker) compared to treatment with carboxylated SWNTs (0.23 wt% of iron) [70]. The higher iron content of pristine SWNT than carboxylated SWNTs also led to significant increase in the formation of intracellular reactive oxygen species following incubation with rat NR8383 macrophages [71]. The length of the CNT could also determine the CNTs' biocompatibility. LPS-primed, human primary macrophages treated with long pristine MWNT (~13µm) showed higher production of the NLRP3 inflammasome-mediated inflammatory cytokine IL-1β than shorter pristine MWNTs (1-10µm) treated macrophages [61,72].

Wang et al. have shown that treating human monocyte-derived DCs with carboxylated-MWNTs at 10-100 µg/ml for 48 h was not associated with a significant decrease in cell viability [73]. In addition, the carboxylated-MWNT treatment did not increase the DCs expression of the CD80 or CD86 co-stimulatory molecules that suggested lack of MWNTs adjuvanticity. However, cytokines production by MWNTs-treated DCs was not evaluated in this study. Dumortier et al. have demonstrated that culturing mice-derived B or T lymphocytes in the presence of SWNTs functionalized using 1,3-dipolar cycloaddition reaction did not induce cell death, provoke cell proliferation or stimulate IFN-γ production [74]. Nevertheless, SWNTs functionalized via acid-oxidation and amide coupling reactions that exhibited lower aqueous dispersibility stimulated the production of TNF-α and IL-6 by macrophages in vitro. Although this study highlighted the effect of SWNTs surface chemistry, and consequently the aqueous dispersibility, on the cytokine production by immune cells in vitro, it would be also useful to investigate the effect of different sized SWNTs.

Pescatori et al. have also reported that incubating carboxylate or amine-functionalized MWNTs with Jurkat T cell line or THP-1 monocytic cell line did not induce cell apoptosis [75]. The uptake of the functionalized MWNTs by the THP-1 monocytic cells, but not the Jurkat T cells, increased the production of IL-6 and TNF-α Pro-inflammatory cytokines. On the other hand, Medepalli et al. have found that DNA-functionalized SWNTs did not alter the cell phenotypes or activation markers expression following the incubation with human blood-derived monocytes or lymphocytes [76]. Such discrepancy could be attributed to the CNTs' functionalization density, the used doses and incubation time.

These studies, therefore, suggested that the increased purity of functionalized CNTs could be accompanied by improved cytocompatibility. However, functionalized CNTs could still exert dose-dependent cytotoxic effects.

3.4. CNTs' Biodistribution

Biodistribution and clearance of the CNTs are considered among the main obstacles clinical application of CNTs is facing. The utilization of CNTs for the delivery of therapeutic agents demanded studying their biodistribution to determine their organ accumulation and toxicity following systemic administration. Yang et al. have demonstrated that

pristine SWNTs intravenously injected to KM mice were distributed mainly to liver, spleen and lung 24 h post injection [77]. The pristine SWNTs were retained in these organs at high levels over a period of 28 days post injection. In addition, the pristine SWNTs were undetectable in the urine or feces samples collected from injected mice, which further indicated the retention and accumulation of the injected pristine SWNTs in the mentioned organs.

It has been shown that the functionalization density of MWNTs affected their biodistribution and excretion following intravenous injection in BALB/c mice [78]. On comparing three types of ¹¹¹In--radiolabelled MWNTs that were amine-functionalized to varying degree, the highest bladder accumulation and lowest liver retention detected at 0.5 h and 24 h post injection, respectively, were demonstrated by the MWNT that possessed the highest content of amine moieties. Thus, it was suggested that increasing the amine-functionalization density of MWNTs assisted their individualizations, hence glomerular filtration and renal clearance. However, other factors that are, theoretically, expected to affect the MWNTs biodistribution such as frequency of administration and injected doses were not studied.

Liu et al. used Raman spectroscopy to qualitatively and quantitatively assess the long-term fate of SWNTs functionalized with polyethylene glycol (PEG) of varying chain length intravenously administered to BALB/c mice [79]. Raman spectroscopic analysis of ex vivo tissues isolated 1 day post-injection of 20 µg SWNTs/mouse showed retention of SWNTs-PEG mainly in liver and spleen. The retained SWNTs-PEG, especially if functionalized with a long PEG chain, were almost cleared from the liver and spleen 3 months after injection with no apparent toxic effects detected in histology specimens and blood chemistry. Administration of higher doses (100 µg/mouse), presumably due to improvement in signal-to-noise-ratio, provided evidence of SWNTs presence in the bladder and feces at 24 h post-injection suggesting elimination via the renal and biliary routes. On the other hand, the biodistribution and clearance of the injected 100 µg SWNTs over longer period of time, e.g. 1 and 3 months, were not evaluated.

Schipper et al. have reported that on monitoring the blood count of nude mice over a period of 4 months after the intravenous injection of PEG-functionalized SWNTs, no significant differences were detected between the naïve and SWNT-injected mice groups [80]. Histological analysis of tissues from the organs excised 4 months post SWNT injection showed the presence of dark aggregates that were confirmed by Raman spectroscopy to be SWNTs in the liver and spleen macrophages with no obvious pathological features. This observation comes despite the fact that mice were injected with SWNTs two times (on day 0 and 7), the injected dose of SWNTs was 17 µg/mouse. It is quite probably that higher doses of SWNTs as nanocarriers will be required and this could be addressed in future work using a similar model.

Guo et al. studied the biodistribution and excretion of radiolabelled glucosamine-functionalized MWNTs following

intraperitoneal administration to mice [81]. Tracing the radioactivity 1 h post injection revealed the distribution of MWNTs–glucosamine to the main organs and almost complete clearance after 24 h with less than 70% of the total initial radioactivity excreted in urine and feces. However, free radiolabelled glucosamine released from the functionalized MWNTs *in vivo* could provide misleading data about the MWNTs biodistribution, thus a more reliable method, e.g. detection of MWNTs Raman signals, could have been applied to further support the presented conclusion.

Meng et al. investigated the organ toxicity and immunological reactions induced following subcutaneous administration of 1 mg of carboxylated MWNTs to BALB/c mice [82]. Histological analysis of heart, liver, kidney and spleen excised from the mice over a period of 2 to 90 days post MWNTs injection revealed normal histology with no apparent accumulation of MWNTs. However, histological examination of axillary lymph nodes excised 30 days post injection showed accumulation of MWNTs that increased and then decreased 60 and 90 days, respectively. Nevertheless, the administered MWNTs were not completely eliminated and the study did not investigate the fate of the accumulated MWNTs. Levels of pro-inflammatory cytokines such as TNF- α and IL-17 were detected at a higher level in the sera of the MWNT-injected mice compared to naïve mice 2 days post injection, however, the cytokine levels returned to normal 7 days post injection [82].

In light of the research gaps highlighted in the mentioned studies, future studies could provide more conclusive assessment of the CNTs by considering critical factors such as administered doses, frequency of administration, reliability of the methods applied to track the injected CNTs and long-term tracking following administration.

3.5. CNTs' biodegradability

Once the loaded cargo is delivered to its intended intracellular target, CNTs need to be eliminated from the cells. To this end, there have been growing interests in studying the CNTs biodegradability and susceptibility to enzymatic degradation. Allen et al. have shown that oxidized SWNTs incubation with the plant-derived horseradish peroxidase enzyme at 4 °C in the presence of hydrogen peroxide (H₂O₂) led to length shortening and then complete loss of the tubular structure of the SWNTs, as revealed by TEM imaging, over a period of 12 weeks [83]. It was suggested that the SWNTs were subjected to biodegradation that was further demonstrated using other methods such as mass spectrometry. Despite the harsh conditions applied, complete biodegradation was not observed as the TEM images revealed the presence of the carbonaceous material at the end of the 12 weeks. In addition, the biodegradation of the SWNTs at conditions resembling the intracellular environment was not evaluated. The described mechanism behind this degradation relies on the interaction of the peroxidase enzyme with H₂O₂ to generate potent oxidizing intermediates that oxidize the CNTs into aromatic oxidized fragments and eventually carbon dioxide.

Kagan et al. have demonstrated that incubating human neu-

trophil– derived myeloperoxidase enzyme and H₂O₂ with a suspension of oxidized SWNTs in buffered saline changed the dark SWNTs suspension into a translucent solution after 24 h [84]. The SWNT biodegradation was assessed by the complete disappearance of the tubular SWNT structure in TEM images and the distortion of the characteristic SWNT Raman signals. Raman spectroscopic analysis of SWNTs internalized by neutrophils *in vitro* was also used to assess intracellular biodegradation. However, the disappearance of the SWNTs characteristic tubular structure or Raman signals cannot be considered as the carbonaceous material persists. The study investigated the biocompatibility of the carbonaceous material by demonstrating that administration of 40 μ g of the biodegraded SWNTs via pharyngeal aspiration was not associated with acute pro-inflammatory response in mice. Nevertheless, factors such as other administration routes, higher doses and possibility of chronic toxicity were not studied. In a similar manner, the same group has also studied the biodegradation of oxidized SWNTs following incubation with eosinophil peroxidase enzyme and H₂O₂ or internalisation by murine–derived eosinophils *in vitro* [85]. It would have been interesting to assess the biodegradation of various SWNTs doses following incubation with the eosinophils at different time points. Furthermore, the biocompatibility of the persisted carbonaceous material was not assessed *in vitro* or *in vivo*.

Interestingly, Shvedova et al. found that pulmonary inflammatory responses induced by pharyngeal aspiration of oxidised SWNTs were more intense in myeloperoxidase enzyme knockout B6.129 \times 1 mice compared to wild type C57BL/6 mice [86]. The authors attributed this observation to the SWNTs intracellular degradation by myeloperoxidase enzyme in the C57BL/6 mice. This was supported by the presence of a high proportion of SWNTs with shortened length and oxidative defects, in solubilized lung sample preparations, 28 days following exposure to the SWNTs as revealed from TEM and Raman spectroscopic analysis. However, the carbon material that withstood degradation appeared aggregated under TEM and the biocompatibility of the persisted material over the long term was not assessed. Moreover, biodegradation of the SWNTs following repeated administration or administration via other routes that are more frequently used in the biological applications of CNTs, e.g. intravenous or subcutaneous injection, were not investigated.

It has been previously studied the degradation of amine-functionalized MWNTs in brain tissue following stereotactic brain injection [87]. TEM analysis of mouse brain tissue 2 days after the MWNTs administration (0.5 μ g/mouse) showed the existence of intact cylindrical nanotubes and clustered non-tubular material in the microglia's cytoplasm, suggesting MWNTs biodegradation. This observation was further investigated via Raman spectroscopic analysis of brain tissues 2- and 14-days post MWNTs administration. Decreased intensity was observed in the MWNTs characteristic Raman spectra that could be attributed to biodegradation-induced defects, further suggesting degradation in brain tissue. However, dose-dependent degradation of the MWNTs and the possibility of complete degradation were not investigated.

Although the findings of these studies provide evidence for the tendency of CNTs towards intracellular biodegradation, the studies did not resolve the issue of the carbon-based material cellular persistence. Future studies have to investigate the cellular capacity to fully degrade the carbonaceous material and to find out how long would it take to completely degrade and eliminate a specified amount of CNTs. Furthermore, complete degradation of CNTs should not be the only concern of future studies, as the previous studies reported that CNTs biodegradation is achieved by the aid of intracellular-generated reactive oxygen species. Thus, it is also important to carry out a Long-term assessment of the cellular damage that may occur as a result of the increased oxidative stress following cellular uptake of CNTs.

Biodegradability and elimination can be considered as one of the major hurdles that could impede the clinical assessment of CNTs as delivery carriers to therapeutics. In a recent study published by Alidori et al., SWNTs functionalized using 1,3-dipolar cycloaddition were intravenously administered to non-human primates (cynomolgus monkey), the injected SWNTs exhibited biodistribution profile and rapid renal elimination in a manner similar to that observed in mice [88]. Despite such encouraging results, clinical investigations of the CNTs proficiency as nanocarriers might not be possible until pre-clinical assessments of their biosafety, biodegradation and elimination are conclusive. In addition, clinical application of functionalized CNTs-based delivery systems could be also hindered by the necessity to produce them according to the current Good Manufacturing Practices. Hence, several obstacles will need to be overcome in order to meet these standards including uniformity of CNTs dimensions, functionalization density and antigen loading.

4. SWCNTs in Cancer Therapy

Platinum-based Phase II and Phase III anticancer drugs hold promise in the treatment of cancer with new drugs being discovered, some of which are still under clinical trials. The two main limitations in use of Pt-based anticancer drugs are the anticancer drugs undergo poor circulation in tissue cells and its activity is reduced with time due to the complex formation with plasma and tissue cells, and tumor cells demonstrate resistance toward Pt-based drugs under prolonged exposure, rendering them ineffective as potent anti-tumor agents. Lippard and co-workers incorporated capped f-CNT as longboat delivery vehicles for cisplatin anticancer drug through clathrin-dependent endocytosis and measured the changes in redox potential before and after release of the drug. The substituted c, c, t [Pt(NH₃)₂Cl₂(OEt)(O₂CCH₂CH₂COOH)] pro-drug was attached to SWCNT functionalized with phospholipid tethered amine with PEG to solubilize the nanotube [89-93]. Investigated the encapsulation of cisplatin in a phospholipid formulation. The lipid-coated cisplatin nanocapsules exhibit drug-lipid ratio and in vitro cyto-

toxicity 1000 times higher than free cisplatin. This method thus formed an effective approach in drug delivery and the means of producing lipid-based nanocapsules for encapsulating different bio- and therapeutic molecules. Hilter and Hill suggested three preferred orientations of cisplatin toward the entry into CNT and probable interactions using mechanical principles and mathematical modeling [94]. The atomic interaction between nanotubes and cisplatin was calculated using hybrid-discrete-continuum approximation. In this approximation, cisplatin was taken as a collection of discrete atoms and the CNT was treated as a continuum body of repeating carbon atoms. Non-bonded interaction, suction, and acceptance energies were calculated using the Lennard-Jones (LJ) potential. For nanotube radius of 5.3 Å, cisplatin exhibited maximum suction energy, depending on the orientation of nanotubes as a function of radii.

It has been performed density functional studies on the non-covalent functionalization of non-Pt-based anticancer drug camptothecin (CPT) on graphene-based nanomaterials and its prototypes, including graphene oxide (GO) [95]. The non-covalent adsorption of CPT induces a significant strain within the nanosheets and the interaction was thermodynamically favored from energetics perspective. In case of GO, surface incorporation of functional groups resulted in significant crumpling along the basal plane and the interaction was mediated by H-bonding rather than π - π stacking. The molecular docking studies of CPT onto Top1 (Figure 4a) showed CPT to be stacked between the Watson Crick AT and GC base pairs and the interaction was mediated via π - π stacking (Figure 4b). For the binding of CPT functionalized graphene and GO with topoisomerase I (top 1) CPT interacts through π stacking with AT and GC base pairs of DNA. The optimum interacting distance of CPT from AT and GC bases was calculated at 3.87 and 3.38 Å, from the central aromatic rings (Figure 4b). The re-rank score of bare CPT drug was calculated as -89.01 a.u. with an H-bond score of -2.53 a.u. as shown in Table 1.

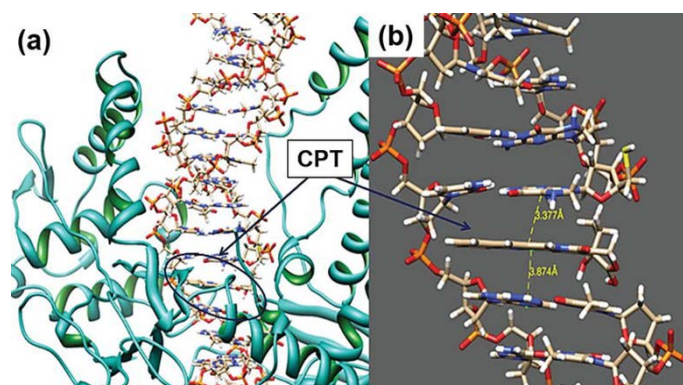


Figure 4: (a) Secondary structure of Top1 protein with the CPT drug docked within the DNA, (b) interacting distance between CPT and the DNA base pairs of top 1. Reprinted with permission from Ref. [95]. Copyright 2017, Elsevier.

Table 1: The re-rank scores and H-bond scores for the best docked conformations of CPT and CPT/8 × 8 graphene, and CPT/8 × 8 GO sheets, respectively.

System	Re-rank score CPT	Re-rank score nanosheet	H-bond score CPT	H-bond score nanosheet
CPT_Top1	-89.01	—	-2.53	—
8 × 8 graphene/CPT docked onto Top1	-89.10	95.87	-2.57	0.00
8 × 8 GO/CPT docked onto Top1	-90.21	126.21	-2.29	-4.44

Likewise, for the docking of CPT/8 × 8 graphene with Top1 (Figure 5a) CPT gets docked between the AT and GC base pairs. However, graphene gets docked along the phosphate backbone of the ds-DNA helix as shown from Figure 5b indicating a strong interaction between the polar phosphate groups of the DNA helix. Compared to the docking of bare CPT drug, presence of graphene stabilizes the intercalation of CPT between the AT and GC base pairs, as observed from the increase in re-rank score values.

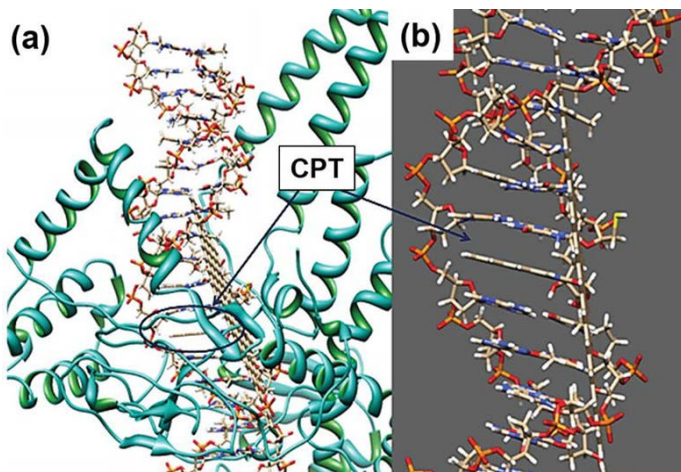


Figure 5: (a) Secondary structure of Top1 with the CPT/8 × 8 graphene sheet docked within the DNA, (b) binding of CPT/8 × 8 graphene sheet with DNA base pairs of top 1. Reprinted with permission from Ref. [95]. Copyright 2017, Elsevier.

The docking of CPT/GO with Top1 as illustrated in Figure 6a, depicts CPT to get docked between AT and GC base pairs of DNA, mediated by π - π stacking interaction similar to that observed for bare CPT and CPT/8 × 8 graphene. However, in the presence of GO, GO undergoes strong interactions with DNA bases and gets docked between the DNA helix and the interaction is stabilized by intermolecular H-bond between the polar functional units on the basal plane of GO and DNA nucleobases (Figure 6b). The molecular docking studies on bare CPT and CPT functionalized graphene and GO systems showed that the interaction of CPT with Top1 is mediated by π -stacking interaction between the aromatic rings of CPT and the A and C bases of DNA. In presence of graphene and GO, CPT undergoes a similar trend in adsorption while the graphene and GO nanomaterial gets docked along the phosphate backbone indicating a strong preferential interaction with DNA.

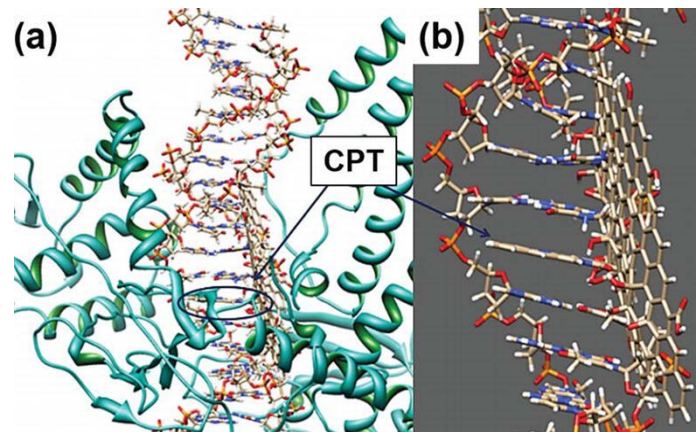


Figure 6: (a) Secondary structure of Top1 protein with the CPT/8 × 8 GO sheet docked within the DNA, (b) the binding of CPT/8 × 8 GO sheet with DNA base pairs of top 1. Reprinted with permission from Ref. [95]. Copyright 2017, Elsevier.

Boucetta et al. [96] investigated the supramolecular MWCNT-DOX-copolymer complex for anticancer activities. Since DOX, a clinically acclaimed anticancer drug belonging to the family of anthracyclines exhibit fluorescence properties, its uptake and interaction with nanotubes upon administration can be monitored using fluorescent spectrophotometry. The copolymer coated MWCNT formed supramolecular complexes with DOX via π -stacking and revealed enhanced cytotoxicity leading to highly efficient cell killing efficiency [97]. reported the use of DOX loaded PEG functionalized CNT for targeted delivery of anticancer drugs in tumor cells [97]. The SWCNT was pre-functionalized with PEG and DOX and a fluorescence probe (fluorescein) was loaded onto the nanotube via π stacking. The loading and subsequent release of DOX were found to be pH dependent; decrease in pH from 9 to 5 showed a decrease in DOX loading. Under acidic conditions (pH 5.5), DOX exhibited increased hydrophilicity and solubility with lysosomes and endosomes, facilitating the release of drug molecules from the nanotube. On decreasing the pH, surface loading of DOX onto nanotube surface lowered and at lower acidic pH, amine group of DOX underwent protonation resulting in increased solubility of DOX molecules.

5. Functionalized CNTs as Cancer Vaccine Delivery System

Various types of particulate carriers have been utilized in vaccine delivery [98–102]. The efficacy of particulate vaccines has been assigned to a number of suggested mecha-

nisms. Particulate delivery systems can accommodate multiple copies of the antigen and adjuvant. Hence, the uptake of particulate vaccine delivery systems by APCs could increase the antigen and adjuvant intracellular concentrations, thus the presented antigen density.

Potent anti-tumour immune response induction could be achieved via combinatorial therapeutic approaches consisting of tumour antigens and immune modulators capable of overcoming tumour-induced immune suppression [16, 103]. Examples of nanoscopic particulates previously employed to co-deliver tumour-derived antigen and adjuvant include liposomes (spherical vesicles consisting of lipid bilayers enclosing an aqueous core), lipopolyplexes (lipid and DNA complex), nanoparticles made up of emulsified poly(lactic-co-glycolic acid) (PLGA), virus-like nanoparticles (self-assembled capsid protein lacking the viral nucleic acids), albumin-based nanoparticles or mesoporous silica nanoparticles (synthetic nanoparticles possessing porous structure) [109]. Examples of micro-sized carriers exploited in tumour antigen and adjuvant simultaneous delivery are polymeric systems consisting of PLGA or diamino sulfide polymers. Despite the differences in the composition and size of these nanoparticles or microparticles, they share the property of being spherical in shape. The efficacy of particulate delivery systems to deliver cancer vaccines comprised of antigen and adjuvant has been investigated in various studies [104–120]. These studies have shown that nanoparticles (e.g. liposomes, PLGA nanoparticles or albumin nanoparticles) or microparticles (e.g. PLGA or diamino sulfide-based microparticles) co-incorporating antigen and adjuvant delayed the growth of cancer cells inoculated in mice. This observation was attributed to the capacity of the nanoparticles or microparticles to augment the antigen-specific CD8⁺ T cell immune response elicited by the co-loaded antigen and adjuvant as demonstrated in these studies *in vitro* or *in vivo* [106,108–120].

Inspired by the demonstrated potentials of the conventional spherical nano-systems as vaccine delivery vectors and by the CNTs capacity to enter the cells via different mechanisms, various studies have investigated the exploitation of CNTs as vaccine nanocarriers. As summarized in, these studies focused on functionalized CNTs using various approaches to deliver antigens expressed by cancer cells and/or adjuvants to APCs and tested the efficacy of the CNTs–delivered vaccines through the assessment of specific immune responses elicited *in vitro* and *in vivo* [121].

5.1. Functionalized CNTs as delivery vector for tumour-derived antigen

As a cancer vaccine delivery system, Sun et al. investigated the use of carboxylated MWNTs to deliver MCF7 breast cancer cells-derived tumour lysate protein (TumourP) to APCs, specifically the DCs [122]. Flow cytometry showed that the MWNTs improved the uptake of the covalently incorporated TumourP by DCs *in vitro*. Furthermore, DCs pre-treated with MWNT-TumourP were more efficient than DCs pre-treated with free TumourP in inducing lymphocyte-mediated cyto-

toxicity against the MCF7 cells *in vitro*. However, the capability of MWNT-TumourP in retarding the MCF7 breast cancer cells growth *in vivo* was not studied.

Assessed the potentials of carboxylated MWNTs to augment the anti-tumour immune response elicited against covalently immobilised H22 liver cancer cell-derived tumour lysate protein (H22P) [123]. The H22 cells were subcutaneously inoculated into BALB/c mice and the mice were subcutaneously injected with MWNT–H22P or free H22P starting 2 days post H22 cells inoculation. The injected treatments were further potentiated by the additional administration of inactivated H22 tumour cells as a tumour cell vaccine. The maximum anti-tumour response was observed in mice injected with MWNT–H22P. Lymphocytes isolated from MWNT–H22P injected mice showed higher cytotoxicity against the H22 cells *in vitro* than lymphocytes isolated from free H22P–injected mice. Additionally, some of the mice free of H22 tumour, as result of MWNT–H22P treatment, successfully inhibited H22 cell growth following re-administration. This was due to the induction of antigen-specific memory T cells, since challenging ‘cured’ mice with the unrelated breast cancer cell line EMT led to successful tumour growth. The authors suggested that the augmented antigen-specific immune response elicited by MWNT–H22P was due to increased uptake of MWNT-conjugated H22P by the APCs, however, the MWNTs ability to enhance antigen uptake by the APCs *in vivo* was not tested. In addition, to evaluate the therapeutic efficiency of MWNT–H22P, it would have been informative to treat H22–tumour bearing mice with the vaccine rather than to challenge mice with tumour cells post vaccination.

In order to potentiate the immune response elicited by the poorly immunogenic Wilms’ tumour protein (WT1) Villa et al. covalently conjugated WT1-derived peptide with amine-functionalized SWNTs [124]. The SWNTs were internalized by the DCs *in vitro*, as determined using live confocal imaging, with no effects exerted on cell viability. The free WT1 peptide or SWNT–WT1 peptide conjugate were mixed with an oil-based adjuvant and then subcutaneously administered to BALB/c mice. The highest levels of anti-WT1 peptide IgG were detected in the sera collected from mice vaccinated with SWNT–WT1 peptide. However, tumour therapy experiments using WT–1 expressing cells were not carried out.

5.2. Functionalized CNTs as Delivery Vector for Adjuvants

Appropriate activation of APCs is crucial for unlocking their full T cell stimulatory capacity [125]. Innate activation of APCs is mediated by pattern recognition receptors (PRRs) such as Toll-like receptors (TLRs), C-type lectin receptors (CLRs) and NOD-like receptors (NLRs) [126, 127]. These receptors recognize ligands associated invading pathogens known as pathogen-associated molecular patterns (PAMP). Naturally occurring PAMPs or their synthetic analogues have been widely explored in vaccine formulations as adjuvants with the aim to promote immunity induction [127,128]. In particular, synthetic TLR9 agonists in form of oligodeoxynu-

cleotides (ODN) containing unmethylated deoxycytidine-deoxy guanosine dinucleotide (CpG) motifs have been included as adjuvant in many clinically investigated cancers vaccine formulations (Fig. 7) [129, 130].

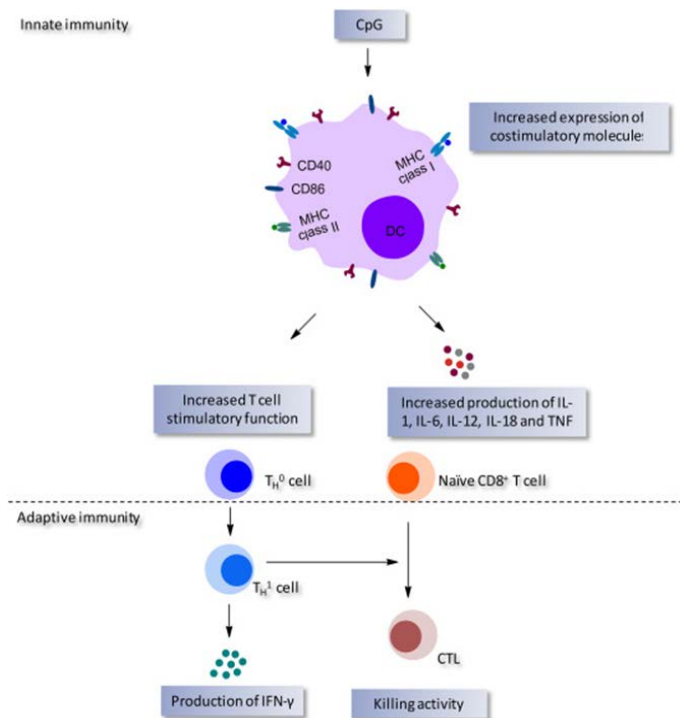


Figure 7: Immune stimulatory activities of CpG. Stimulation of the DCs' TLR9 by CpG induces DC maturation by upregulating the MHC, CD40 and CD86 expression, and provokes the immune stimulatory cytokines production that ultimately determines the DC ability to induce CD4⁺ and CD8⁺ T cells priming. Adapted by permission from Nature (Nature Reviews Immunology) ref. [131] (© 2004).

The delivery of TLR9 agonist to APCs using CNTs has also been studied. Zhao et al. investigated whether SWNT-mediated delivery of CpG ODN could enhance the cellular uptake and the immune stimulatory properties of the vaccine and promote potent anti-tumour immune response induction [132]. The authors showed that the uptake of fluorescently labeled CpG by bone marrow-derived monocytes *in vitro* was increased by its non-covalent conjugation to SWNTs. The SWNT-CpG conjugate also increased the CpG-induced production of interleukin (IL)-12 and tumour necrosis factor (TNF)- α by the monocytes *in vitro*. Moreover, intratumoural injection of the SWNT-CpG conjugate effectively delayed the growth of GL261 glioma cells intracranially-implanted in mice, which was not observed in mice injected with SWNT alone or free CpG. SWNT-CpG treatment failed to delay the growth of GL261 glioma cells intracranially implanted into mice depleted of CD8⁺ T cells or natural killer cells. This observation indicates the joint involvement of these cells in the induction of anti-tumour immune responses by SWNT-CpG conjugate.

Fan et al. have reported that intracranial administration of SWNT-CpG could also inhibit metastatic tumour growth in C57BL/6 mice [133]. This was demonstrated by showing

that injection of SWNT-CpG was more efficient than free CpG in delaying the growth of subcutaneous and intracranial inoculated B16F10 melanoma cells. Furthermore, testing the therapeutic efficacy against a more challenging glioma model, Ouyang et al. have shown that SWNT-CpG along with the chemotherapeutic drug temozolomide, intratumorally administered, to mice bearing intracranial K-Luc glioma cells led to significantly prolonged survival in contrast to the injection of free CpG and temozolomide [134].

5.3. Functionalized CNTs as Delivery Vector for both Tumour-Derived Antigen and Adjuvants

In 2014 Faria et al. have reported the delivery of antigen and adjuvant to APCs using CNTs [135]. In this study the model antigen OVA and the TLR9 agonist CpG were both non-covalently linked to carboxylated MWNTs. Mice immunised with MWNT-conjugated OVA and CpG showed higher sera levels of anti-OVA IgG and IFN γ production by *ex vivo* stimulated splenocytes than mice immunized with free OVA and CpG. The authors also tested the ability of the carboxylated MWNTs to co-deliver NY-ESO-1 (tumour antigen expressed in various human cancers) in combination with CpG to the APCs. The immune response induced *in vivo* by NY-ESO-1 and CpG was intensified following their non-covalent linkage to MWNTs. In addition, testing the ability to induce protective immunity, mice pre-injected with NY-ESO-1 and CpG-loaded MWNTs demonstrated a markedly retarded growth of NY-ESO-1 expressing B16F10 melanoma cells in subcutaneous tumour model. However, to assess the therapeutic efficacy of the designed MWNT-based vaccine, tumour-inoculated mice were vaccinated three days post tumour cell inoculation, when tumour growth was still undetectable. Therefore, it is unclear whether therapeutic vaccination with carboxylate MWNTs co-delivering antigen in combination to CpG ODN would lead to effective remission of a well establish tumour.

In a previous study, it has been compared the efficacy of MWNTs functionalized using 1,3-dipolar cycloaddition, oxidation or amide coupling reactions in delivering non-covalently immobilised OVA to APCs [136]. The MWNTs functionalized via amide coupling were more efficient in enhancing the OVA-specific immune response both *in vitro* and *in vivo*. In a follow-up study, the functionalized MWNT possessing surface chemistry that was found optimal for OVA delivery was then utilized for the co-delivery of OVA along with the adjuvants CpG and anti-CD40 antibody (α CD40) to the APCs in form of a (α CD40) MWNT (OVA-CpG) conjugate [137]. In addition to the immune stimulatory properties that can be acquired by the inclusion of α CD40 [103,138,139], it has been hypothesised that α CD40 contained in the aforementioned conjugate will target it to the CD40 receptor on APCs, including cross-priming DC subsets, and thereby further enhance antigen cross-presentation to CD8⁺ T cells. Previous studies have demonstrated the ability α CD40-antigen conjugates to mediate uptake via CD40 receptor and enable translocation of the conjugate to the early endosomes [140-142]. It has been suggested that antigen translocation to early endosomes could support antigen escape into the cytosol and thereby promote antigen cross-presentation (Fig. 8). It was observed that DCs treated with (α CD40) MWNT (OVA-CpG)

in vitro possessed significantly lower surface expression of CD40 receptor compared to DCs treated with MWNT (OVA-CpG). This finding could support the hypothesis that CD40 receptor was internalized following its ligation with the α CD40 contained in (α CD40) MWNT (OVA-CpG) [140, 141]. However, to conclusively support this hypothesis it would be interesting to investigate the intracellular trafficking of the CD40 receptor following the incubation of DCs with (α CD40) MWNT (OVA-CpG). Antigen presentation to CD8+ T cells in vitro was more efficient when DCs were treated with (α CD40) MWNT(OVA-CpG) compared to treatment with free

α CD40 in combination with MWNT(OVA-CpG). The (α CD40) MWNT (OVA-CpG) conjugate also amplified the OVA-specific CTL response in vivo at reduced OVA and CpG doses. Lastly, (α CD40) MWNT (OVA-CpG) demonstrated significant proficiency in delaying tumour growth in the subcutaneous and lung pseudo-metastatic B16F10-OVA tumour models. However, it is unclear whether antigen-specific memory was induced in this model since tumour-inoculated mice treated with (α CD40) MWNT (OVA-CpG) that remained tumour-free were not re-challenged with B16F10-OVA tumour cells.

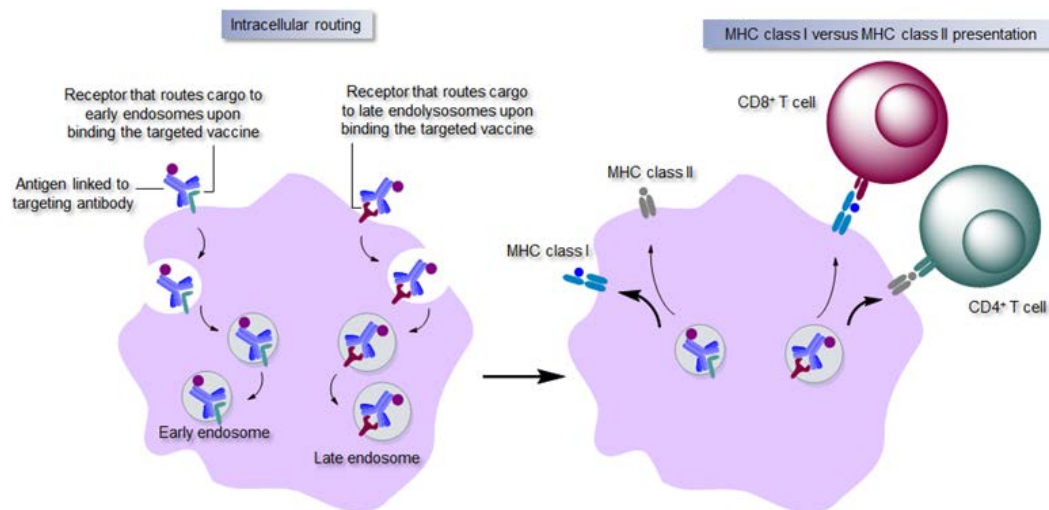


Figure 8: Impact of intracellular routing of antibody-conjugated antigen on antigen presentation. Delivering antigens through a linked targeting antibody to a specific receptor expressed by APCs is followed by cellular internalization of the formed cargo. Relying on the targeted receptor, the internalized cargo could be routed to a specific intracellular compartment. For instance, it has been found that mannose and CD40 receptors are intracellularly routed to the early endosomes, whereas CD205 receptor is routed to the late endosomes. In the late lysosome-containing endosomes, internalized antigen is subjected to rapid degradation by the lysosome enzymes and presentation of the processed antigenic fragments via MHC class II molecules. In the early endosomes, the slow rate by which antigen is degraded could facilitate antigen escape from the endosome to cytosolic compartments that allows proteasome antigen degradation and, subsequently, presentation via the MHC class I molecules. The thicker arrow denotes that this route of presentation of processed antigen is more predominant than the other pathway. Adapted by permission from Nature (Nature Reviews Immunology) ref. [142] (© 2014).

6. Carbon Nanotubes' Surface Chemistry Determines their Potency as Vaccine Nanocarriers in Vitro and in Vivo

It has been hypothesized that altering the physical properties of multi-walled CNTs (MWNTs)-antigen conjugates, e.g. length and surface charge, can affect the internalization of MWNT-antigen by DCs, hence the induced immune response potency. For this purpose, pristine MWNTs (p-MWNTs) were exposed to various chemical reactions to modify their physical properties then conjugated to ovalbumin (OVA), a model antigen. The yielded MWNTs-OVA conjugates were long MWNT-OVA (~386 nm), bearing net positive charge (5.8mV), or short MWNTs-OVA (~122 nm) of increasing negative charges (-23.4, -35.8 or -39 mV). Compared to the short MWNTs-OVA bearing high negative charges, short MWNT-OVA with the lowest negative charge demonstrated better cellular uptake and OVA specific immune response both in vitro and in vivo. However, long positively-charged MWNT-OVA showed limited cellular uptake and OVA specific immune response in contrast to short MWNT-OVA dis-

playing the least negative charge. It has been suggested that reduction in charge negativity of MWNT-antigen conjugate enhances cellular uptake and thus the elicited immune response intensity. Nevertheless, lengths of MWNT-antigen conjugate might also affect the cellular uptake and immune response potency; highlighting the importance of physical properties as a consideration in designing a MWNT-based vaccine delivery system.

Spherical nanosized vaccine delivery systems, ranging from 15 to 1000 nm, have demonstrated a marked capability in augmenting immune response against the delivered antigens [143–145]. This has led to clinical investigations of these delivery systems with respect to enhancing the body's immune response against challenging diseases such as cancer [146, 147]. Cylindrical-shaped nanosized delivery systems have also attracted increased interest over the last decades [148]. CNTs are among the most extensively studied cylindrical-shaped delivery systems in the biomedical field [149, 150]. CNTs, owing to high aspect ratio (length to width

ratio), have been shown to internalize into cells utilizing both energy-dependent and independent routes. For example, single walled CNT (SWNT) conjugated to fluorescently labeled-DNA or protein was shown to be internalized by HeLa cells via energy-dependent endocytosis [151]. Another study reported the internalization of fluorescently labeled ammonium-functionalized-MWNTs in Jurkat cells, under endocytosis inhibiting conditions, suggesting utilization of energy independent uptake mechanisms [152].

CNTs have been reported as antigen delivery systems in a number of studies for enhancing the immune response against infectious agents or cancer. In one study, peptide derived from the foot and mouth disease virus (FMDV) was conjugated to SWNT. The binding specificity and biological activity were confirmed using surface Plasmon resonance, *in vitro* and *in vivo*, respectively [153–155]. A stronger immune response, shown by a higher level of anti-FMDV antibodies, was obtained in BALB/C mice immunized with the SWNT-FMDV conjugate compared to the free FMDV [154]. Another study illustrated that conjugation of a malaria-derived peptide to MWNTs induced higher levels of specific antibodies in mice immunized with the conjugate compared to the free peptide [156]. Furthermore, a shift from Th2 to Th1 immune response, marked by increased interferon gamma (IFN- γ) production, was obtained following immunization with SWNT-conjugated tuberculin [157].

Cancer is another disease where CNTs have shown promise as a vaccine delivery tool. Earlier studies explored enhancing delivery of cancer antigens using SWNT or MWNT. Meng et al. reported that immunization with tumor lysate proteins, derived from H22 liver cancer, conjugated to MWNT reduced tumor volume and prolonged the survival of H22 tumor-bearing mice [158]. Conjugation of tumor lysate proteins, derived from MCF7 breast cancer cells, to MWNTs resulted in enhanced DCs uptake and anti-tumor T cell response *in vitro* [159]. Lastly, Villa et al. reported an augmented humoral immune response against a weak immunogenic peptide derived from Wilm's tumor protein, following conjugation to SWNTs [160].

CNT have also been exploited for the delivery of immunoadjuvants such as the synthetic oligodeoxynucleotides containing cytosine-phosphate-guanine motifs (CpG-ODN). Bianco et al. demonstrated improved immune-stimulatory properties of CpG-ODN *in vitro* following non-covalent loading onto cationic SWNTs [161]. Similarly, Zhao et al. reported enhanced cellular uptake of CpG-ODN *in vitro* and *in vivo*. This was associated with an eradication of established intracranially implanted glioma in mice [162]. In a more sophisticated approach, de Faria et al. utilized MWNTs for the co-delivery of NY-ESO-1 (cancer testis antigen) and CpG-ODN (immunoadjuvant) to DCs *in vivo*. This approach resulted in reduced tumor size and prolonged survival of NYESO-1-expressing B16F10-tumor bearing mice challenged with this treatment [135].

All the outlined studies highlighted the immune modulating potential of these cylindrical-shaped nanocarriers and their

use as an emerging vaccine delivery system [163, 164]. Despite this, only one study has investigated the relationship between CNT's physical properties, specifically their dimension, and the elicited immune response [165]. In that study, functionalized MWNTs (f-MWNTs) of altered physical properties were synthesized to address the structure–activity relationship with respect to influencing antigen presenting cells uptake and immune response *in vitro* and *in vivo* [166].

In that study, it has been investigated the ability of MWNTs-OVA with different surface functionalities and physical properties to induce antigen-specific immune responses following internalization by the antigen presenting cell. *In vitro* studies highlighted differences in T cell activation and cytokine production, for both CD4+ and CD8+ T cells induced by the different MWNTs-OVA conjugates, which correlated with their cellular internalization. Interestingly, no change in the expression of co-stimulatory molecules was detected among BM-DCs treated with f-MWNTs, and the same was observed for MWNTs-OVA treated BMDCs. This lack of f-MWNT's adjuvant properties is in agreement with previously reported studies [159, 161, 167,168]. These observations might indicate that the pattern of induced immune response was determined by the conjugated antigen uptake by antigen presenting cell and not due to the adjuvanticity of f-MWNT. Lastly, cellular uptake and CD8+ T cell responses observed *in vivo* were in a good agreement with the *in vitro* studies.

p-MWNTs were exposed to various functionalization approaches that yielded long positively charged L+ or short negatively charged S--, S-/+ or S-. OVA conjugation with the f-MWNTs yielded MWNTs-OVA of increased negativity. This was in agreement with work reported by de. where an increase in the negativity of oxidized MWNT following conjugation with OVA was observed [135]. This could be due to the acidic amino acids content of OVA. Fadel et al. observed the same behavior following the interaction of negatively charged CNTs with streptavidin, neutravidin or avidin bearing net negative, neutral or positive charges, respectively [169]. Taking advantage of their high surface area and surface hydrophobicity, CNTs have been shown to be able to adsorb peptides or proteins of various molecular weights [170]. Based on our findings, it has been concluded that OVA and its MHC class I-restricted epitope SIN were non-covalently conjugated to f-MWNT, possibly via π - π stacking or hydrophobic interaction [171].

Assessed the immune response induced by CpG-ODN complexed with either ammonium-functionalized SWNT (ammonium-SWNT) or lysine-functionalized SWNT (lysine-MWNT). The study demonstrated a higher enhancement in immunostimulatory activity of CpG-ODN loaded on the lysine-SWNT than ammonium-SWNT *in vitro* [161]. It was suggested that the more positive lysine-SWNT neutralized the negative charge of CpG-ODN and enhanced its cellular uptake. Li et al. examined the uptake efficiency of 4 types of MWNTs functionalized using 1,3-dipolar cycloaddition (12.95 mV), oxidation (-52.61 mV), amidation reaction (-2.35 mV) or polyetherimide modification (53.33 mV) in BEAS-2B (epithelial cells) and THP-1 (monocytes) cells *in vitro* [172]. A

direct correlation between f-MWNT's surface positivity and cellular acquisition was found. It has been also reported similar findings using a series of cationic dendron-modified MWNT in cancer cells [173, 174]. This was attributed to the enhanced electrostatic interactions between the anionic cell membranes and the cationic f-MWNTs.

In case of the shortened f-MWNTs series, it is possible that the differences in biological activity, DCs uptake and immune response are due to reduction in the overall negative charge. One, however, cannot ignore the differences in the chemical structures introduced, which may also have influenced uptake in DC's. Nevertheless, it can be concluded from this study that alteration in f-MWNT's surface chemistry may influence the degree of uptake in DC's. The former is directly proportional to the intensity of immune response produced, agreeing with previously reported studies. Previous studies have also demonstrated a correlation between enhanced cellular uptake of positively charged particulate vaccine delivery systems and immune response augmentation. For instance, cationic poly-L-lysine coated nanoparticles (1000 nm in diameter) in vitro, polystyrene spheres (1000 nm) in vitro, liposomes (200 nm) of varying lipid composition and surface charges in vitro, PLGA microspheres loaded with hepatitis B Ag (HBAG) in vivo, tetanus toxoid-loaded chitosan nanoparticles (40–400 nm) in vivo or OVA-conjugated rod-shaped hydrogel nanoparticles in vitro and in vivo [175-180].

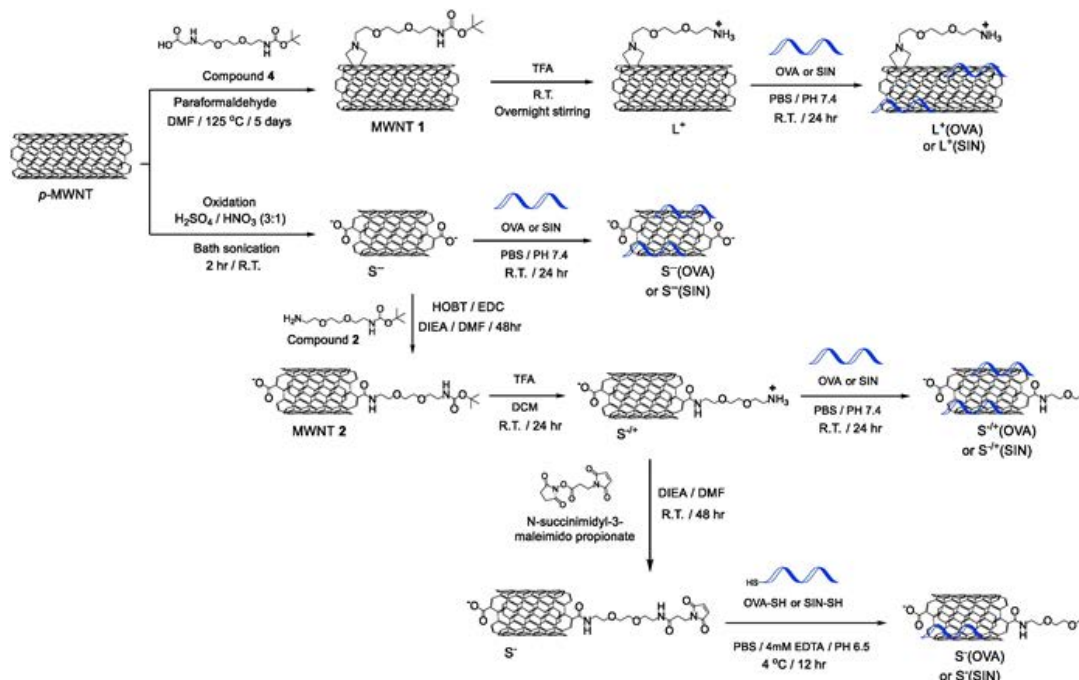
"The positively charged L+(OVA) and L+(SIN) showed lower immune response intensity compared to the negatively charged S-/+(OVA) and S-/+(SIN), respectively. These observations might be related to the longer length possessed by L+ (~386 nm) in contrast to S-/+ (~122 nm) affecting cellular uptake. The effect of MWNT's length on specific antibody response was previously investigated in vivo in New Zealand rabbits and BALB/c mice immunized with protein hapten-MWNTs of two lengths but similar surface charge, and shorter MWNTs (500 nm) induced higher antigen-specific antibody response than the longer MWNTs (>2 μm) [165].

Size-dependency was also reported for spherical nanoparticles. Previous studies concluded that higher uptake by the antigen presenting cells and a subsequently more potent immune response was induced using smaller sized spherical-shaped particulate vaccine delivery systems [179,181-183]. Interestingly, Foged et al. showed that 100 nm nanoparticles, despite being negatively charged, can be taken up more efficiently in DCs than positively charged nanoparticles of bigger size (1000 nm) [176].

Results [166] are expressed as mean value ± standard deviation (S.D.). Statistical analysis was performed using GraphPad Prism version 5.01, California, USA. Statistical differences were determined using one-way ANOVA followed by Bonferroni post-test".

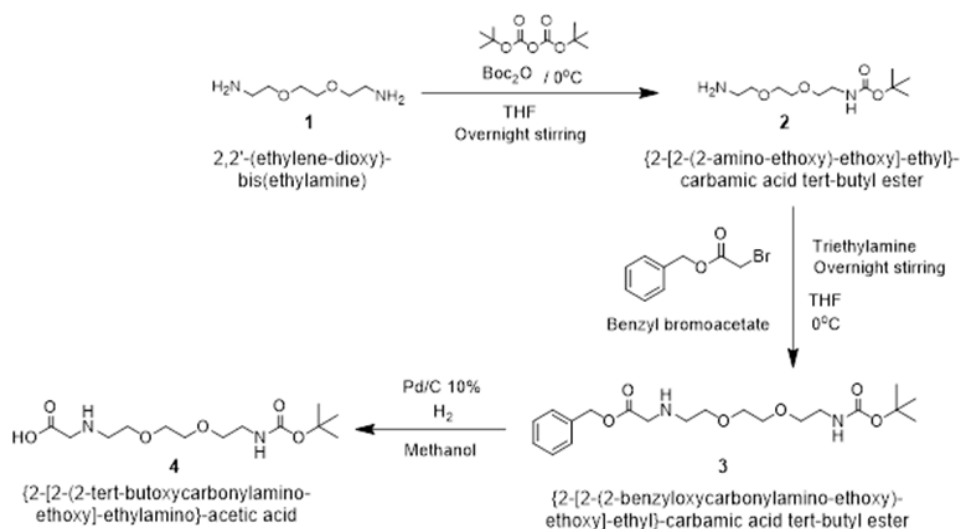
6.1. Synthesis and characterization of functionalized MWNTs (f-MWNTs)

The synthetic steps to prepare f-MWNTs are described in Scheme 1 [166].



Scheme 1: Synthesis of f-MWNTs, MWNTs-OVA and MWNTs-SIN. p-MWNT was functionalized either via 1,3-dipolar cycloaddition or oxidation reactions yielding L+ (long f-MWNT) or S-- (shortened f-MWNT), respectively. S-- was used as a precursor for the synthesis of S-/+ that was further functionalized to yield S-. Non-covalent conjugation approach was used for OVA loading onto L+, S--, or S-/+ yielding L+(OVA), S--(OVA), or S-/+(OVA), respectively. Similarly, non-covalent conjugation was applied for SIN loading onto L+, S--, or S-/+ yielding L+(SIN), S--(SIN), or S-/+(SIN), respectively. Covalent conjugation was employed for OVA-SH or SIN-SH loading onto S-, yielding S-(OVA) or S-(SIN), respectively.

Synthetic steps and NMR spectra of compounds 2, 3 and 4 are illustrated in Scheme 2 and Fig. 9, respectively. Details on the synthesis of f-MWNT and the compounds are described in Fig. 9.



Scheme 2: Synthetic scheme of compounds 2 and 4.

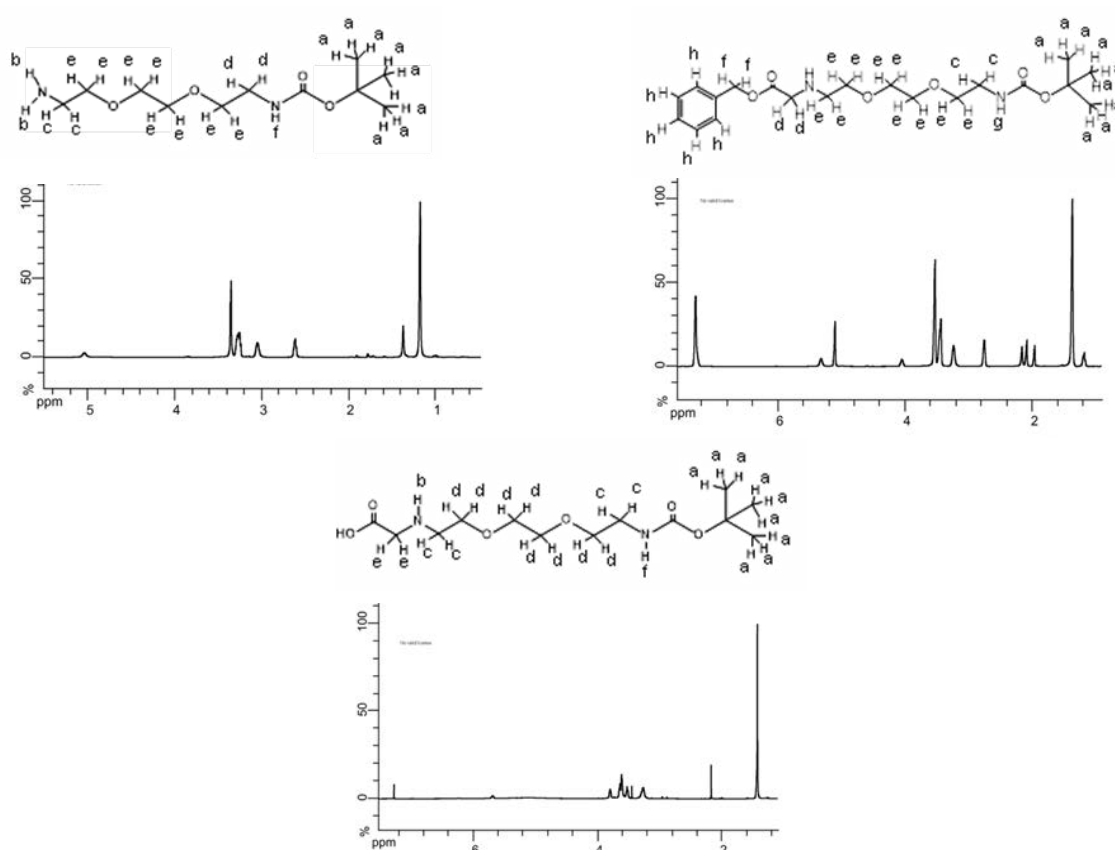


Figure 9: ¹H NMR spectra of compounds 2, 3 and 4.

The surface of the p-MWNTs was chemically modified via the incorporation of functional groups to yield f-MWNTs (Scheme 1). The first functionalization approach relied on reacting the aromatic rings at the sidewalls of p-MWNTs with compound 4 utilizing the previously described 1,3-dipolar cycloaddition reaction [150, 184, 185]. Yielding MWNT 1. The Boc group protecting the amine of MWNT 1 was removed using an acidic treatment that yielded L+ with positively charged primary amine groups. The second functionalization approach involved shortening p-MWNTs by treatment

with oxidizing acids that introduce surface defects and negatively charged carboxylic acids yielding S-- [186–190]. MWNT 2 was synthesized by reacting compound 2 with S— via amide coupling reaction [191, 192]. Boc-deprotection of MWNT 2 liberated the primary amines of S-/+. To incorporate functional groups capable of establishing covalent interaction with OVA, S-/ + was reacted with a maleimide-terminated spacer, yielding S-. Characterization of f-MWNTs was achieved using TGA (Figs. 10 A and 11).

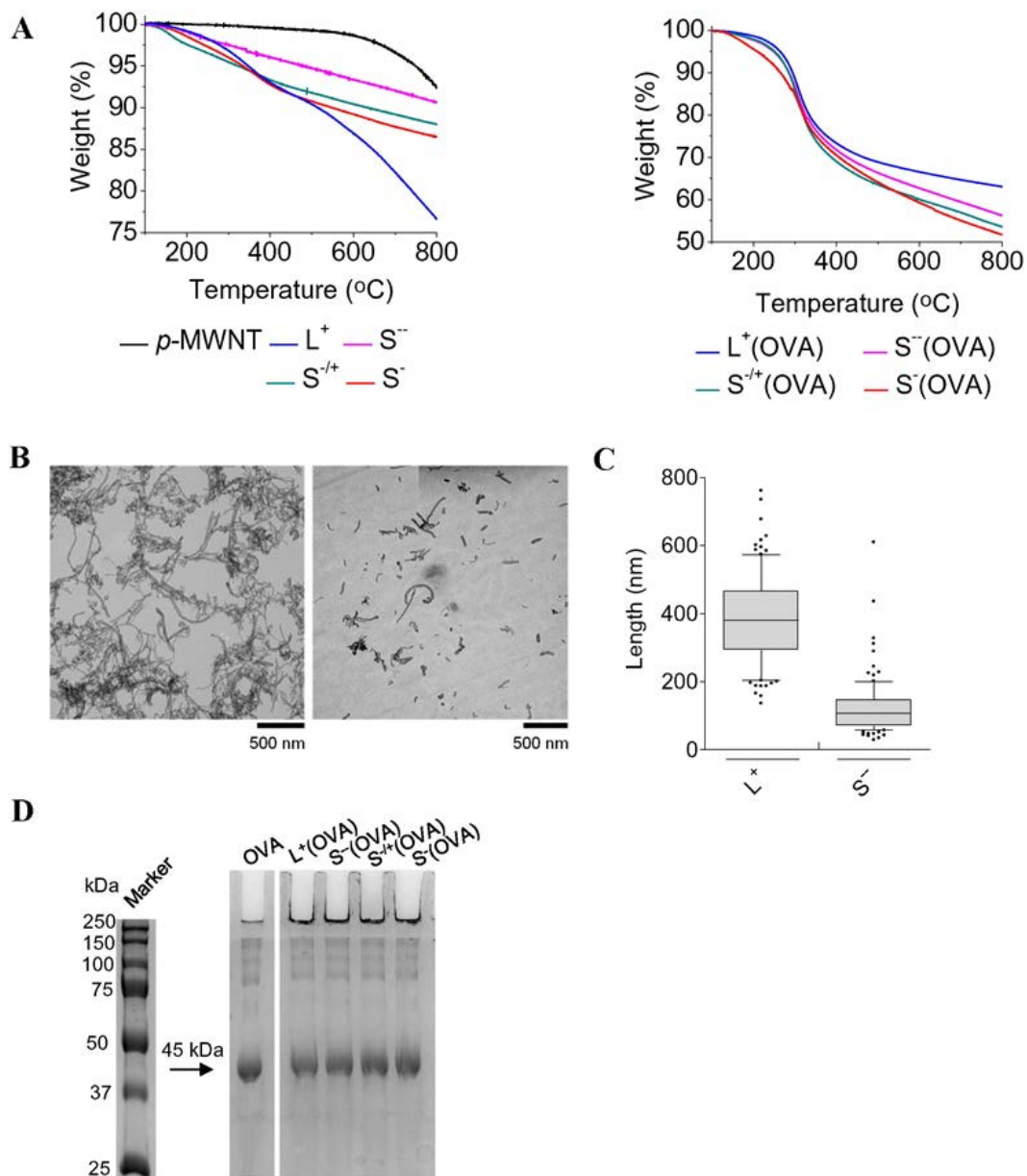


Figure 10: Physicochemical characterization of f-MWNTs and MWNTs-OVA. (A) Thermogravimetric profiles of f-MWNTs (left) or MWNTs-OVA (right). A known weight of MWNT was exposed to gradually increasing temperature and the weight loss was detected as the temperature increased. p-MWNTs were thermally stable up to 600 °C. The weight loss at 600 °C was directly correlated to the amount of introduced functional groups or OVA. Representative thermogravimetric profiles are shown (n = 3). (B) Morphology of f-MWNTs. Representative TEM images of L⁺ (left) and S⁻ (right), deposited on carbon grid from aqueous dispersions. S⁻ displayed shorter lengths compared to L⁺. (C) Box plot of L⁺ or S⁻ length distribution. The horizontal line inside the box indicates the median value; the black dots indicate values outside the 10–90 percentiles. Measurements were carried out on 100 individualized nanotubes and analyzed using ImageJ software. (D) Polyacrylamide gel electrophoresis of MWNTs-OVA. MWNTs-OVA were gel electrophoresed using 10% polyacrylamide gel under native gel condition. 10 µg of free OVA or OVA conjugated with MWNTs were loaded in the well. OVA bands were detected by gel staining with brilliant-Coomassie blue. Matching band intensities were observed for both the free OVA and MWNT-conjugated OVA.

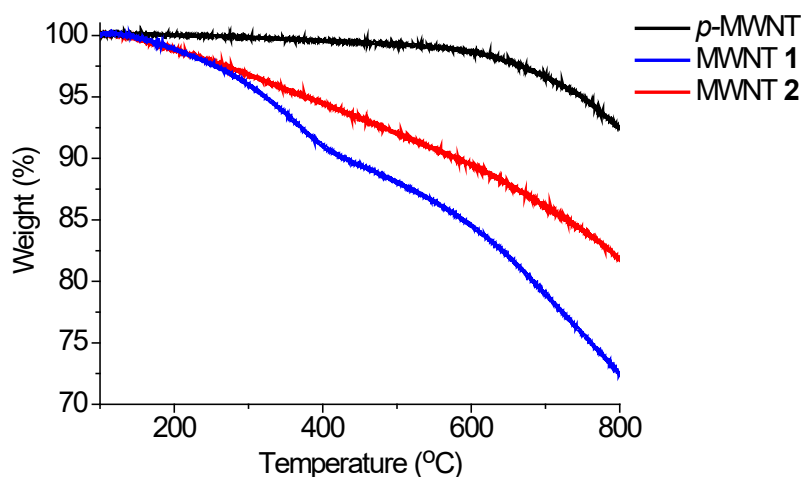


Figure 11: Characterization of f-MWNTs by TGA.

A known weight of MWNT was exposed to gradually increasing temperature and the weight loss was detected as temperature increased. p-MWNTs were thermally stable up to 600°C. The weight loss at 600°C was directly correlated to the amount of introduced functional groups. Representative Thermogravimetric profiles are shown (n=3).

TGA has shown to be one of the useful techniques to characterize MWNT functionalization [193]. It is based on measuring the weight of the sample being analysed upon exposing it to a gradually increasing temperature under inert gas (nitrogen). Normally, p-MWNTs are thermally stable up

to 600 °C above which they dramatically decompose. Functional groups incorporated onto the surface of the f-MWNT are, however, less thermally stable and decompose at lower temperatures. The weight loss measured at 600 °C is directly related to the functional groups loading density. The degree of chemical functionalization was calculated using TGA and are summarized in Table 2. Furthermore, the primary amine content of S-/ + and S- was qualitatively determined using Kaiser Test [194]. The UV-Vis spectra (Fig. 12A) confirmed the reduced primary amine content of S- compared to S-/ + as a consequence of the maleimide-terminated spacer addition.

Table 2: Physicochemical properties of f-MWNTs and MWNTs-OVA conjugate [166]

MWNT	Initial primary amine [final maleimide] ^{abc} (μmole/g MWNT)	OVA loading (mg/g f-MWNT)		MWNT length ^{bd} (nm)	Zeta potential ^{bce} (mV)
		TGA ^{bc}	BCA assay ^{bc}		
L+	263 ± 72	—	—	386 ± 133	17.3 ± 5.0
L+(OVA)	263 ± 72	317 ± 31.1	329 ± 44.0	386 ± 133	5.8 ± 3.2
S--	—	—	—	122 ± 82	-21.2 ± 3.4
S--(OVA)	—	431 ± 40.0	449 ± 32.5	122 ± 82	-39.0 ± 4.0
S-/ +	140 ± 48	—	—	122 ± 82	-10.1 ± 3.0
S-/ +(OVA)	140 ± 48	435 ± 28.6	441 ± 36.0	122 ± 82	-23.4 ± 5.1
S-	140 ± 48 [80 ± 25]	—	—	122 ± 82	-16.4 ± 4.0
S-(OVA)	140 ± 48 [80 ± 25]	438 ± 30.5	445 ± 42.2	122 ± 82	-35.8 ± 3.3

^[a] Analyzed by TGA.

^[b] Data are represented as mean ± SD.

^[c] n = 3.

^[d] Determined from TEM images (n= 100 nanotubes).

^[e] Analyzed by electrophoretic mobility using 10× diluted PBS buffer.

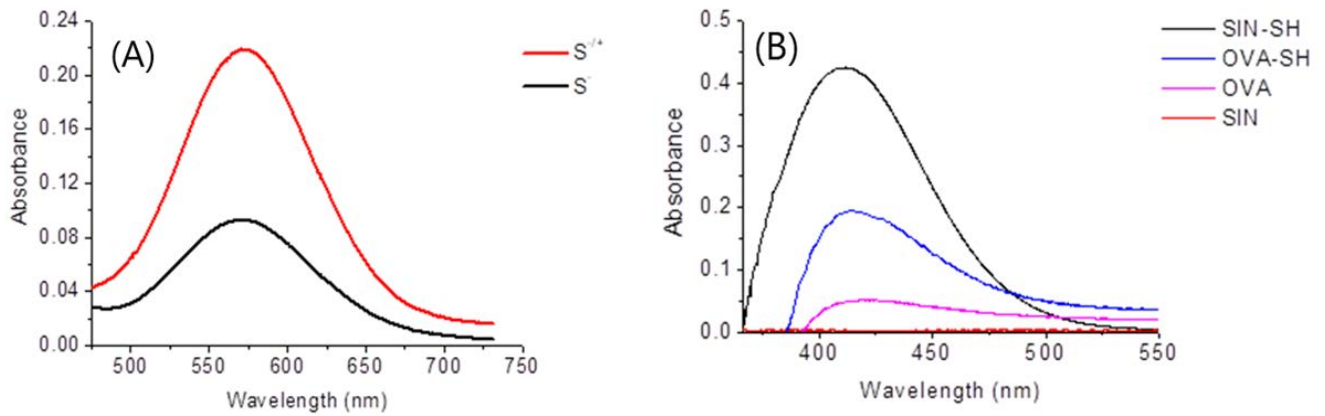


Figure 12: Detection of primary amine or sulfhydryl groups using Kaiser Test or Ellman's assays, respectively. (A) UV-Vis spectra of the chromophoric compound formed between Ninhydrin and primary amines, showing the characteristic absorbance at λ_{max} of 570 nm (S-/+) that was reduced following the maleimide group introduction (S-). (B) UV-Vis spectra of OVA, OVA-SH, SIN or SIN-SH following the reaction with Ellman's reagent showing the increase in absorbance at the λ_{max} after modification with sulfhydryl groups using Traut's reagent or cysteine as expected.

The morphology of an aqueous dispersion of f-MWNTs was studied using TEM (Figs. 10B-C and 13).

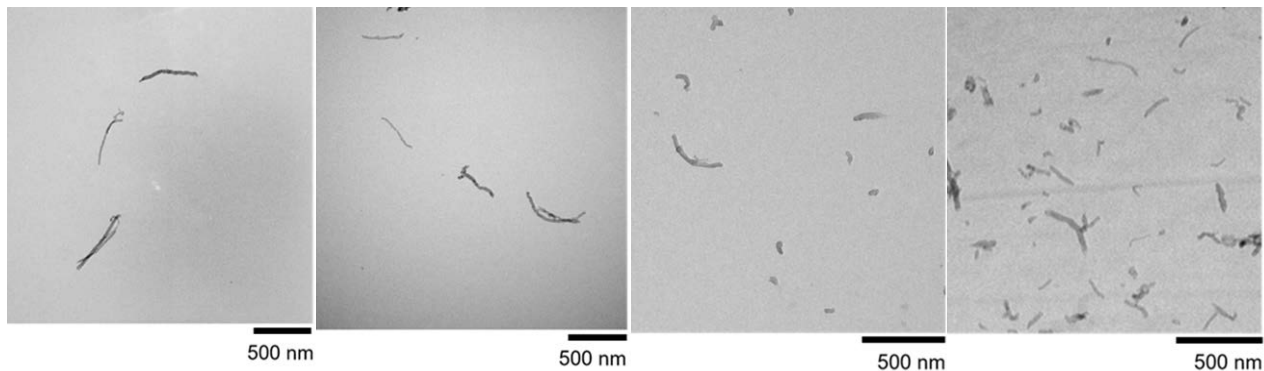


Figure 13: Additional TEM images of L+ (A-B) or S-- (C-D), dispersed at 1 mg/ml in de-ionized water. The mean and median lengths of L+ were found to be 386 ± 133 nm and 380.6 nm, respectively, whereas S-- exhibited mean and median lengths of 122 ± 82 nm and 107.5 nm, respectively (Tables 2 and 3).

Table 3: Descriptive analysis of L+ or S-- length distribution.

f-MWNT	Number of nanotubes measured	Minimum (nm)	25% Percentile (nm)	Median (nm)	75% Percentile (nm)	Maximum (nm)	Lower 95% confidence interval of mean (nm)	Upper 95% confidence interval of mean (nm)
L+	100	136.131	292.6	380.6	465.9	761.3	359.6	412.8
S--	100	28.607	70.1	107.5	146.9	610.0	106.5	139.3

Since S-- was the precursor for the synthesis of S-/+ and S-, the mean length of S-/+ and S- was considered to be 122 ± 82 nm. A maximum of one-minute sonication steps were applied during washing cycles with organic solvents so that further shortening of f-MWNT can be avoided. MWNT-OVA and MWNT-SIN lengths were extrapolated from their f-MWNT precursors. Zeta potential of f-MWNTs was measured and expressed in Table 2. The fact that S-/+ possessed a reduced overall negative charge compared to S-- indicated the presence of residual un-reacted carboxylic acid moieties

in S-/+. Zeta potential values measured agreed with chemical structures.

6.2. Synthesis and Characterization of MWNTs-OVA and MWNTs-SIN Conjugates

Initially the aim was to conjugate OVA or SIN to f-MWNTs, using non-covalent or covalent approaches. Thiol-modification of OVA was achieved using Traut's reagent [195, 196]. SIN and SIN-SH synthesized using solid phase peptide synthesis were characterized using mass spectrometry (Fig. 14).

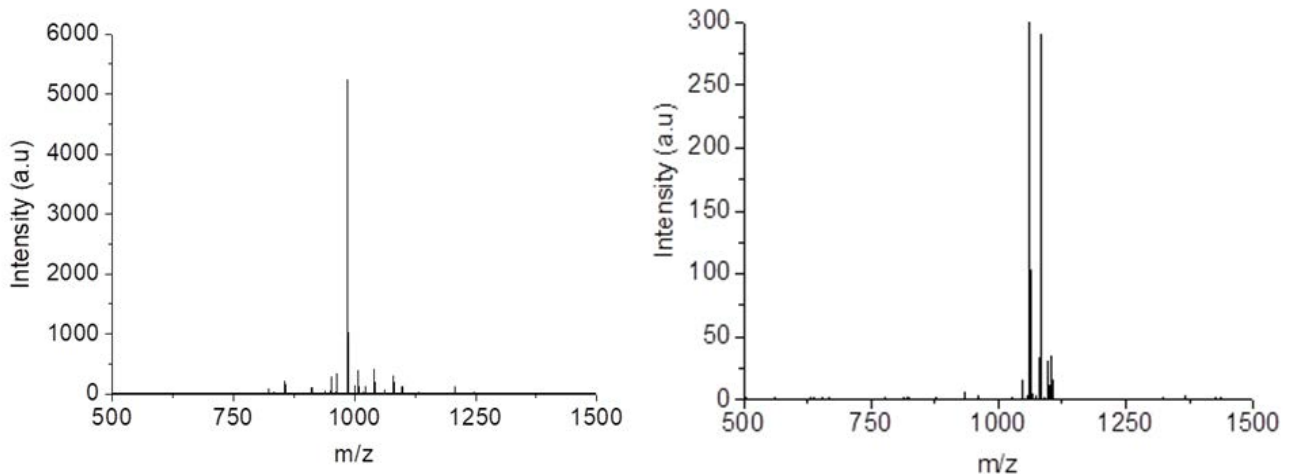


Figure 14: MALDI Mass Spectra of SIN (MW= 963 g/mol) and SIN-SH (MW= 1066.29 g/mol).

The concentration of the sulfhydryl groups determined using Ellman's assay [197] was 0.5 μmol or 0.8 μmol per mg of OVA-SH or SIN-SH, respectively (Fig. 12B). As depicted in Scheme 1, L+(OVA), S--(OVA) or S-/+(OVA) were prepared by non-covalent conjugation of non-modified OVA, while thiol-modified OVA (OVA-SH) was used in preparation of S-(OVA) [154, 194]. The same approaches were applied for the conjugation of SIN with f-MWNTs yielding L+(SIN), S--(SIN), S-/+(SIN) or S-(SIN). Following their reaction with OVA or SIN, the solids of MWNTs recovered by filtration were analyzed using TGA while the unreacted OVA or SIN contained in the filtrates was quantified using BCA assay. From the thermogravimetric profiles of MWNTs-OVA (Fig. 10A) and the BCA assay, the OVA contents in MWNTs-OVA were calculated and are summarized in Table 2. SIN loading values determined from the thermogravimetric profiles of MWNTs-SIN (Fig. 15) or BCA assay are summarized in Table 4.

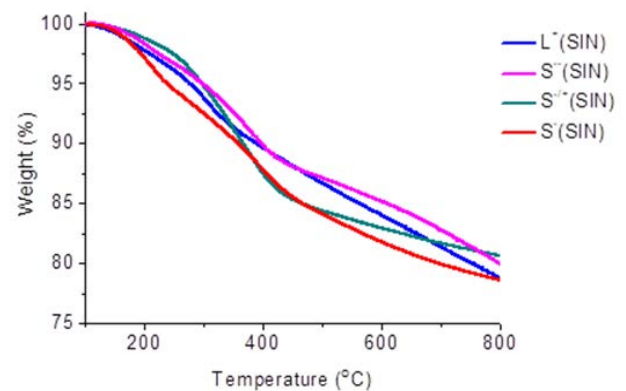


Figure 15: Thermogravimetric profiles of MWNTs-SIN conjugates. Representative thermogravimetric profile of 3 runs is shown.

Table 4: Physicochemical properties of f-MWNTs and MWNTs-SIN conjugates.

MWNT	Initial primary amine [final maleimide] ^[a] ^[b] ^[c] ($\mu\text{mole/g}$ MWNT)	SIN loading (mg/ g f-MWNT)		MWNT length ^[b] ^[d] (nm)	Zeta potential ^[b] ^[c] ^[e] (mV)
		TGA ^[b] ^[c]	BCA assay ^[b] ^[c]		
L+	263 \pm 72	-	-	386 \pm 133	17.3 \pm 5.0
L+(SIN)	263 \pm 72	57 \pm 10.8	52 \pm 15.1	386 \pm 133	12.3 \pm 3.6
S--	-	-	-	122 \pm 82	-21.2 \pm 3.4
S--(SIN)	-	97 \pm 27.6	86 \pm 32.0	122 \pm 82	-25.5 \pm 5.1
S-/+	140 \pm 48	-	-	122 \pm 82	-10.1 \pm 3.0
S-/+(SIN)	140 \pm 48	88 \pm 16.6	83 \pm 27.8	122 \pm 82	-13.1 \pm 4.3
S-	140 \pm 48 [80 \pm 25]	-	-	122 \pm 82	-16.4 \pm 4.0
S-(SIN)	140 \pm 48 [80 \pm 25]	90 \pm 21.8	93 \pm 25.4	122 \pm 82	-21.2 \pm 3.9

[a] Analyzed by TGA.

[b] Data are represented as mean \pm SD.

[c] n= 3.

[d] Determined from TEM images (n= 100 nanotubes).

[e] Analyzed by electrophoretic light scattering using 10x diluted PBS buffer.

TGA showed a mean OVA or SIN loading of 404 or 81 μg per mg f-MWNT, respectively. The mean OVA or SIN loading determined using BCA assay was 412 or 78 μg per mg f-MWNT, respectively, in agreement with the loading values determined by TGA. reported a similar observation on determining the protein loading on CNTs using TGA or by measuring the absorbance of unreacted protein using UV-vis spectroscopy [194]. The surface charges of MWNTs-OVA or MWNTs-SIN are summarized in Tables 2 or 4, respectively.

To further assess OVA and SIN interaction with f-MWNTs, MWNTs-OVA and MWNTs-SIN was subjected to native gel electrophoresis (PAGE). OVA contained in MWNTs-OVA exhibited the same migration pattern and band intensity as free OVA (Fig. 10D), suggesting that OVA conjugation with the f-MWNTs, even with S-, was achieved using non-covalent conjugation. A similar trend was observed for MWNTs-SIN (Fig. 16).

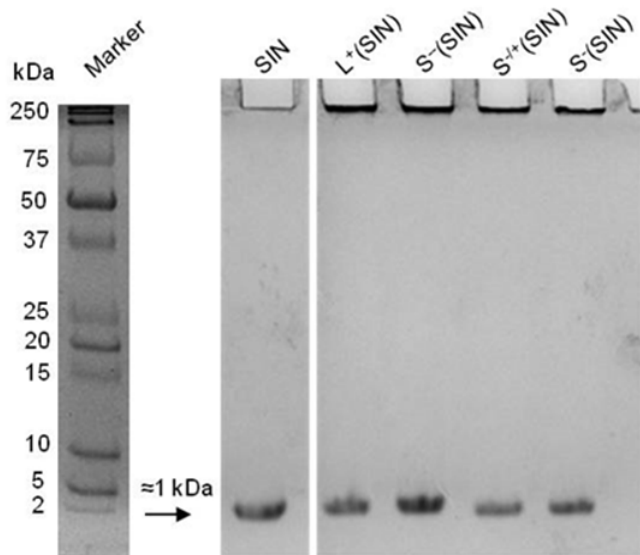


Figure 16: Polyacrylamide gel electrophoresis of MWNTs-SIN conjugates. MWNTs-SIN conjugates were gel electrophoresed using 15% polyacrylamide gel under native gel condition. 10 μg of free SIN or SIN conjugated with MWNTs were loaded in the well. SIN bands were detected by staining the gel with brilliant-coomassie blue. Matching band intensities were observed for both free SIN and MWNT-conjugated SIN.

6.3. Cellular Uptake of F-MWNTs by BM-DC Does not Affect their Viability or Phenotype *In Vitro*

In order to study the effect of f-MWNTs on DCs, CD11c+ ve BM-DCs were generated from the bone marrow of C57BL/6 mice (Fig. 17) [198,199].

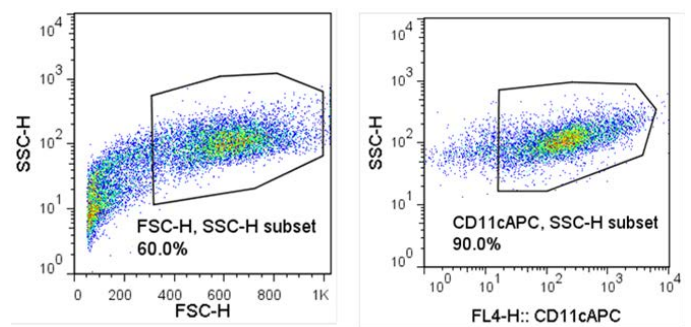


Figure 17: Characterization of BM-DCs by immunostaining. The viable BM-DCs were gated (Left) to determine their CD11c marker expression (Right) using flow cytometry.

First, whether these cells were able to uptake f-MWNTs and the effect on BM-DC viability was assessed prior to undertaking further studies. Light microscopy images of f-MWNT treated BM-DC revealed the association of the BM-DCs with dark aggregates of f-MWNT; however, it was difficult to distinguish between cellular uptake of f-MWNTs and aggregation of f-MWNTs on the cell surface (Fig. 18A). To further assess the cellular uptake of the f-MWNTs, BM-DCs were treated with 10 $\mu\text{g}/\text{ml}$ of f-MWNTs for 24 h before Image Stream analysis.

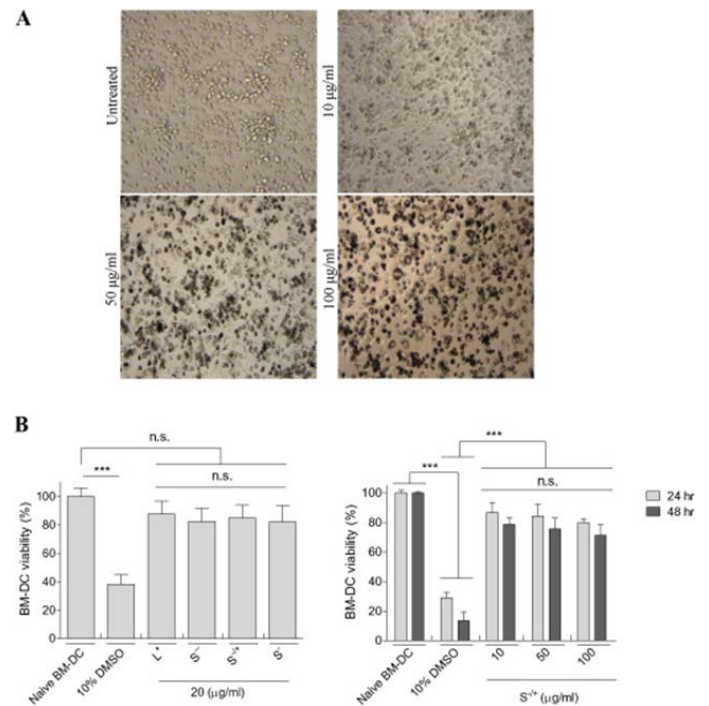


Figure 18: Viability of BM-DCs following treatment with f-MWNTs. (A) Light microscopy images of BM-DCs after 24 h incubation with S-/+, at 10–100 $\mu\text{g}/\text{ml}$. Images were captured at 20 \times magnification. (B) Assessment of f-MWNT cytotoxicity using the modified LDH assay. 10% DMSO was used as a positive control. LDH content in the viable BM-DCs was determined in triplicates for each treatment. Results are expressed as mean \pm SD ($n = 3$).

To overcome the need for fluorescent probes, ImageStream analysis have been previously used to quantify cellular uptake of CNTs for an individual cell, utilizing the CNT ability to absorb and scatter light [200–202].

As illustrated in Fig. 19A, the scatter plot of naïve BM-DCs appeared as main single population. Following the internalization of f-MWNTs, and the associated light scattering, two populations of BM-DCs, namely f-MWNT positive (f-MWNT+ve) or negative (f-MWNT-ve) BM-DC population were observed (Figs. 19B and 20). In contrast to the f-MWNT-ve BM-DC population, the f-MWNT+ve BM-DC population had light-absorptive black spots of internalized f-MWNTs (Fig. 19B). Employing the direct correlation between the reduction in the bright-field intensity and the increase in cellular

uptake of CNTs [200,201], the mean bright-field intensity of BM-DCs treated with the various f-MWNTs was measured to quantify f-MWNT internalization (Fig. 19C). ImageStream analysis showed that S-/+ was significantly acquired by BM-DCs in comparison to L+ or S--, while the difference in uptake between S-/+ and S- was not significant. Interestingly, positively charged long f-MWNT (L+) showed the least uptake. The same trend was obtained for f-MWNT conjugated to OVA with the highest uptake efficiency being attributed to S-/(OVA) (Fig. 19D).

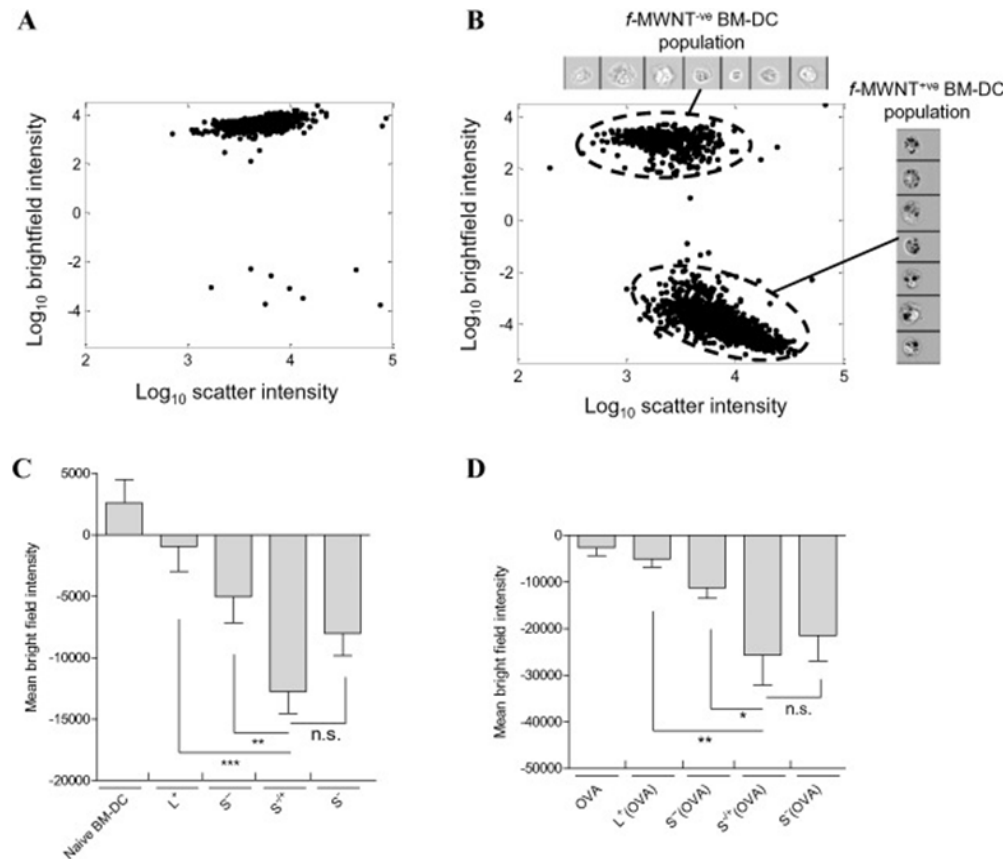


Figure 19: Intracellular uptake of f-MWNTs or MWNTs-OVA in vitro. BM-DCs were incubated with f-MWNTs or MWNTs-OVA each at MWNT concentration of 10 $\mu\text{g/ml}$ for 24 h then analyzed with image stream analysis. (A) Scatter plot of naïve BM-DCs. (B) Scatter plot of BM-DCs incubated with S-/, as a representative plot for f-MWNT treated BM-DC, showing the S-/+ positive and S-/+ negative BM-DC populations, identified from mean image intensity in the bright field and scatter channels (cell images are shown in an inset). (C) Relative f-MWNTs uptake indirectly determined by measuring the bright field intensity of BM-DCs following treatment with f-MWNT. Naïve BM-DCs were used as a control. (D) Relative MWNTs-OVA uptake indirectly determined by measuring the bright field intensity of BM-DCs following treatment with MWNTs-OVA. Soluble OVA treated BM-DCs were used as a control. Results are expressed as mean \pm SD (n = 3).

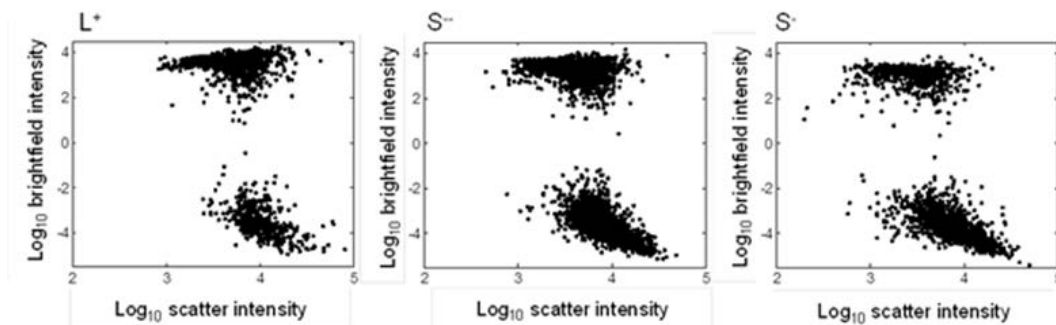


Figure 20: Intracellular uptake of f-MWNTs in vitro. Scatter plot of BM-DCs incubated with L+, S- or S- determined using Image Stream analysis. Acquisition of these molecules was not associated with significant loss of BM-DC viability, as determined by the modified LDH assay, even following incubation of these cells with 10–100 $\mu\text{g/ml}$ S-/+ for up to 48 h (Fig. 18B) [203].

Materials used in formulating particulate delivery system might have an impact on the induced immune response. For instance, it has previously been reported that DC treatment with poly (lactic-co-glycolic acid) (PLGA) film or PLGA microparticles increased the expression of CD40, CD80 and CD86 [204]. To evaluate whether treatment with f-MWNTs or MWNTs-OVA for 24 h affected these co-stimulatory molecules as well as major histocompatibility complex (MHC) levels, BM-DCs were assessed by flow cytometers following incubation with antibodies specific to MHC class I, MHC class II, CD40, CD80 or CD86 (Fig. 21). No significant difference in

expression of any of these molecules was detected following f-MWNTs-treatment compared to untreated cells. Furthermore, no significant differences were observed following incubation with MWNTs-OVA or OVA.

In conclusion, S-/+ and S-/(OVA) treatment of BM-DCs resulted in a higher uptake efficiency compared to f-MWNTs and MWNTs-(OVA), respectively. Exposure to these compounds did not affect BM-DC viability or maturation of these cells.

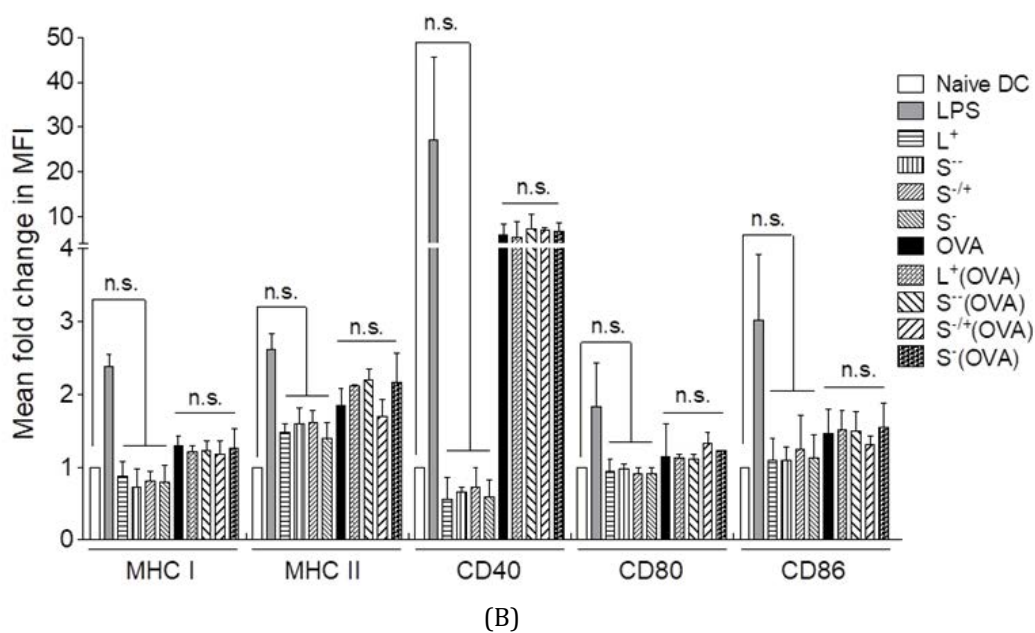
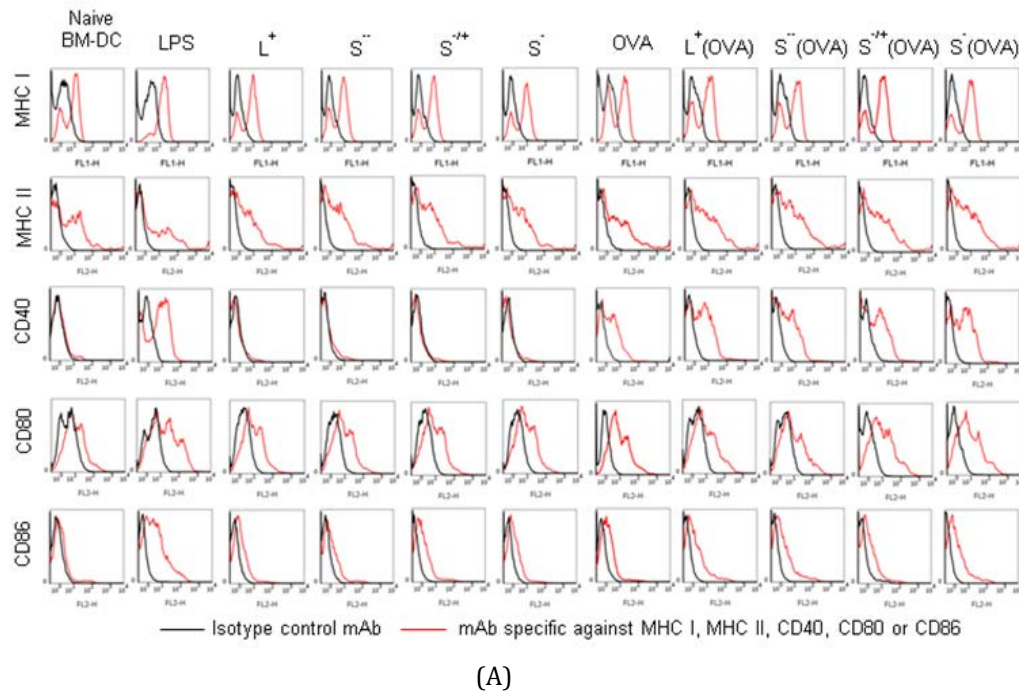


Figure 21: Effect of f-MWNTs or MWNTs-OVA on BM-DCs phenotypes. BM-DCs were left untreated or incubated with f-MWNTs, OVA or MWNTs-OVA for 24 hr. LPS were used as a positive control. (A) Representative histograms for BM-DCs stained with fluorescently labelled antibodies specific to MHC I, MHC II, CD40, CD80, CD86 or their respective isotype controls. The mean fluorescence intensity (MFI) of the positive cells was determined for 10 x 10⁴ cells with flow cytometry and results were analysed using FLOWJO 7.6.5 software. (B) The mean fold change in the MFI of each marker compared to naive BM-DC. The mean values of results obtained from two separate experiments ± SD are shown.

6.4. Assessment of f-MWNTs or MWNTs-OVA Cellular Uptake in Vitro

A 1mg/ml dispersion of f-MWNTs or f-MWNTs conjugated to OVA in PBS was prepared. Details on generation of DCs from bone marrow of C57BL/6 are described in SI. Bone marrow derived DCs (BM-DCs) were treated with f-MWNTs or MWNTs-OVA each at 10 µg/ml. As a control, BM-DCs were treated with PBS or OVA alone. After 24 h, BM-DCs were harvested, washed with RPMI 1640 medium (Life Technologies, UK) then fixed by the incubation with 4% paraformaldehyde and analyzed using Image Stream 100 cell analyzer (Amins Corporation, USA).

6.5. Assessment of the Immune Response Induced by MWNTs-OVA in Vitro using 3H-Thymidine Incorporation assay

A 0.5 mg/ml dispersion of OVA alone, OVA conjugated to f-MWNTs in PBS was prepared. f-MWNTs alone were dispersed in PBS at 1 mg/ml. BM-DCs were treated with each of the conjugates at 5 µg/ml OVA. As a control, BM-DCs were treated with PBS or uncoupled f-MWNTs. After 24 h, treated BM-DCs were harvested, washed and gamma-irradiated (3000 Gys). CD8+ or CD4+ T cells were isolated from spleens of OT-I or OT-II mice, respectively, as described in SI. In a 96-well round-bottom plate, CD8+ or CD4+ T cells were co-cultured with the irradiated BMDCs at 1:4 in complete medium. The 1:4 ratios were decided from optimization studies (SI). CD8+ or CD4+ T cells cultured without BM-DCs or with naive BM-DCs were used as controls. Cells were maintained for 3 days/37 °C and the proliferation was measured by adding 1 µCi of 3H-thymidine (Perkin Elmer, USA) per well for the last 18 h of culture. Proliferation of CD8+ or CD4+ T cells was determined by measuring the radiation emitted from the incorporated 3H-thymidine using liquid scintillation counter (Wallac 1205 Betaplate) and read as counts per minute (c.p.m.).

6.6. Quantification of IFN-γ Production using ELISA

IFN-γ present in the culture supernatants collected from BM-DC: T cell co-cultures was determined using anti-mouse IFN-γ sandwich ELISA kit following the manufacturer's protocol (eBioscience). The ELISA plates were measured at 450 nm using FLUOstar Omega, BMG LABTECH (Germany).

6.7. MWNTs-OVA and MWNTs-SIN augment T cell specific response in vitro with varying intensities

To further assess the efficiency of f-MWNTs, to deliver OVA or the MHC I-restricted OVA peptide epitope (SIN) to BM-DCs,

we measured their ability to activate antigen specific T cell proliferation and cytokine production. CD8+ or CD4+ T cells were isolated from the spleens of mice expressing a T cell receptor capable of recognizing OVA peptide SIN (OVA257–264) or OVA323–339 presented by H-2Db (MHC I) or I-Ab (MHC II), respectively (Fig. 22).

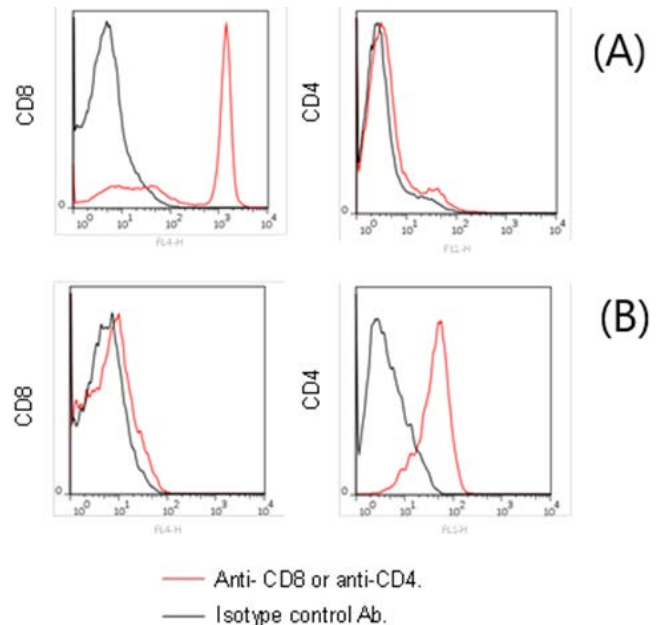


Figure 22: Characterization of CD8+ T cells and CD4+ T cells by immunostaining. (A) Purity of CD8+ T cell isolated from spleen of OT1 Rag^{-/-} using flow cytometric analysis assessed by CD8 (CD8+ T cell marker) expression and absence of CD4 (CD4+ T cell marker). (B) Purity of CD4+ T cell isolated from spleen of OT2 Rag^{-/-} using flow cytometric analysis assessed by CD4 (CD4+ T cell marker) expression and absence of CD8 (CD8+ T cell marker).

Initially, it has been titrated the ratio of SIN pulsed BM-DCs to CD8+ T cells and found a DC: T cell ratio of 1:4 allowed maximal activation of OVA-specific CD8+ T cells (Fig. 23A) [166]. In addition, it has been titrated the concentration of soluble OVA to determine maximum and minimal OVA concentration required to induce T cell stimulation (Fig. 23B). A suboptimal concentration (5 µg/ml) of soluble OVA or OVA contained in MWNTs-OVA was used to determine the differences in T cell activation induced by MWNTs-OVA. BM-DC were cultured with OVA in free form or conjugated with f-MWNT and T cell proliferation was assessed by 3H-thymidine incorporation.

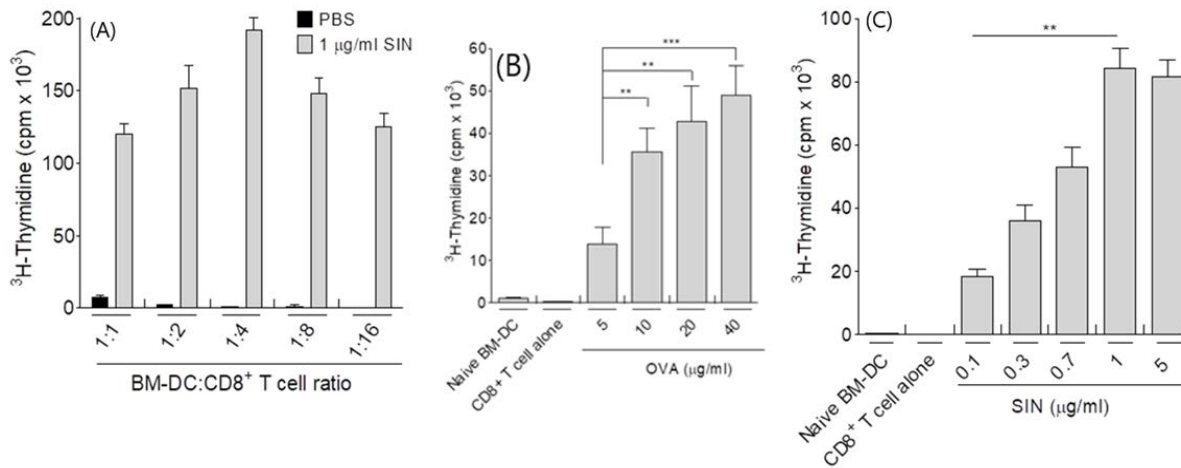


Figure 23: Optimization of CD8+ T cell: DC ratio, OVA-dose and SIN-dose response in vitro. (A) 3H-Thymidine incorporation assay of CD8+ T cell co-cultured with BM-DCs, for determination of optimal CD8+ T cell: DC number ratio to be used in subsequent studies. BM-DCs stimulated with 1 µg/ml SIN were co-cultured with CD8+ T cells at different cell number ratios. CD8+ T cells proliferation was determined with 3H-thymidine incorporation in CD8+ T cells. (B) Determination of the in vitro CD8+ T cell proliferation induced by OVA in a dose-dependent manner. BM-DCs were treated with OVA at concentration ranging from 5 to 40 µg/ml, and then co-cultured with CD8+ T cells at 1:4 ratios. CD8+ T proliferation was measured using 3H-thymidine proliferation assay. Results are expressed as mean ± SD (n=3). (C) Determination of the CD8+ T cells proliferation induced by SIN in a dose-dependent manner. BM-DCs were treated with SIN at concentration ranging from 0.1 to 5 µg/ml, then co-cultured with CD8+ T cells at 1:4 ratio. CD8+ T proliferation was measured using 3H-thymidine proliferation assay. Results are expressed as mean ± SD (n=3).

As illustrated in Fig. 24A, MWNTs-OVA treated BM-DCs significantly increased the proliferation of CD8+ antigen specific T cells compared to soluble OVA treated BM-DCs. However, significantly higher CD8+ T cell proliferation was induced by S-/(OVA) treated compared to L+(OVA), S--(OVA) or S-(OVA) treated BM-DCs. A similar pattern of proliferation was observed with antigen-specific CD4+ T cells. The results

[166] showed that treatment of BM-DCs with MWNTs-OVA derivatives lead to more efficient antigen presentation compared to antigen in a soluble form and that L+(OVA) and S-/(OVA) pulsing induced the least and the highest T cell proliferation rates, respectively. Additionally, IFN-γ production was assessed by ELISA. IFN-γ production correlated with T cell proliferation assay (Fig. 24A).

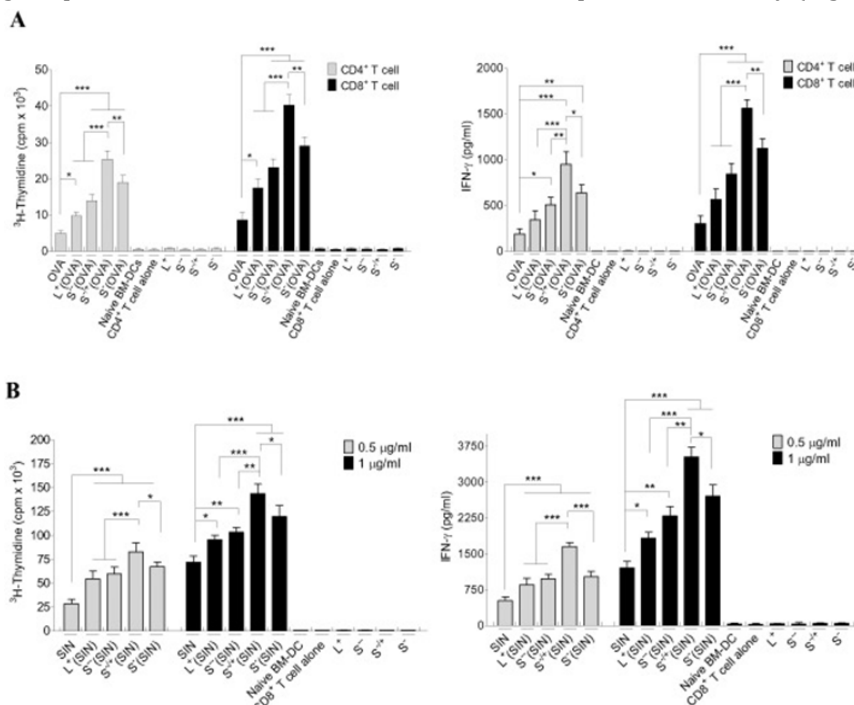


Figure 24: Assessment of the immune response induced in vitro. (A, B; left) Determination of T cells proliferation using 3H-Thymidine incorporation assay. BM-DCs were incubated with OVA, SIN, MWNTs-OVA, or MWNTs-SIN, each at 5 µg/ml OVA, 0.5 or 1 µg/ml SIN for 24 h. Incubated BM-DCs were harvested, irradiated then co-cultured with CD4+ or CD8+ T cells at 1:4 ratio for 3 days. CD8+ and CD4+ T cells proliferation was assessed with 3H-thymidine incorporation assay. (A, B; right) Measurement of IFN-γ production in the supernatants of CD4+ or CD8+ T cells co-cultured for 3 days with OVA, SIN, MWNTs-OVA, or MWNTs-SIN stimulated BM-DCs, by ELISA. Results are expressed as the mean value ± SD (n = 3).

"A dose-dependent CD8+ T cell proliferation was obtained on treating the BM-DCs with soluble SIN up to 1 µg/ml (Fig. 23C). As illustrated in Fig. 24B, MWNTs-SIN treated BM-DCs induced significantly stronger CD8+ T cell proliferation compared to SIN treated BM-DCs, at concentrations of 0.5 or 1

µg/ml. Furthermore, S-/+ (SIN) induced a significantly higher CD8+ T cell response compared to L+(SIN), S--(SIN) or S-(SIN). The overall pattern of T cell stimulation and IFN-γ production elicited by MWNTs-SIN was similar to MWNTs-OVA (Figs. 24B and 25).

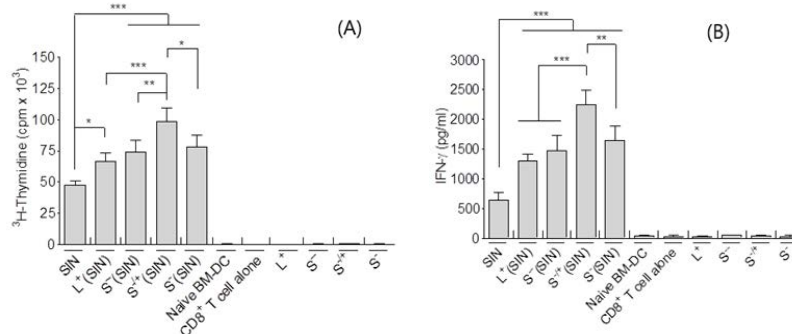


Figure 25: Assessment of the immune response induced by MWNTs-SIN in vitro. BM-DCs were incubated with SIN or MWNTs-SIN, each at 1 µg/ml SIN for 24 hr. Treated BM-DCs were harvested, irradiated then co-cultured with CD8+ T cells at 1:8 ratio for 3 days. (A) Assessment of CD8+ T cell proliferation with 3H-thymidine incorporation assay. (B) Measurement of IFN-γ production in the supernatants of CD8+ T cells co-cultured with stimulated BM-DCs, by ELISA.

Although it was demonstrated that the f-MWNTs were not capable of affecting the BM-DC phenotypes, further studies were performed to assess the innate immune activation of BM-DCs by f-MWNTs. To do this, S-/+ was added separately to SIN-pulsed BM-DCs then co-cultured with CD8+ T cells. A comparable CD8+ T cell proliferation was induced by SIN-pulsed BM-DCs in presence or absence of S-/+ (Fig. 26) [166] suggests that f-MWNTs lack adjuvanticity and require the antigen to be coupled to them.

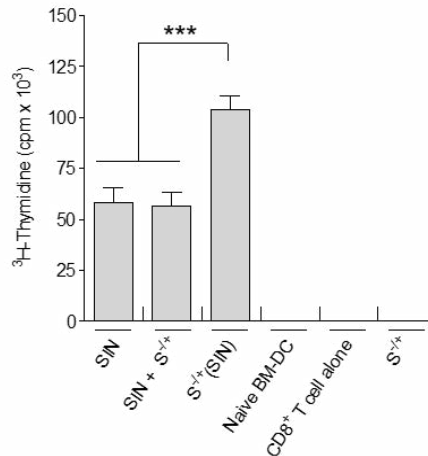


Figure 26: Assessment of CD8+ T cell proliferation induced by SIN in presence or absence of S-/. BM-DCs were treated with free SIN, SIN and S-/+ or S-/(SIN), each at 1 µg/ml SIN, then co-cultured with CD8+ T cells at 1:4 ratio. CD8+ T cell proliferation was assessed with 3H-thymidine incorporation. Experiments were carried out in triplicates. Results are expressed as mean ± SD (n=3).

Taken together, from these observations we conclude that MWNTs-OVA derivatives were able to induce better CD8+ and CD4+ T cell responses than soluble OVA, with L+(OVA) and S-/(OVA) inducing the least and highest T cell proliferation, respectively, which correlated with the cellular uptake

profile. Furthermore, and importantly, conjugation of antigen to f-MWNT did not appear to interfere with the process of antigen processing.

6.8. Assessment of f-MWNTs Uptake in Vivo

C57BL/6 mice (n=3) were injected via the footpad with 100 µg of f-MWNTs. Mice were sacrificed 24 h post injection and the draining popliteal lymph nodes were dissected. The lymph node cells were isolated by incubating the harvested lymph nodes with 50 µl RPMI 1640 medium containing 5 µl of 40 mg/ml collagenase and 2 µl of 0.8 mg/ml DNase (Roche Diagnostics, USA) for 30 min at 37 °C, followed by straining the cells through a 70 µm cell strainer (Becton Dickinson, USA) and washing in PBS (1×). Isolated lymph node cells were resuspended in 150 µl PBS and incubated for 30 min at 4 °C with 0.86 µg/ml PE-conjugated mAb against CD11c (PE-CD11c) (Becton Dickinson, USA). Lymph node cells were then washed in PBS and analyzed for side scatter and bright-field intensity using Image Stream 100 cell analyzer (Amnis Corporation, USA).

6.9. Assessment of MWNTs (DQ-OVA) Uptake and Antigen Processing by DCs in Vivo

MWNTs (DQ-OVA) were synthesized as described in SI. C57BL/6 mice (n = 3) were injected via the footpad with MWNTs (DQ-OVA) each containing 10 µg of DQ-OVA [205]. Mice were sacrificed 24 h post-injection, the draining popliteal lymph nodes were dissected, and cells were isolated and stained with PE-CD11c as described before. Lymph node cells were then analyzed on a FACSCalibur, using Cell Quest software (BD Bioscience, CA). Subsequent analysis was done using FlowJo software (Tree Star, Ashland, OR).

6.10. Assessment of the immune response induced by the MWNTs-OVA in mice using in vivo specific cytotoxic T lymphocyte killing assay

An in vivo cytotoxic T lymphocyte (CTL) killing assay was performed using a previously reported method [206]. Briefly, C57BL/6 mice (n=3) were injected via the footpad with PBS, OVA or MWNTs-OVA, each at 50 µg OVA, on days 0, 7 and 14 [181]. On day 21, a 1:1 mixture of 0.5 µM carboxy-

fluorescein diacetate succinimidyl ester (CFSE, eBioscience, UK)-labeled SIN-pulsed splenocytes and 5 μ M CFSE-labeled un-pulsed splenocytes (prepared as described in SI) were administered iv into treated or untreated mice. At 18 h post-injection, mice were scarified; spleens were harvested and splenocytes analyzed using flowcytometric analysis to determine the percentage of SIN-pulsed (0.5 μ M CFSE/SIN) and un-pulsed (5 μ M CFSE/no SIN) cells present. Antigen specific killing was calculated using the following equation:

$$\left[1 - \frac{\text{Percentage of } 0.5 \mu\text{M CFSE}^{\text{SIN/FEKL}}}{\text{Percentage of } 5 \mu\text{M CFSE}^{\text{no SIN/FEKL}}} \right] \times 100$$

6.11. Cellular uptake of MWNTs-OVA is correlated with the potency of CTL responses induced in vivo

To study the cellular uptake of f-MWNTs in vivo, C57BL/6 mice were injected with f-MWNTs and the popliteal lymph nodes were dissected 24 h later [166]. Image Stream analysis revealed that the lymph node cells and the CD11c+ ve

lymph node cells internalized S-/+ in a significantly higher manner compared to L+ or S- [Fig. 27A–B], judging from the bright-field intensity signals. Furthermore, in vivo internalization and processing of f-MWNT conjugated OVA by the antigen presenting cells was studied by substituting OVA with DQ-OVA in the conjugates. DQ-OVA are dye-labeled OVA that emit green fluorescence following exposure to proteolytic enzymes [207]. Administration of S-/+ (DQ-OVA) was associated with highest green fluorescence intensity in the CD11c+ lymph node cells [Fig. 27C], determined with flow cytometry analysis. Thus, indicating that more DQ-OVA was delivered to CD11c+ lymph node cells when conjugated to S-/+ than other the other f-MWNTs. No significant differences were detected among the phenotypes of the CD11c+ve lymph node cells derived from MWNTs (OVA) injected mice [Figs. 27D and 28], which was consistent with the in vitro phenotypic characterization of BM-DCs. Histological analysis of the main organs excised from injected mice showed no accumulation of MWNTs in lungs, liver, spleen or kidneys.

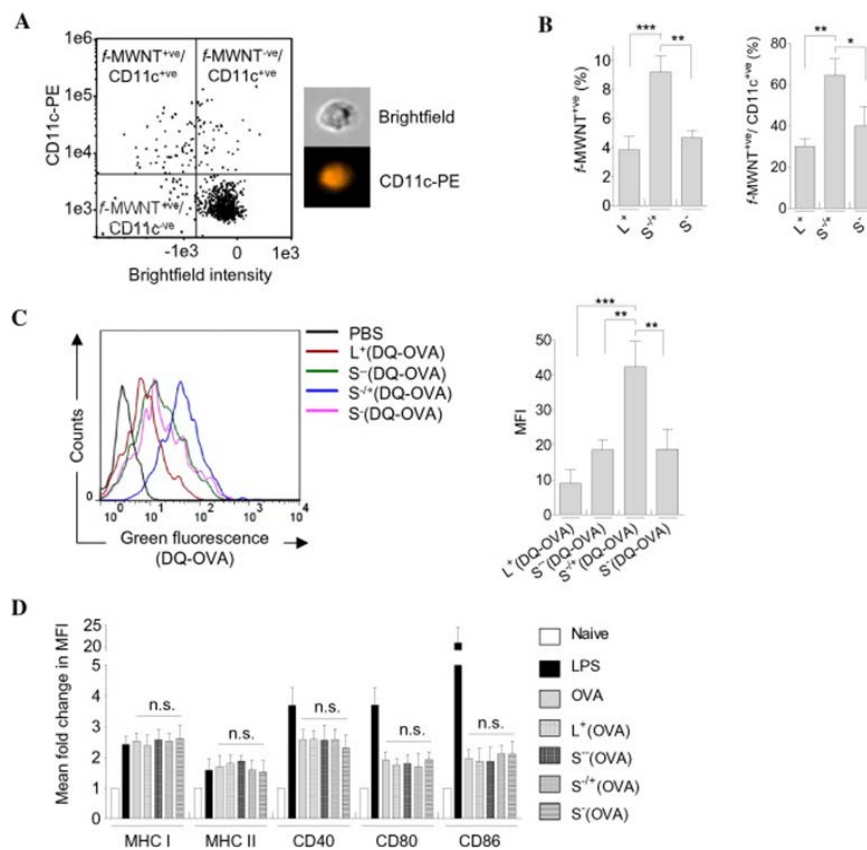


Figure 27: In vivo uptake and phenotypic characterization. (A) Uptake of f-MWNTs in draining popliteal lymph nodes. C57BL/6 mice ($n = 3$) were injected via the footpad with 100 μ g of f-MWNTs, and the draining popliteal lymph nodes were dissected 24 h later. The isolated lymph node cells were stained for DCs using PE anti-CD11c (PE-CD11c) and analyzed using Image Stream analysis. Scatter plot of lymph node cells isolated from S-/+ injected mouse is shown, as a representative plot, illustrating the gating strategy applied to determine the f-MWNT+ ve and CD11c+ ve cells based on the reduction in bright-field intensity and the increase in PE-CD11c fluorescence intensity, respectively (cell images are shown in an inset). (B) Quantification of f-MWNTs uptake in popliteal lymph nodes. (Left) Percentage of f-MWNT+ ve cells in the whole cell population. (Right) Percentage of f-MWNT+ ve cells in the CD11c+ ve cells. (C) Uptake and processing of f-MWNT conjugated OVA in draining popliteal lymph nodes. C57BL/6 mice ($n = 3$) were injected with MWNTs (DQ-OVA), each contained 10 μ g DQ-OVA. The isolated lymph node cells were stained with PE-CD11c and analyzed using flow cytometry. (Left) Representative histograms showing the processed DQ-OVA fluorescence, determined using the FL-1 detector. (Right). The MFI of processed DQ-OVA. (D) Effect of MWNTs-OVA on CD11c+ ve lymph node cells phenotypes. C57BL/6 mice ($n = 2$) were injected with OVA or MWNTs-OVA, each at 50 μ g OVA. The isolated lymph node cells were stained with fluorescently-labeled antibodies and analyzed using flow cytometry. The MFI of the positive cells was determined to measure the fold change in the MFI of each marker compared to the naive cells. Results are expressed as mean \pm S.D. Statistical analyses were performed using one-way ANOVA with Bonferroni post-test.

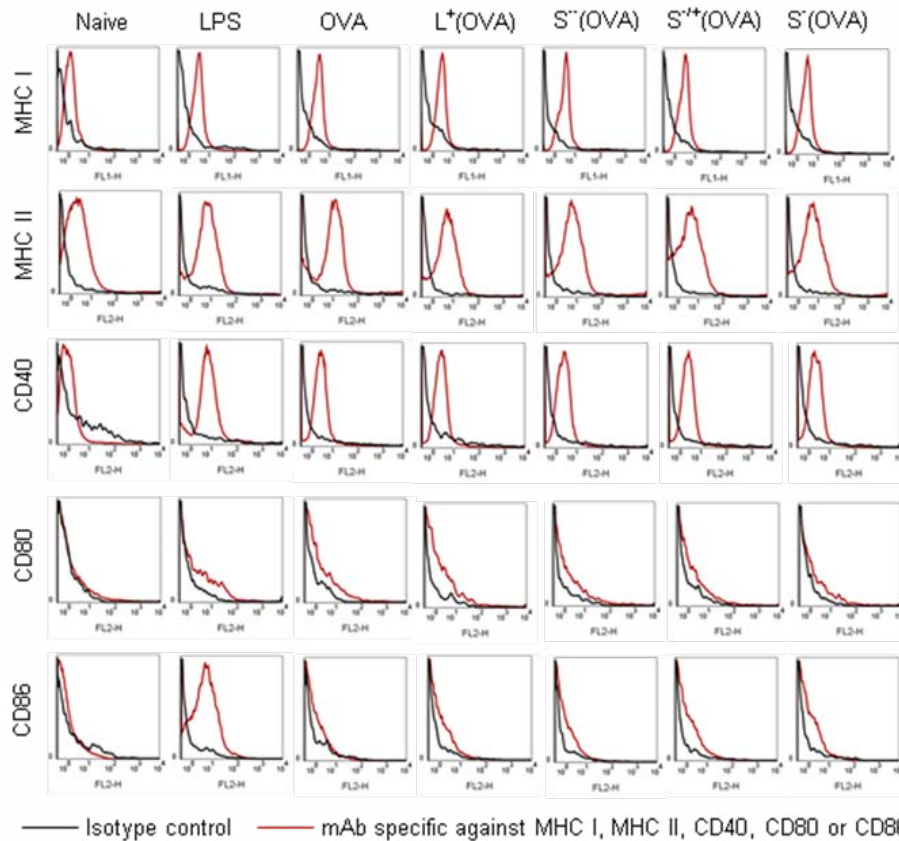


Figure 28: Effect of MWNTs-OVA on CD11c+ve lymph node cells. C57BL/6 mice (n=2) were injected via the footpad with OVA or MWNTs-OVA, each contained 50 μ g OVA, and the draining popliteal lymph nodes were dissected 24 hrs later. Uninjected or LPS injected mice were used as negative or positive controls, respectively. The lymph node cells were stained with APC anti-CD11c and other fluorescently-labelled antibodies against MHC I, MHC II, CD40, CD80, CD86, or their respective isotype controls and analysed using flow cytometry. Representative histograms are shown.

Given the above findings, the *in vivo* efficacy of the MWNTs-OVA conjugates to induce T cell activation *in vivo* was assessed using an *in vivo* CTL assay [181, 206]. C57BL/6 mice were treated with soluble OVA or MWNTs-OVA on days 0, 7 and 14. On day 21 post immunization, mice were injected with a 1:1 splenocyte mixture consisting of 0.5 μ M CFSE labeled SIN-pulsed splenocytes (target cells) and 5 μ M CFSE labeled un-pulsed splenocytes (control cells). The ratio of the target: control splenocytes was assessed after 24 h using flow cytometry to determine the percentage of antigen specific killing (Fig. 29). Treatment with S-/(OVA) induced the highest percentage of antigen specific killing (18.7% \pm 3.1) ($P < 0.0001$) compared to uncoupled OVA. No significant dif-

ferences were found between S--(OVA) (10.4% \pm 2.86) and S-(OVA) (10.6% \pm 1.1). Both conjugates, however, showed better efficacy than soluble OVA (3.3% \pm 0.6) ($P < 0.01$) or L+(OVA) (5.2% \pm 0.58) ($P < 0.05$). Interestingly, administration of soluble OVA and S-/+ did not improve CTL induction compared to treatment with S-/(OVA). It is important to note that overall levels of CTL induction were rather low not exceeding 18.7% of antigen-specific killing. However, this is not surprising taking into account the lack of adjuvanticity of MWNT. In conclusion, consistent with the *in vitro* findings, S-/(OVA) demonstrated the same capabilities on ensuing significantly higher antigen specific immune response than the other MWNTs-OVA *in vivo*.

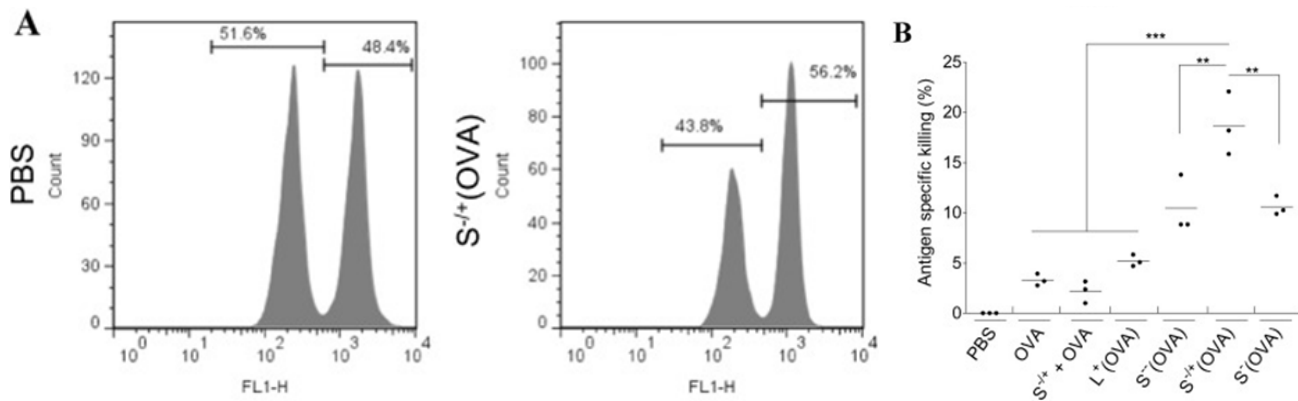


Figure 29: In vivo CTL assay. C57BL/6 mice ($n = 3$) were injected via the footpad with OVA or MWNTs-OVA, each at 50 μg OVA on day 0, 7 and 14. Mice injected with PBS were used as a negative control. On day 21 following immunization, target cells derived from naive C57BL/6 mice were intravenously administered to the immunized mice. Splenocytes were harvested from the immunized mice 18 h later and analyzed by flow cytometry to determine the specific killing of the target cells. (A) Representative histograms for splenocytes analyzed by flow cytometry. (B) Specific killing of target cells induced by the different treatments. CTL induced by each individual mouse is represented as a dot, bars represent the mean antigen specific killing for each treatment.

It is possible that the differences in immune responses found in the study are due to MWNT's dispersibility characteristics. Short oxidized f-MWNTs exhibited enhanced dispersibility and a higher degree of individualization, as observed in the TEM, compared to long non-oxidized f-MWNT (L+), which displayed a higher tendency of agglomeration. This could be due to the shortening induced by acid-assisted bath sonication [166, 189]. Interestingly, Iannazzo et al. conjugated HIV inhibitor to oxidized-MWNTs or oxidized-MWNTs modified with hydrophilic moieties and found that increasing the MWNT's dispersibility is associated with higher therapeutic effect of the loaded drug [208]. In that study [166], the in vitro uptake studies demonstrated increased uptake of S^{-/+} or S^{-/+}(OVA) on treating the BM-DCs with fixed concentration of f-MWNTs or MWNTs contained in MWNTs-OVA, and similar findings were observed in vivo. However, variations in antigen loading density among MWNTs-OVA or MWNTs-SIN cannot be ignored among the factors leading to the induced immune response intensities.

Despite the suggestion that differences in immune response efficacy in vitro and in vivo are related to differences in amounts of nanocarriers and antigen internalized, one cannot exclude the possibility of f-MWNT affecting the process of antigen processing by BM-DCs. Exogenous antigens processed in the endocytic compartments of the DCs are loaded onto MHC II molecules and presented to CD4⁺ T cells, while those processed in the cytosolic compartments are loaded onto the MHC I molecules and presented to CD8⁺ T cells. The latter is called cross presentation [209–211]. The similar pattern of CD8⁺ T cell stimulation induced by MWNTs-OVA and MWNTs-SIN treated BM-DCs propose the absence of MWNT's interference with antigen presentation. Thus, suggesting that the pattern of induced immune response was dependent on the tendency of MWNTs to enhance the cellular uptake of the conjugated antigen, whether it is an already processed antigen (SIN) or not (OVA).

7. Dual stimulation of antigen presenting cells using carbon nanotube-based vaccine delivery system for cancer immunotherapy

We hypothesized that harnessing MWNT for concurrent delivery of cytosine-phosphate-guanine oligodeoxynucleotide (CpG) and anti-CD40 Ig (αCD40), as immunoadjuvants, along with the model antigen ovalbumin (OVA) could potentiate immune response induced against OVA-expressing tumour cells. It has been initially investigated the effective method to co-deliver OVA and CpG using MWNT to the APC. Covalent conjugation of OVA and CpG prior to loading onto MWNTs markedly augmented the CpG-mediated adjuvanticity, as demonstrated by the significantly increased OVA-specific T cell responses in vitro and in C57BL/6 mice [212]. A CD40 was then included as a second immunoadjuvant to further intensify the immune response. Immune response elicited in vitro and in vivo by OVA, CpG and αCD40 was significantly potentiated by their co-incorporation onto the MWNTs. Furthermore, MWNT remarkably improved the ability of co-loaded OVA, CpG and αCD40 in inhibiting the growth of OVA-expressing B16F10 melanoma cells in subcutaneous or lung pseudo-metastatic tumour models. Therefore, the study suggests that the utilization of MWNTs for the co-delivery of tumour-derived antigen, CpG and αCD40 could be a competent approach for efficient tumours eradication [212].

Cancer therapeutic vaccines rely on the ability of professional antigen presenting cells (APCs), specifically dendritic cells (DCs), to detect, process and then present administered tumour-antigens via the major histocompatibility complex molecules class (MHC) II or I to CD4⁺ or CD8⁺ T cells, respectively, leading to anti-tumour immune responses induction [213]. However, tumour-induced immunosuppression and abundance of immunosuppressive regulatory T cells in the tumour micro-environment hinder the immune system to effectively eradicate established tumours [214]. This could be overcome by the use of combinatorial immunotherapeutic approaches, for instance by administration of tumour antigens along with different types of immunoadjuvants, rather

than the single immunotherapeutic ones [215].

Carbon nanotubes (CNTs) have been developed as needle-like nanoscopic carriers capable of improving therapeutic agents delivery to the intracellular compartments via energy-dependent and/or passive mechanisms of cellular uptake [216-218]. It has been previously demonstrated that altering the surface chemistry of multi-walled CNTs (MWNTs) conjugated to the model antigen ovalbumin (OVA) can affect the extent of their cellular internalization into APCs, and thus the intensity of the resulting immune responses elicited *in vitro* and *in vivo* [219]. As a delivery vector for tumour antigens, MWNTs have markedly improved antitumour immune response against breast or liver cancer-derived tumour proteins *in vitro* [220] or *in vivo* [221], respectively. Single-walled CNTs (SWNTs) conjugation with the immunoadjuvant cytosine-phosphate-guanine oligodeoxynucleotide (CpG) enhanced the CpG-induced stimulatory activities *in vitro* [222] and amplified the anti-tumour response in glioma-bearing mice [223,224]. Despite the demonstrated proficiencies of CNTs as an efficient delivery vector for antigen or immunoadjuvant, the utilization of CNTs to co-deliver antigen along with various types of immunoadjuvants has not been studied yet.

Agonist for Toll-like receptors (TLRs) expressed by APCs have shown marked capabilities in augmenting the antigen-specific immune response via various mechanisms, including the ability to enhance antigen presentation by APCs [225]. CpG, an agonist for endosomal TLR9, has been included in various cancer vaccine formulations tested in clinical trials [226]. The co-internalization of both antigen and TLR agonist by the same APC has been shown to influence the TLR agonist-mediated improvement of antigen presentation, thus the induced T cell responses. Yarovinsky et al. showed that potent induction of antigen-specific CD4+ T cell response in mice required the activation of TLR11 and an-

tigen presentation via MHC II to occur "in cis" in the same DC instead of separate DCs [227]. Wilson et al. demonstrated the significance of APC activation by TLR agonists at the time of antigen uptake showing that pre-treatment of mice with CpG reduces the ability of DCs to take up and present viral antigens to the CD8+ T cells [228]. Posing additional complexity, Blander et al. reported that more efficient antigen presentation by DCs could be achieved following the internalization of antigen and TLR4 agonist into the same rather than separate phagosome (s) *in vitro* [229]. In light of these studies, we hypothesized that designing an efficient method to co-incorporate antigen and CpG onto MWNT could improve their concomitant delivery to APC, and thus the induction of an antigen-specific immune response.

APCs express a number of receptors known as tumour necrosis factor receptors (TNFRs) such as CD40. Anti-CD40 Ig (α CD40), an agonist for the CD40 co-stimulation molecule, has exhibited potential benefits in amplifying antigen-specific immune responses [230,231]. It has been reported that DC stimulation with α CD40 chemically conjugated to peptide antigens increased the DC capacity to induce antigen-specific CD8+ T cell response *in vitro* [232,233]. This has been attributed to the demonstrated α CD40 ability to intracellularly target the conjugated antigen to the early endosomes of DCs. Antigen routing to the early endosomes of DCs has shown to facilitate antigen proteasomes degradation, loading onto MHC I and, subsequently, presentation to CD8+ T cells [234]. Thereby, by utilizing the α CD40-mediated enhancement of antigen presentation, stimulation of DCs with MWNT loaded with α CD40 in addition to OVA could further improve the induction of OVA-specific CD8+ T cell response [235]. CD40 interaction with α CD40 has been found to provide APCs with the CD4+ T cell-derived licensing signals required for CD8+ T cell stimulation. This has been demonstrated by the ability of administered α CD40 to restore antigen specific CD8+ T cell response in CD4+ T cell-depleted mice [236,237].

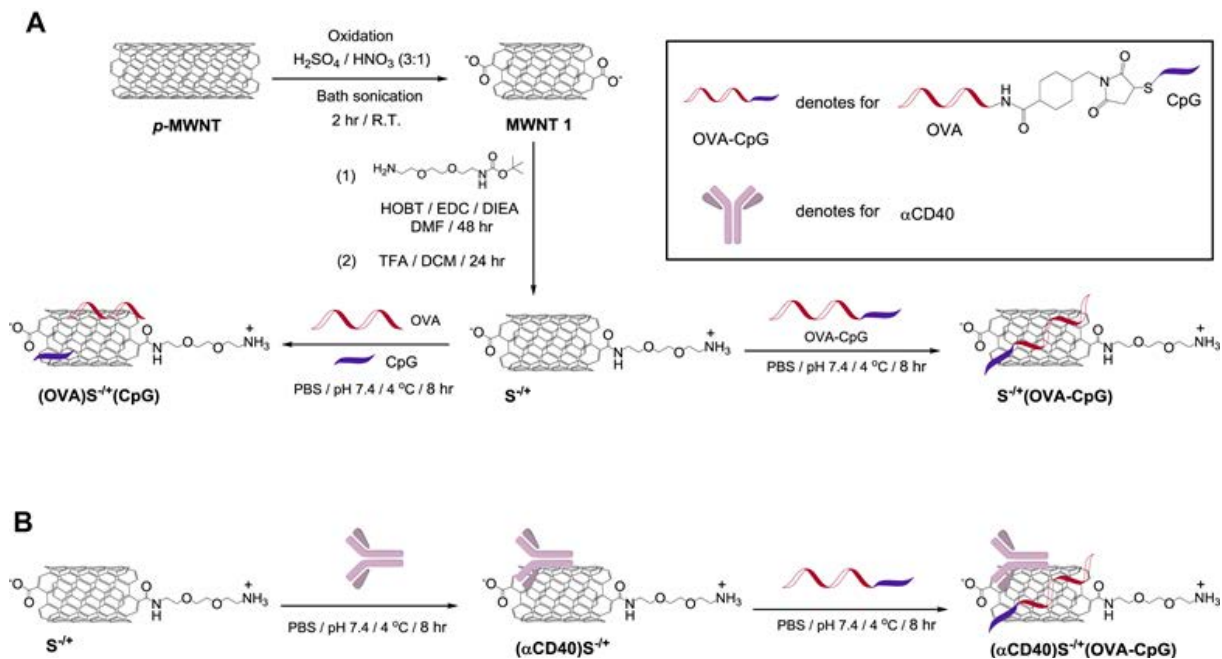
7.1. Synthesis and characterization of (OVA)S-/(CpG), S-/(OVA-CpG) and (α CD40) S-/(OVA-CpG) conjugates

7.1.1. Synthesis of S-/(OVA-CpG) or (OVA)S-/(CpG)

Synthesis of chemically functionalized MWNT has been described as shown in Scheme 3 [219].

In addition, for an efficient CD8+ T cell response induction, the process of antigen recognition by both CD4+ and CD8+ T cells has to occur via the same APC [238]. Hence, theoretically, higher immune response intensity could be achieved using delivery approaches that co-deliver the antigen and α CD40 signal to the same APC.

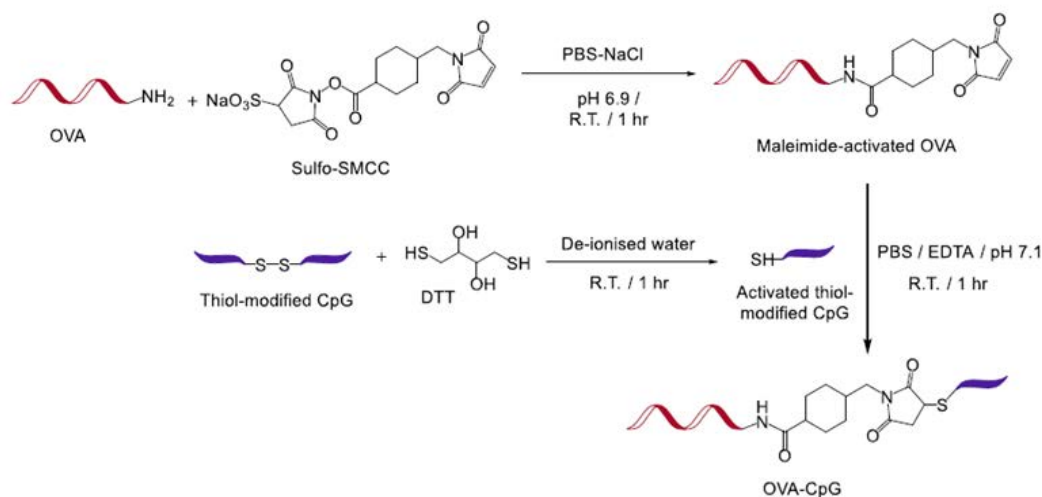
It has been hypothesized that CpG and α CD40 co-incorporation onto MWNT carrying the model antigen OVA would synergistically and significantly improve the OVA-specific immune responses, and effectively retard the growth of OVA-expressing B16F10 melanoma cells in solid or pseudo-metastatic tumour models.



Scheme 3: Synthesis of the conjugates. (A) Synthesis of (OVA)S^{-/+}(CpG) or S^{-/+}(OVA-CpG) conjugates. p-MWNT was oxidized using acidic mixture yielding MWNT 1. The carboxylic acid moieties of MWNT 1 were reacted with Boc-protected amine-terminated spacer via amide coupling reaction yielding S^{-/+}. (OVA)S^{-/+}(CpG) was synthesized by the simultaneous addition of OVA and CpG to S^{-/+}, while S^{-/+}(OVA-CpG) was synthesized by reacting the OVA-CpG with S^{-/+}. (B) Synthesis of (αCD40)S^{-/+}(OVA-CpG). αCD40 was first conjugated with S^{-/+} yielding (αCD40)S^{-/+} that following conjugation with OVA-CpG yielded (αCD40)S^{-/+}(OVA-CpG).

Briefly, pristine MWNTs (p-MWNTs) (20–30 nm diameter, 0.5–2 μm length, Nanostructured and Amorphous Materials, USA) were oxidized using acidic mixture, followed by incorporation of amine-terminated spacer using amide coupling reaction yielding a functionalized MWNT named S^{-/+}. The synthesis of OVA-CpG is illustrated in Scheme 4 and described in [239, 240]. For the synthesis of (OVA)S^{-/+}(CpG), 0.5 ml of PBS (PAA Laboratories Ltd, UK) containing 1 mg OVA (Endo Grade® Ovalbumin, Hyglos GmbH, Germany) and 1.1 mg CpG (phosphonothioate ODN CpG 1668 (5′-(TC-CATGACGTTCCCTGATGCT) -3′), Neurogenetic, Belgium) were mixed with a dispersion of 2 mg S^{-/+} in 2 ml PBS. For the synthesis of S^{-/+}(OVA-CpG), OVA-CpG containing 1 mg OVA and 1.1 mg CpG in 0.5 ml PBS was mixed with a dispersion of 2 mg S^{-/+} in 2 ml PBS. Both reactions were mixed for 8 h at 4 °C. The reaction mixtures were briefly sonicated then vacu-

um filtered through 0.22 μm polycarbonate membrane filter (Isopore™ Membrane, Merck Millipore, Germany). The solids recovered were re-dispersed in 2.5 ml PBS and the obtained dispersion was briefly sonicated and then vacuum filtered. Unreacted OVA and CpG contained in the collected filtrates were quantified using bicinchoninic acid protein (BCA) assay reagent (Fisher Scientific, UK) and NanoDrop (ND-1000 spectrophotometer, NanoDrop Technologies, USA), respectively, as described in [212]. The recovered S^{-/+}(OVA-CpG) or (OVA)S^{-/+}(CpG) solids were further washed with methanol (Fisher Scientific, UK) and then vacuum filtered through 0.22 μm polycarbonate membrane filter, dried and recovered. Synthesized conjugates were characterized using thermogravimetric analysis (TGA) and polyacrylamide gel electrophoresis (PAGE) that were performed as described before [219].



Scheme 4: Synthesis of OVA–CpG conjugates. OVA were maleimide–activated using sulfo–SMCC then covalently conjugated with the thiol–modified CpG via thioether linkage yielding OVA–CpG.

7.1.2. Synthesis of (α CD40) S–/+(OVA–CpG)

To a dispersion of 3 mg S–/+ in 2 ml PBS, 1 mg of α CD40 (purified rat anti-mouse CD40 monoclonal antibody, BD Biosciences, USA) in 0.5 ml PBS was added. The reaction was mixed for 8 h at 4 °C. The reaction mixture was briefly sonicated then vacuum filtered through 0.22 μ m polycarbonate membrane filter. The solids recovered were re-dispersed in 2.5 ml PBS and the obtained dispersion was briefly sonicated and then vacuum filtered. Unreacted α CD40 contained in the collected filtrates was quantified using BCA assay as described in Supplementary Information. The recovered (α CD40) S–/+ solids were washed with methanol, vacuum filtered through 0.22 μ m polycarbonate membrane filter, dried and re-dispersed in 2 ml PBS. To the (α CD40) S–/+ dispersion, OVA–CpG containing 1 mg OVA and 1.1 mg CpG in 0.5 ml PBS was added. The reaction was mixed for 8 h at 4 °C. The reaction mixture was briefly sonicated then vacuum filtered through 0.22 μ m polycarbonate membrane filter. The solids recovered were re-dispersed in 2.5 ml PBS and the obtained dispersion was briefly sonicated and then vacuum filtered. Unreacted OVA and CpG contained in the collected filtrates were quantified using BCA assay and NanoDrop, respectively, as described in Supplementary Information. The recovered (α CD40) S–/+(CpG) solids were further washed with methanol and then vacuum filtered through 0.22 μ m polycarbonate membrane filter, dried and recovered.

As depicted in Scheme 3A, the length of p-MWNTs was shortened by oxidation reaction using sulphuric and nitric acids mixture and bath sonication, yielding MWNT 1. This step was followed by partial neutralization of the incorporated negatively charged carboxylic acid moieties using an amine terminated spacer, yielding S–/+. It has been previously reported that this functionalization approach, compared to other chemical functionalization methods, yields a functionalized MWNT (S–/+) capable of significantly improving the loaded antigen internalization by APCs in vitro and in vivo [219].

Utilizing the ability of CNTs to non-covalently interact with proteins [241] and ssDNA [242], OVA and CpG were incorporated onto S–/+ surface using two distinct methods (Scheme 3A). (OVA)S–/+(CpG) was synthesized by mixing an aqueous dispersion of S–/+ with OVA and CpG. Alternatively, OVA and CpG were covalently conjugated to yield OVA–CpG (Scheme 4) prior to the reaction with S–/+, yielding S–/+(OVA–CpG). The third conjugate, (α CD40) S–/+(OVA–CpG), was prepared by prior mixing of α CD40 with S–/+ followed by OVA–CpG loading (Scheme 3B). The zeta potential values of S–/+, (OVA)S–/+(CpG) and S–/+(OVA–CpG) were found to be –7.27, –43.7 and –41.9 mV, respectively (Table 5) [212].

Table 5: Zeta potential of the functionalized MWNTs and synthesized conjugates.

	Zeta potential ^a (mV)
MWNT 1	–20.9
S–/+	–7.27
(OVA)S–/+(CpG)	–43.7
S–/+(OVA–CpG)	–41.9

^aAnalyzed by electrophoretic mobility using 10 \times diluted PBS buffer.

Transmission electron microscopy (TEM) revealed individualized nanotubes with a mean length of 122 ± 82 nm (Fig. 30A). OVA or α CD40 loading was quantified using a BCA assay [219], while CpG quantification was performed using NanoDrop Spectrophotometer [223]. The loading values and

loading efficiency are summarized in Table 6 and Table 7, respectively. OVA: CpG molar ratios of 1:10, 1:7.3 and 1:7.4 were reported for (OVA)S-/+(CpG), S-/+(OVA-CpG) and (α CD40) S-/+(OVA-CpG), respectively.

Table 6: Physicochemical characterization of conjugates.

	Length ^{a,b} (nm)	Primary amine loading ^{b,c} (μ mole/g S-/+))	OVA loading ^{b,d} (μ mole/g S-/+)) [μ mole/g S-/+]	CpG loading ^{b,e} (μ mole/g S-/+)) [μ mole/g S-/+]	α CD40 loading ^{b,d} (mg/g S-/+)) [μ mol/g S-/+]
(OVA)S-/+(CpG)	122 ± 82	263 ± 72	205 ± 24 [4.5 ± 0.53]	288 ± 20 [45 ± 3.1]	—
S-/+(OVA-CpG)	122 ± 82	263 ± 72	130 ± 21 [2.9 ± 0.47]	136 ± 18 [21.2 ± 2.8]	—
(α CD40)S-/+(OVA-CpG)	122 ± 82	263 ± 72	55 ± 15 [1.2 ± 0.33]	57 ± 11 [8.8 ± 1.7]	188 ± 17 [1.3 ± 0.1]

Stability studies were carried out up to 7 days by stirring in PBS at 37 C ° ; the stability of the loaded cargo was confirmed (Figure 31).

Table 7: Loading efficiencies of the conjugates.^a

	OVA loading efficiency (%)	CpG loading efficiency (%)	α CD40 loading efficiency (%)
(OVA)S-/+(CpG)	41 ± 6.8	52.4 ± 5.2	—
S-/+(OVA-CpG)	26 ± 5.9	24.8 ± 4.6	—
(α CD40)S-/+(OVA-CpG)	16.5 ± 6.4	15.5 ± 4.2	56.4 ± 7.2

^a Calculated as the percentage of OVA, CpG or α CD40 bound to S-/+ of the starting material. Data are represented as mean \pm SD (n= 3).

OVA, CpG and/or α CD40 loading onto S-/+ was also confirmed using TGA [243]. TGA was performed under inert gas (nitrogen) by exposing the tested samples to gradually increasing temperature (up to 800 °C). The graphitic structure of the pristine CNT (p-MWNT) is stable against sublimation within the applied temperatures. However, surface defects and impurities such as amorphous carbon (that con-

stitute approximately 2% of p-MWNT) are less stable and thermally decompose by sublimation at 600 °C [244, 245]. Organic functional groups decomposition also occurs at temperatures lower than 600 °C. It was previously reported that thermally degraded functional groups or biomolecules decompose mainly into carbon dioxide, carbon monoxide, ammonia [246].

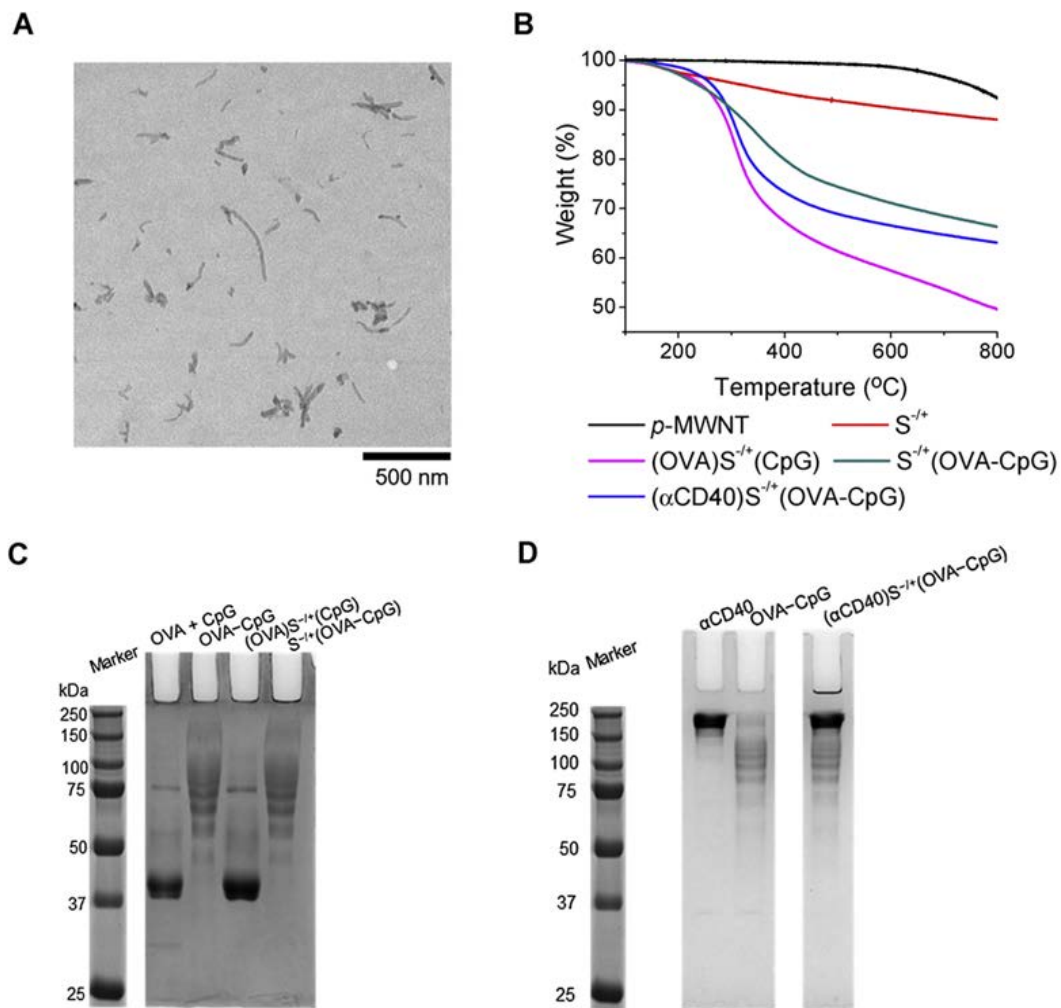


Figure 30: Characterization of the conjugates. (A) Representative TEM image of an aqueous dispersion of $S^{-/+}$. (B) Thermogravimetric profiles. $S^{-/+}$ or the conjugates, of known weights, were subjected to increasing temperatures and the weight loss was measured at the increased temperature. (C) PAGE of (OVA) $S^{-/+}$ (CpG) or $S^{-/+}$ (OVA-CpG). Free OVA, or OVA contained in the conjugates, each at 10 μ g OVA, were loaded in the appropriate lane of 10% native, non-reducing gel. (D) PAGE of $(\alpha$ CD40) $S^{-/+}$ (OVA-CpG). OVA-CpG conjugate containing 3 μ g OVA, 10 μ g of α CD40 or $(\alpha$ CD40) $S^{-/+}$ (OVA-CpG) containing 3 μ g OVA and 10 μ g α CD40 were loaded in the appropriate lane of 10% native, non-reducing gel. Bands were detected by gel staining with Coomassie Brilliant blue.

The density of the loaded functional groups and biomolecules is directly related to the sample weight loss 600 °C, as a result of thermal decomposition. As demonstrated in Fig. 30B, a greater reduction in the thermal stability was observed for $S^{-/+}$ compared to p -MWNT as a result of decomposition of the functional groups. Expectedly, (OVA) $S^{-/+}$ (CpG), $(\alpha$ CD40) $S^{-/+}$ (OVA-CpG) and $S^{-/+}$ (OVA-CpG) achieved higher weight losses than $S^{-/+}$, in the same order. This observation could be assigned to the fact that (OVA) $S^{-/+}$ (CpG) possessed the highest content of incorporated biomolecules followed by $(\alpha$ CD40) $S^{-/+}$ (OVA-CpG) then $S^{-/+}$ (OVA-CpG) (Table 6). TGA confirmed the success of

chemical modification of $S^{-/+}$ and loading of OVA, CpG and α CD40 onto $S^{-/+}$.

PAGE electrophoresis was employed to visualize the loaded OVA and/or α CD40. Similar to unconjugated OVA, the OVA contained in (OVA) $S^{-/+}$ (CpG) appeared as an intense band of ~45 kDa (Fig. 30C). In case of OVA-CpG or $S^{-/+}$ (OVA-CpG), an increase in OVA molecular weight was observed (>45 kDa) due to successful conjugation with CpG. Exposing $(\alpha$ CD40) $S^{-/+}$ (OVA-CpG) to gel electrophoresis confirmed the presence of α CD40 as a main intense band of ~150 kDa and CpG-conjugated OVA bands (Fig. 30D).

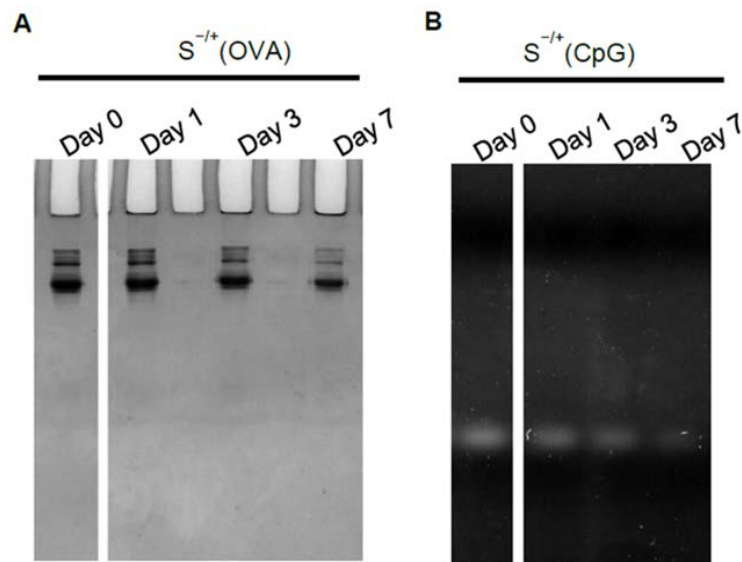


Figure 31: In vitro stability. (A) Assessment of in vitro stability of S^{-/+}(OVA) using PAGE. S^{-/+}(OVA) was dispersed in PBS (pH 7.4) at 1 mg/ml and exposed to constant agitation for 1, 3 or 7 days at 37 °C. At the indicated time points, S^{-/+}(OVA) containing 10 µg OVA was transferred to the wells of 15% native, non-reducing gel. Bands were detected by gel staining with Coomassie Brilliant blue. (B) Assessment of in vitro stability of S^{-/+}(CpG) using agarose gel electrophoresis. S^{-/+}(CpG) was dispersed in PBS (pH 7.4) at 1 mg/ml and exposed to constant agitation for 1, 3 or 7 days at 37 °C. At the indicated time points S^{-/+}(CpG) containing 1 µg CpG was transferred to the wells of a 2% agarose gel. Bands were detected by gel staining with SYBR Gold.

7.2. Assessment of OVA presentation induced by (OVA) S^{-/+}(CpG) or S^{-/+}(OVA-CpG) treated BM-DCs in Vitro

DCs were generated from the bone marrow of C57BL/6 mice and characterized for their purity as previously described [219]. Bone marrow-derived DCs (BM-DCs) were incubat-

ed for 24 h with OVA, mixture of unconjugated OVA and CpG (referred to as OVA + CpG), OVA-CpG, (OVA)S^{-/+}(CpG) or S^{-/+}(OVA-CpG) each containing 5 µg/ml OVA. The used doses were determined from the optimization studies described in (Figure 32).

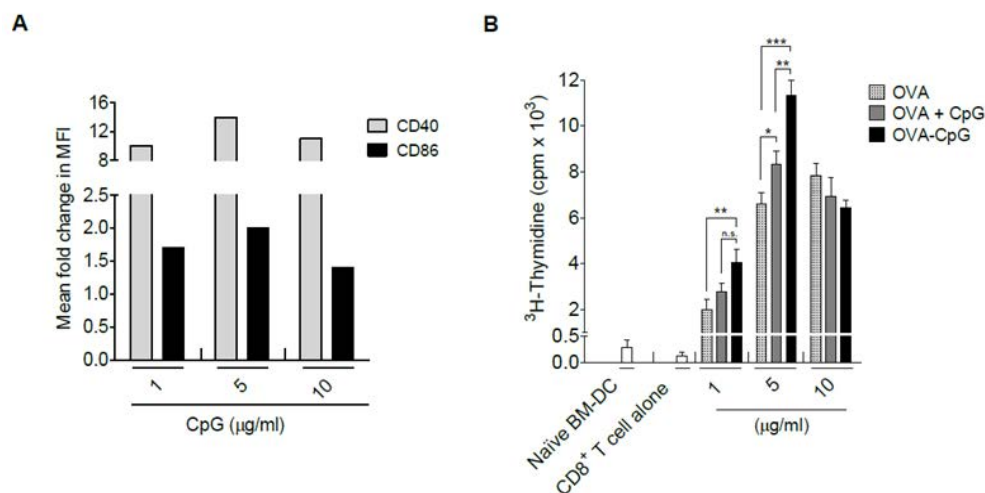


Figure 32: Optimization of CpG or OVA/CpG doses required for induction of BM-DC maturation or OVA presentation in vitro, respectively. (A) Dose-dependent stimulation of BM-DC maturation by CpG in vitro. BM-DCs were incubated for 24 h with 1, 5 or 10 µg/ml CpG and then analyzed for CD40 or CD86 expression using flow cytometry. BM-DCs were stained with specific fluorescently labelled antibodies or their corresponding isotype control antibodies, 10 x 10⁴ cells were acquired using flow cytometry and the analysis was performed using FLOWJO 7.6.5 software. The MFI of the positive CD11c-expressing BM-DCs was measured to assess the fold change in the expression of each marker with respect to the naïve BM-DCs. The optimal CpG dose for induction of BM-DC maturation was found to be 5 µg/ml. (B) Dose-dependant stimulation of CD8⁺ T cell proliferation in vitro by OVA + CpG or OVA-CpG. BM-DCs were incubated for 24 h with OVA + CpG or OVA-CpG each contained 1, 5 or 10 µg/ml of both OVA and CpG. As a control, BM-DCs were incubated for 24 h with OVA alone at 1, 5 or 10 µg/ml. Treated BM-DCs were co-cultured with CD8⁺ T cells, isolated from the spleen of OT-I C57BL/6 mice, at 1:4 ratio for 3 days. On the last 18 h, CD8⁺ T were pulsed with 1 µCi of 3H-thymidine and the CD8⁺ T cell proliferation was measured using 3H-thymidine incorporation assay. Measurements were performed in triplicates for each condition, results represent the mean ± S.D. * P < 0.05, ** P < 0.01, *** P < 0.001. Stimulation of BM-DCs with 5 µg/ml of both OVA and CpG contained in with OVA + CpG or OVA-CpG was found optimal for OVA presentation.

BM-DCs were incubated, as a control, with S-/+ alone at concentrations equivalent to those contained in (OVA) S-/(CpG) or S-/(OVA-CpG) (20–38 µg/ml). Treated BM-DCs were harvested, washed several times with RPMI 1640 and gamma-irradiated using Cesium-137 at 3000 Gy for 10 min. CD4+ and CD8+ T cells were isolated from the OT-II and OT-I mice spleen, respectively, and characterized for their purity as described before [219]. In 96-well round-bottom plate, 25 × 10³ of CD4+ or CD8+ T cells were co-cultured with the BM-DCs at 1:4 ratio in a total volume of 200µl complete medium per well. The BM-DCs: T cell co-culture ratio was determined from previous optimization studies [219]. As a control, CD4+ or CD8+ T cells were cultured alone or with naïve BM-DCs. Cultured cells were maintained for 3 days at 37 °C. For the last 18 h of incubation, 50µl of the supernatants were removed and replaced with a fresh 50µl of complete medium containing 1 µCi of 3H-thymidine (Thymidine (Methyl-3H), Perkin Elmer, USA). T cell proliferation was assessed by measuring the incorporated 3H-thymidine emitted radiation using liquid scintillation counter (Wallac 1205 Betaplate) [219]. The levels of IFN-γ in the supernatants collected from BM-DCs co-cultured with CD4+ or CD8+ T cells were quantified using anti-mouse IFN-γ sandwich ELISA kit (eBioscience, USA) following the manufacturer's protocol. The absorbance of each well was measured at 450 nm using a plate reader (FLUOstar Omega, BMG LABTECH, Germany).

7.3. Assessment of OVA presentation induced by (αCD40) S-/(OVA-CpG) treated BM-DCs in vitro

BM-DCs were incubated for 24 h with mixture of unconjugated αCD40 and OVA-CpG (referred to as αCD40 + OVA-CpG), mixture of unconjugated αCD40 and S-/(OVA-CpG) (referred to as αCD40 + S-/(OVA-CpG)) or (αCD40) S-/(OVA-CpG), each containing 0.5 µg/ml of both OVA and CpG, and 1.8 µg/ml αCD40. As a control BM-DCs were incubated for 24 h with OVA-CpG or S-/(OVA-CpG), each containing 1 µg/ml OVA. CD8+ T cell proliferation and IFN-γ production were then determined using 3H-thymidine incorporation assay and ELISA as described before, respectively.

7.4. Loading of OVA-CpG conjugate onto S-/+ offers more potent in vitro antigen presentation than the loading of unconjugated OVA and CpG

To determine the effect of (OVA)S-/(CpG) or S-/(OVA-CpG) on the maturation of DC, the synthesized conjugates were incubated with BM-DCs for 24 h and the expression of MHC as well as co-stimulatory molecules were determined using specific antibodies and flow cytometry as described in [212]. Similar to the CpG treatment alone, incubation of BM-DCs with (OVA)S-/(CpG) or S-/(OVA-CpG) increased the expression of MHC I, MHC II, CD40 and CD86 (Figure 33 and Fig. 34A) with no significant differences seen between groups. OVA-treated BM-DCs showed no signs of maturation. Incubation of BM-DCs with S-/+ alone has been shown previously to not affect the expression of these molecules [219]. Taken together the data suggest that maturation of BM-DCs induced by (OVA)S-/(CpG) or S-/(OVA-CpG) was CpG-dependant.

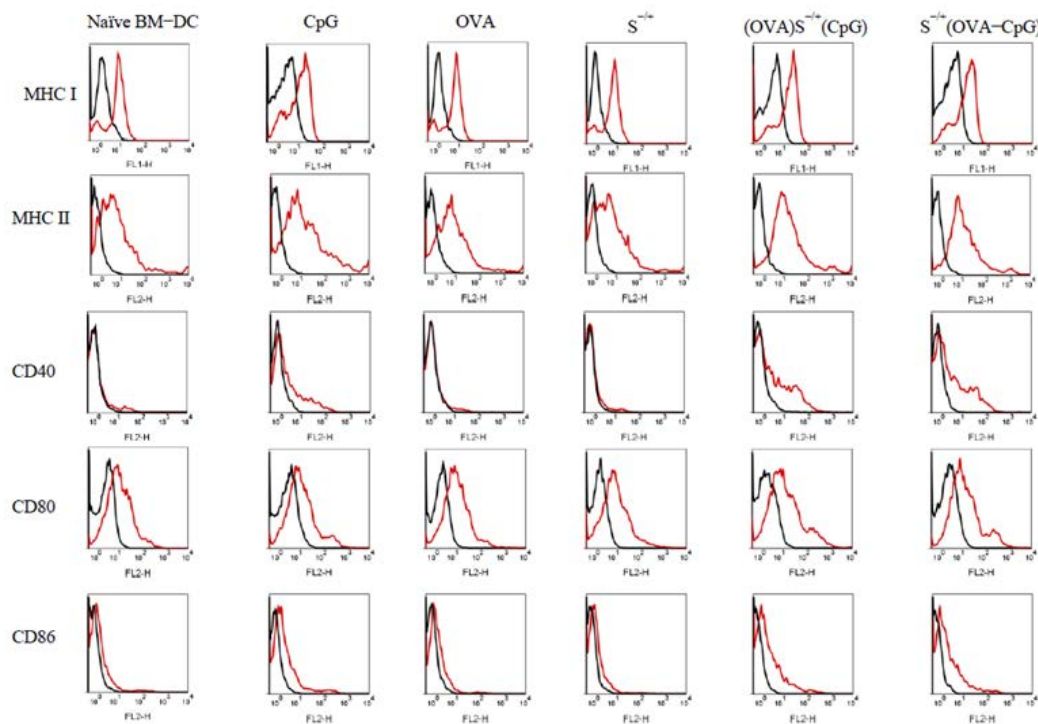


Figure 33: Effect of (OVA)S-/(CpG) or S-/(OVA-CpG) on BM-DC maturation in vitro. BM-DCs were incubated for 24 h with 5 µg/ml CpG, OVA, (OVA)S-/(CpG) or S-/(OVA-CpG), each contained 5 µg/ml OVA. BM-DCs were stained with fluorescently labelled specific antibodies against MHC I, MHC II, CD40, CD80 or CD86, and cell analysis was performed using flow cytometry. Representative histograms are shown for CD11c-expressing BM-DCs stained with specific fluorescently labelled antibodies or their corresponding isotype control antibodies.

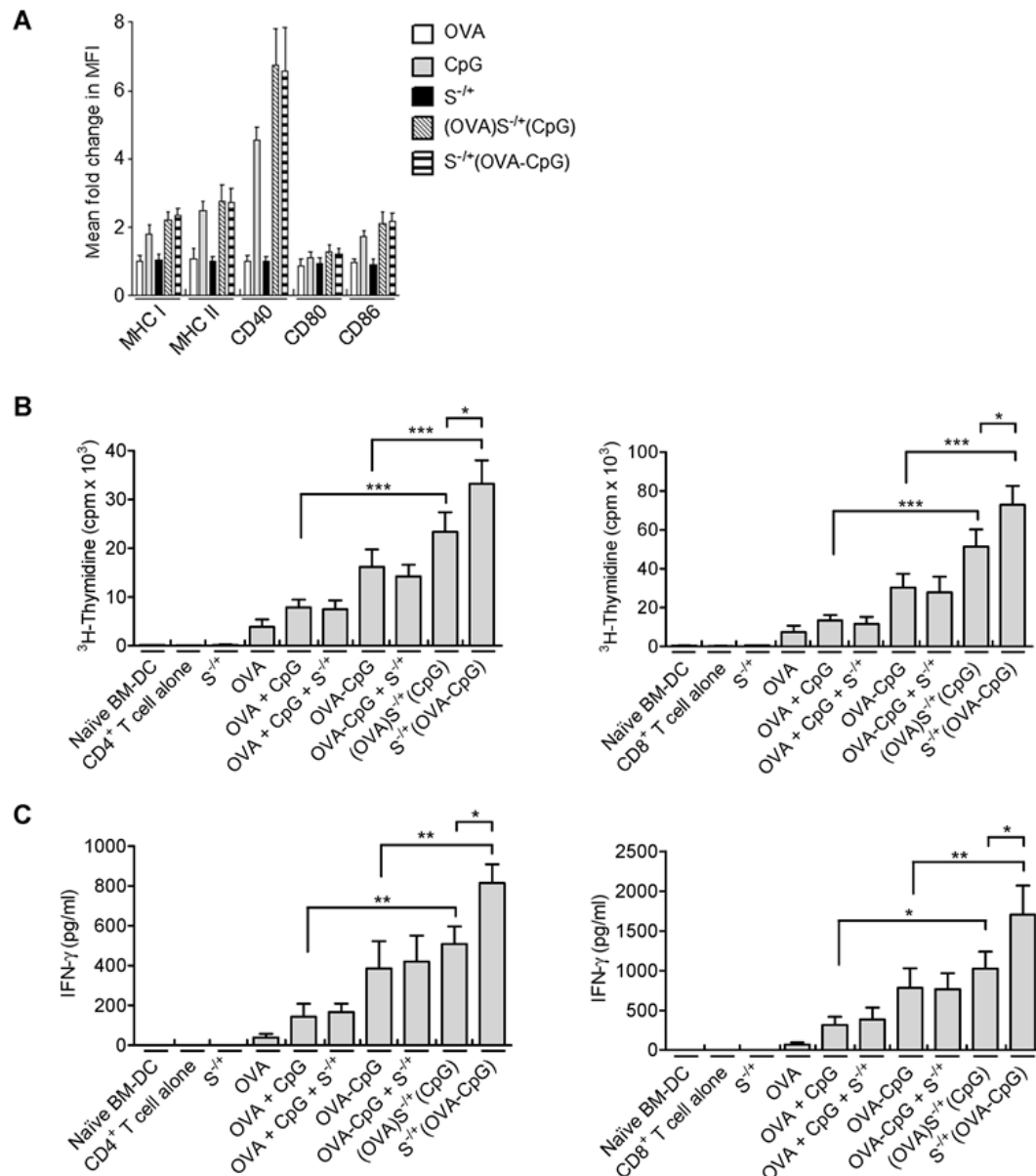


Figure 34: Assessment of BM-DC maturation and OVA presentation induced by treatment with (OVA)S^{-/+}(CpG) or S^{-/+}(OVA-CpG) in vitro. (A) Effect of (OVA)S^{-/+}(CpG) or S^{-/+}(OVA-CpG) on BM-DC maturation. BM-DCs were incubated for 24 h with 5 µg/ml CpG, OVA, (OVA)S^{-/+}(CpG) or S^{-/+}(OVA-CpG), each contained 5 µg/ml OVA. BM-DCs were stained with fluorescently labelled specific antibodies against MHC I, MHC II, CD40, CD80 or CD86, and cell analysis was performed using flow cytometry. The mean fluorescence intensity (MFI) of the positive CD11c-expressing BM-DCs was measured using the fold change in the expression of each marker with respect to the naïve BM-DCs, results represent the mean ± S.D. (B, C) OVA presentation by (OVA)S^{-/+}(CpG) or S^{-/+}(OVA-CpG) treated BM-DCs. BM-DCs were incubated for 24 h with OVA + CpG, OVA-CpG, (OVA)S^{-/+}(CpG) or S^{-/+}(OVA-CpG), each contained 5 µg/ml OVA. Treated BM-DCs were co-cultured with CD4+ or CD8+ T cells isolated from the spleen of OT-2 or OT-1 C57BL/6 mice, respectively, at 1:4 ratio for 3 days. On the last 18 h of incubation, CD4+ T cells (B, left) or CD8+ T cells (B, right) were pulsed with 1 µCi of 3H-thymidine and the proliferation was measured using 3H-thymidine incorporation assay. The content of IFN-γ in the supernatants of the proliferating CD4+ T cells (C, left) or CD8+ T cells (C, right) was quantified using ELISA. Measurements were performed in triplicates for each condition, results represent the mean ± S.D. *P < 0.05, **P < 0.01, ***P < 0.001.

Next, the efficiency of the two approaches in enhancing OVA presentation by BM-DCs was assessed in vitro using OVA-specific transgenic CD4+ or CD8+ T cells. After incubation of BM-DCs with the S^{-/+} based conjugates (containing 5 µg/ml OVA), (OVA)S^{-/+}(CpG) or S^{-/+}(OVA-CpG) significantly enhanced OVA-specific T cells proliferation as compared to their control treatments, namely OVA + CpG or OVA-CpG (p

< 0.001), respectively (Fig. 6.34B). However, treatment with S^{-/+}(OVA-CpG) resulted in elevated responses compared to (OVA)S^{-/+}(CpG) (p < 0.05). This was further confirmed with IFN-γ cytokine production profiles (Fig. 6.34C). Similar T cell responses were obtained when BM-DCs were treated with the synthesized conjugates containing a lower dose of 2.5 µg/ml OVA.

The observations indicated that loading OVA and CpG onto S-/+ in the form of a conjugate can lead to enhanced OVA presentation by BM-DCs in vitro, compared to loading un-conjugated OVA and CpG [212].

7.5. Assessment of the immune response induced by (OVA)S-/(CpG), S-/(OVA-CpG) or (αCD40) S-/(OVA-CpG) in mice using in vivo CTL assay

C57BL/6 mice (n = 3–5) were immunized, via the footpad injection, with OVA-CpG, (OVA)S-/(CpG) or S-/(OVA-CpG) each containing 6 µg OVA in 50 µl PBS. Alternatively, mice were injected via the footpad with αCD40 + OVA-CpG or (αCD40) S-/(OVA-CpG), each containing 3 µg of both OVA and CpG, and 10 µg αCD40 in 50 µl PBS. Mice injected with PBS were used as a control. The in vivo cytotoxic T lymphocyte (CTL) assay was performed following previously described method [219]. Briefly, a 1:1 splenocytes mixture consisting of 0.5 µM CFSE (carboxyfluorescein diacetate succinimidyl ester, eBioscience, USA) -labelled and SIINFEKL-pulsed splenocytes (referred to as 0.5 µM CFSESIINFEKL) and 5 µM CFSE-labelled un-pulsed splenocytes (referred to as 5 µM CFSEno SIINFEKL), were administered in immunized mice or mice injected with PBS via the tail vein at 10×10^6 cells per 200 µl per mouse, on the 8th day post immunization. At 18 h post-injection, mice were scarified; spleens were harvested and digested in collagenase/DNase solution. The percentage of SIINFEKL-pulsed and un-pulsed splenocytes, induced by each treatment, in the harvested splenocytes was determined using flow cytometry. Antigen-specific killing was calculated using the previous equation (1).

7.6. Assessment of the anti-tumour response induced by (αCD40) S-/(OVA-CpG) in subcutaneous tumour model

Luciferase-transfected melanoma B16F10 cells were obtained from Perkin Elmer (USA) and were transduced with vesicular stomatitis virus G pseudo typed retrovirus encoding green fluorescence protein (GFP)-tagged OVA [239, 247]. GFP positive cells were then sorted as single cells using GFP filter. C57BL/6 mice were subcutaneously inoculated in both flanks with 2.5×10^5 OVA-expressing and luciferase-transfected B16F10 (OVA-B16F10-Luc) cells. On the 7th day post tumour inoculation, mice were randomly assigned to 5 groups (n = 7). On the 7th and 14th days post tumour inoculation, mice were immunized via footpad injection with S-/(OVA-CpG), αCD40 + OVA-CpG, αCD40 + S-/(OVA-CpG) or (αCD40) S-/(OVA-CpG), each containing 6 µg OVA, 6 µg CpG and/or 21 µg αCD40 in 50 µl PBS. PBS injected mice were used as untreated controls. A calliper was used to measure the tumour length (L) and width (W), and the tumour volume was calculated using the following equation: Tumour volume = $0.52 \times W^2 \times L$. Mice were sacrificed when the tumour volume reached 1000 mm³.

7.7. Assessment of anti-tumour response induced by (αCD40) S-/(OVA-CpG) in lung pseudo-metastatic tumour model

C57BL/6 mice were intravenously inoculated with 2.5×10^5 OVA-B16F10-Luc cells. On the 4th day post tumour inoculation, mice were randomly assigned to 3 groups (n = 6–8). On the 4th and 9th days post tumour inoculation, mice were immunized via footpad injection with S-/(OVA-CpG)

or (αCD40) S-/(OVA-CpG) containing 6 µg OVA, 6 µg CpG and/or 21 µg αCD40. PBS injected mice were used as untreated controls. Tumour growth was monitored by detecting the bioluminescence emitted from the inoculated OVA-B16F10-Luc cells following D-Luciferin (Perkin Elmer, USA) injection. Every 3–4 days post tumour inoculation, mice were anesthetized and subcutaneously injected with D-Luciferin (150 mg/kg) in PBS. Imaging was performed using IVIS Lumina III and images analysis was conducted with Living Image® 4.3.1 Service Pack 2 software (Perkin Elmer, USA).

7.8. Immunization with S-/+ loaded with OVA-CpG elicits potent cellular and humoral immune responses

The capability of (OVA)S-/(CpG) or S-/(OVA-CpG) to induce a cell-mediated immune response in vivo was determined using an in vivo CTL assay [239]. In these experiments, the OVA immunization dose used in (OVA)S-/(CpG), S-/(OVA-CpG) or their controls was 6 µg, given the observation that in C57BL/6 mice treated with various doses of OVA-CpG, a measureable OVA-specific CTL immune response was detected at OVA content of 6 µg (Figure 35).

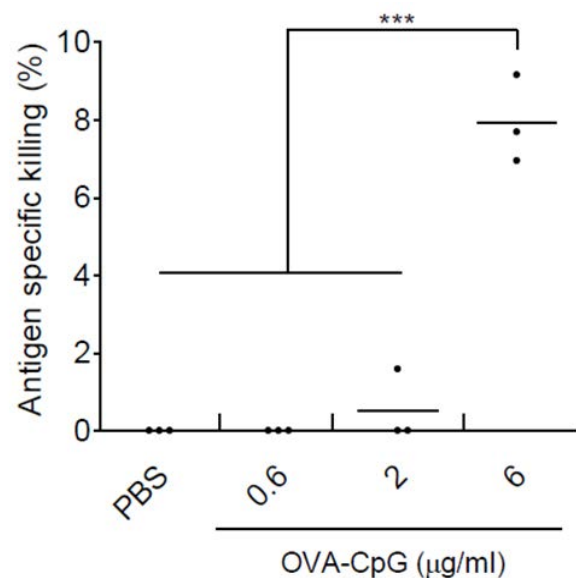


Figure 35: Determination of the optimal dose of OVA-CpG to induce antigen-specific killing using in vivo CTL assay. C57BL/6 mice (n = 3) were immunized, via footpad injection, with OVA-CpG containing 0.6, 2 or 6 µg of both OVA and CpG. On day 7 following immunization, a 1:1 splenocytes mixture consisting of target cells pulsed with 200 nM SIINFEKL and labelled with 0.5 µM CFSE (target cells) and unpulsed control cell labelled with 5 µM CFSE was intravenously administered to the control or immunized mice. Splenocytes were harvested, 18 hr later, from the control or immunized mice and analyzed using flow cytometry analysis. Antigen-specific killing induced by each treatment was determined. Each dot represents killing of target cells by each mouse, the mean value for each treatment is shown as a horizontal bar. *** P < 0.001.

It was revealed that immunization with S-/(OVA-CpG) induced a greater level of antigen-specific killing ($47.7\% \pm 11.7$) in contrast to OVA-CpG ($10.8\% \pm 4.2$) or (OVA) S-/(CpG) ($29.1\% \pm 3.0$) (P < 0.0001) (Fig. 36A and Figure 37).

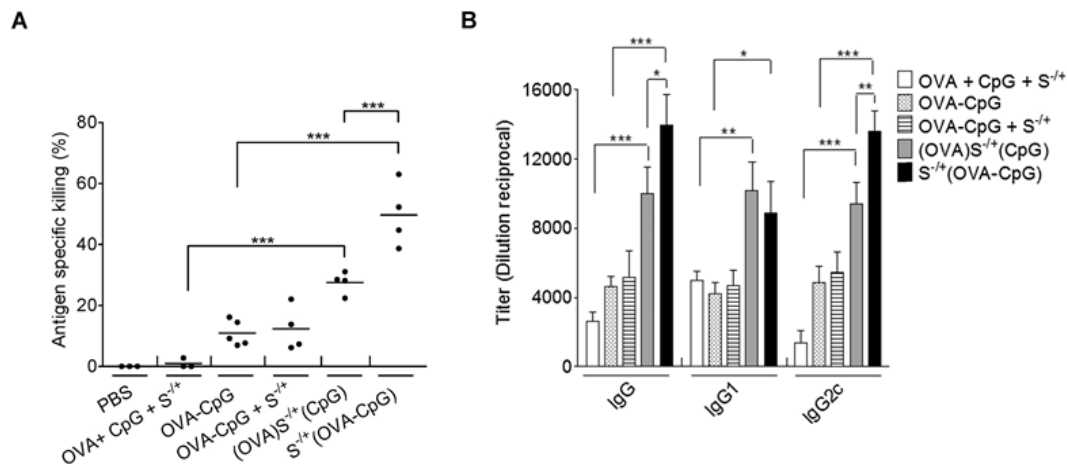


Figure 36: Assessment of immune response induced by (OVA)S^{-/+}(CpG) or S^{-/+}(OVA-CpG) in vivo. (A) Determination of the antigen-specific killing using in vivo CTL assay. C57BL/6 mice (n = 3–5) were immunized with the indicated treatments via footpad injection. Each treatment contained 6 µg of OVA. On day 7 following immunization, a 1:1 splenocytes mixture consisting of target cells pulsed with 200nM SIINFEKL and labelled with 0.5µM CFSE and unpulsed control cell labelled with 5µM CFSE was intravenously administered to the control or immunized mice. Splenocytes were harvested, 18 h later, from the control or immunized mice and analyzed using flow cytometry analysis. Antigen-specific killing induced by each treatment was determined. Each dot represents killing of target cells by each mouse, the mean value for each treatment is shown as a horizontal bar. (B) Quantification of OVA-specific IgG. C57BL/6 mice (n = 3) were immunized with the indicated treatments, via footpad injection, each treatment contained 6 µg of OVA and CpG. On day 21 following injection, control or immunized mice sera were collected. The OVA-specific IgG, IgG1 or IgG2c were determined using ELISA. Data represent the mean value ± S.D. *P < 0.05, **P < 0.01, ***P < 0.001.

To assess the humoral response induced by the conjugates in vivo, C57BL/6 mice were treated with the conjugates or appropriate controls, and OVA-specific antibodies were quantified using an OVA-specific ELISA 21 days post immunization (Fig. 36B). Immunization with S^{-/+}(OVA-CpG) significantly

boosted the production of anti-OVA IgG and IgG2c antibodies titres compared to (OVA)S^{-/+}(CpG) or other treatments. Both conjugates, however, ensued comparable anti-OVA IgG1 titres.

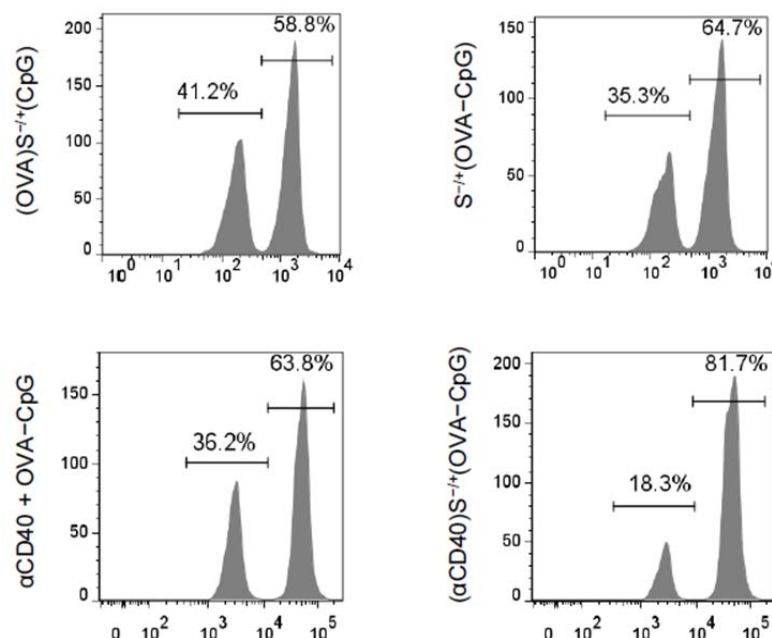


Figure 37: Assessment of in vivo CTL response. C57BL/6 mice (n = 3–5) were immunized, via footpad injection, with either 6 µg OVA (contained in (OVA)S^{-/+}(CpG) or S^{-/+}(OVA-CpG)) or 3 µg OVA (contained in OVA-CpG + αCD40 or (αCD40)S^{-/+}(OVA-CpG)). The S^{-/+} unconjugated or conjugated αCD40 was used at 10 µg. On day 7 following immunization, a 1:1 splenocytes mixture consisting of target cells pulsed with 200nM SIINFEKL and labelled with 0.5µM CFSE (target cells) and unpulsed control cell labelled with 5µM CFSE was intravenously administered to the control or immunized mice. Splenocytes were harvested, 18hr later, from the control or immunized mice and analyzed using flow cytometry analysis. Representative histograms are shown for the detection of target and control cells, in the harvested splenocytes, using flow cytometry.

These findings demonstrated further the augmentation in antigen specific immune response in vivo achieved by S-/(OVA-CpG) over (OVA)S-/(CpG). It has been adopted this conjugate S-/(OVA-CpG) for subsequent studies in combination with α CD40 as a second immunoadjuvant.

7.9. Incorporation of α CD40 as a second immunoadjuvant improves OVA presentation in vitro and intensifies OVA-specific immune response in vivo even at lower OVA doses

To further intensify the antigen-specific immune responses observed, α CD40 antibody was loaded onto S-/+ as a second immunoadjuvant. In order to assess the effect of α CD40 contained in (α CD40) S-/(OVA-CpG) on DC activation mark-

ers, BM-DCs were stimulated with the conjugate or control treatments and known DC markers were assessed using flow cytometry as described in Supplementary Information. BM-DC stimulated with (α CD40) S-/(OVA-CpG) expressed significantly higher levels of MHC I and CD86 compared to those stimulated with S-/(OVA-CpG) or a mixture of unconjugated α CD40 and S-/(OVA-CpG) (α CD40 + S-/(OVA-CpG)) (Fig. 38A). BM-DCs stimulated with (α CD40) S-/(OVA-CpG) showed lower expression of CD40 compared to S-/(OVA-CpG). This could be attributed to the cellular internalization of the CD40 receptor following its ligation with α CD40 contained in (α CD40) S-/(OVA-CpG) [232, 233].

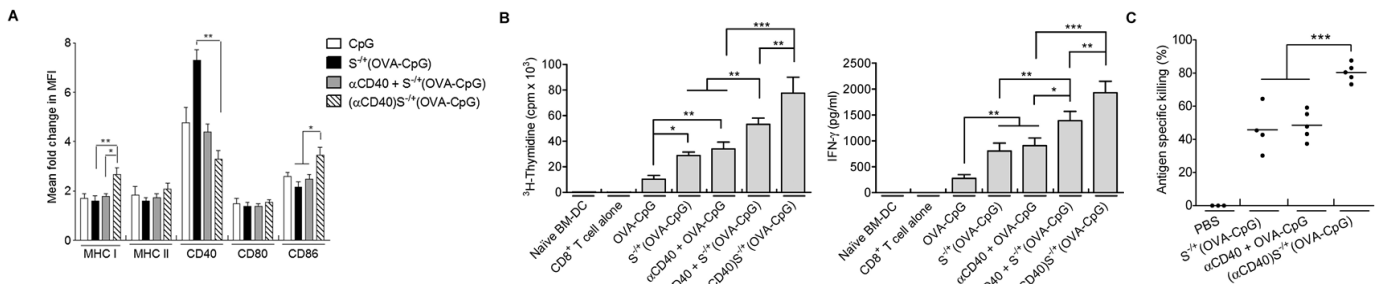


Figure 38: Assessment of immune response induced by (α CD40) S-/(OVA-CpG) in vitro and in vivo. (A) Assessment of BM-DC maturation. BM-DCs were incubated for 24 h with S-/(OVA-CpG), α CD40 + S-/(OVA-CpG) or (α CD40) S-/(OVA-CpG) each contained 0.5 μ g/ml OVA, 0.5 μ g/ml CpG and/or 1.8 μ g/ml α CD40. BM-DCs were stained with fluorescently labelled antibodies and analyzed using flow cytometry. The MFI was measured to assess the fold change in the expression of each marker with respect to naïve BM-DCs. (B) Assessment of OVA presentation. BM-DCs were incubated for 24 h with either 1 μ g/ml OVA (contained in OVA-CpG or S-/(OVA-CpG)) or 0.5 μ g/ml OVA (contained in OVA-CpG + α CD40, S-/(OVA-CpG) + α CD40 or (α CD40) S-/(OVA-CpG)). S-/+ unconjugated or conjugated α CD40 was used at 1.8 μ g/ml. BM-DCs were co-cultured with CD8+ T cells. (Left) CD8+ T cell proliferation. CD8+ T were pulsed with 3H-thymidine and proliferation was measured. (Right) IFN- γ quantification. The content of IFN- γ in the supernatants of the proliferating CD8+ T cell was quantified using ELISA. Measurements were performed in triplicates for each condition, results represent the mean \pm S.D. (C) CTL response. C57BL/6 mice (n = 3-5) were immunized, via footpad injection, with either 6 μ g OVA (contained in S-/(OVA-CpG)) or 3 μ g OVA (contained in OVA-CpG + α CD40 or (α CD40) S-/(OVA-CpG)). The S-/+ unconjugated or conjugated α CD40 was 10 μ g. Each dot represents killing of target cells by each mouse, the mean value for each treatment is shown as a horizontal bar. *P < 0.05, **P < 0.01, ***P < 0.001.

Given the increase in MHC I expression, OVA presentation to CD8+ T cell was assessed, following stimulation with (α CD40) S-/(OVA-CpG). In order to assess the synergy provided by the CpG and α CD40 loaded onto S-/, BM-DCs were incubated with (α CD40) S-/(OVA-CpG) containing half the OVA and CpG amounts present in S-/(OVA-CpG) treatment (Fig. 38B). Higher CD8+ T cell proliferation was induced following stimulation with (α CD40) S-/(OVA-CpG) containing 0.5 μ g/ml of both OVA and CpG compared to the control treatment α CD40 + S-/(OVA-CpG), and S-/(OVA-CpG) treatment that contained 1 μ g/ml of both OVA and CpG. Production of IFN- γ by the stimulated CD8+ T cells correlated well with their pattern of proliferation. These observations reflected the significance of α CD40 conjugation with S-/+ on BM-DC activation.

Immune enhancement induced by (α CD40) S-/(OVA-CpG) was investigated using the in vivo CTL assay. Immunization of C57BL/6 mice with (α CD40)S-/(OVA-CpG) (containing 3 μ g OVA and CpG) led to a robust OVA-specific cellular immune response (80.4% \pm 5.4 antigen-specific killing) (P <

0.0001) compared to the CTL response induced by the control α CD40 + OVA-CpG (containing 3 μ g OVA and CpG) or S-/(OVA-CpG) treatment (containing 6 μ g OVA and CpG) showing 48.6% \pm 8.8 or 46.2% \pm 14.1 antigen-specific killing, respectively (Fig. 38C and Figure 37). Taking the in vitro and in vivo data together we can conclude that inclusion of α CD40 antibody as a second immunoadjuvant resulted in synergy of the MWNT-mediated delivery of OVA-CpG as shown by the marked increase in antigen-specific immune responses at lower OVA and CpG doses.

7.10. α CD40 and OVA-CpG loading onto S-/+ effectively delays the tumour growth in both solid and lung pseudo-metastatic tumour models

The therapeutic efficacy of the conjugates in delaying the growth of a solid tumour was investigated. Immunization of C57BL/6 mice subcutaneously inoculated with Luc-B16F10-OVA cells with S-/(OVA-CpG) containing 12 or 25 μ g of both OVA and CpG led to significant tumour growth retardation compared to unimmunized mice (Figure 39A). Furthermore, administration of S-/(OVA-CpG), containing

25 µg of both OVA and CpG, to mice subcutaneously inoculated with B16 cells (tumour cells which do not express OVA), failed to impede the B16 cells growth (Figure 39B), indicat-

ing that the induced anti-tumour immune response was antigen-specific.

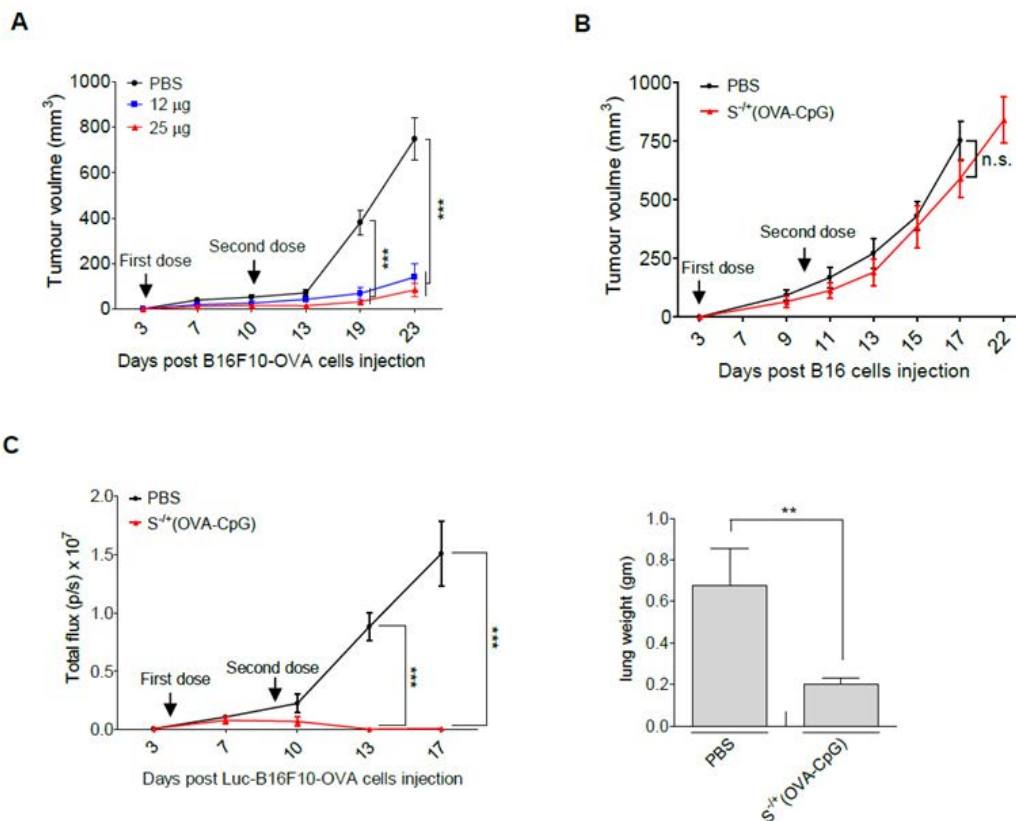


Figure 39: Assessment of anti-tumour immunotherapeutic efficiency of S^{-/+}(OVA-CpG) in subcutaneous or lung pseudo-metastatic tumour models. (A) C57BL/6 mice (n=8) were subcutaneously injected with 2.5×10^5 OVA-B16F10-Luc cells. On the 3rd and 10th days post tumour cells injection, tumour-inoculated mice were immunized via footpad injection with S^{-/+}(OVA-CpG) containing 12 or 25 µg OVA. Tumour volume was monitored using caliper measurement. Results are expressed as mean value \pm SEM. (B) Anti-tumour immune response antigen specificity. C57BL/6 mice (n=8) were subcutaneously injected with 2.5×10^5 B16 cells. On the 3rd and 10th days post tumour cells injection, tumour-inoculated mice were immunized via footpad injection with S^{-/+}(OVA-CpG) containing 25 µg OVA. Tumour volume was monitored using caliper measurement. Results are expressed as mean value \pm SEM. (C) Pseudo-metastatic lung tumour model. C57BL/6 mice (n=6-8) were intravenously injected with 2.5×10^5 OVA-B16F10-Luc cells. On the 4th and 9th days post tumour cells injection, tumour-inoculated mice were immunized via footpad injection with S^{-/+}(OVA-CpG) containing 12 µg OVA. Tumour growth was monitored using whole body imaging. (Left) Quantification of photon flux, expressed as number of photons per second (p/s). Values are expressed as mean value \pm SEM. (Right) The weights of the lung excised from scarified tumour inoculated mice. Values are expressed as mean value \pm S.D. ** P < 0.01, *** P < 0.001.

To determine the ability of (α CD40) S^{-/+}(OVA-CpG) to delay the solid tumour growth at reduced OVA and CpG doses, mice were subcutaneously inoculated with Luc-B16F10-OVA cells and then immunized with (α CD40) S^{-/+}(OVA-CpG), S^{-/+}(OVA-CpG) or other controls at 6 µg of both OVA and CpG. As demonstrated in Fig. 40A, immunization with S^{-/+}(OVA-CpG) at 6 µg OVA did not significantly delay the tumour growth compared to unimmunized mice. However, immunization with (α CD40) S^{-/+}(OVA-CpG) led to significant tumour growth retardation compared to unim-

munized mice, and mice immunized with S^{-/+}(OVA-CpG). Immunization with α CD40 + S^{-/+}(OVA-CpG) failed to delay the tumour growth to the same extent as (α CD40) S^{-/+}(OVA-CpG), highlighting the increase in α CD40-mediated immune enhancement achieved on incorporating α CD40 onto S^{-/+} in addition to OVA-CpG. Additionally, vaccination with (α CD40) S^{-/+}(OVA-CpG) prolonged the tumour-inoculated mice survival in a significant manner compared to the other treatments (Fig. 40A).

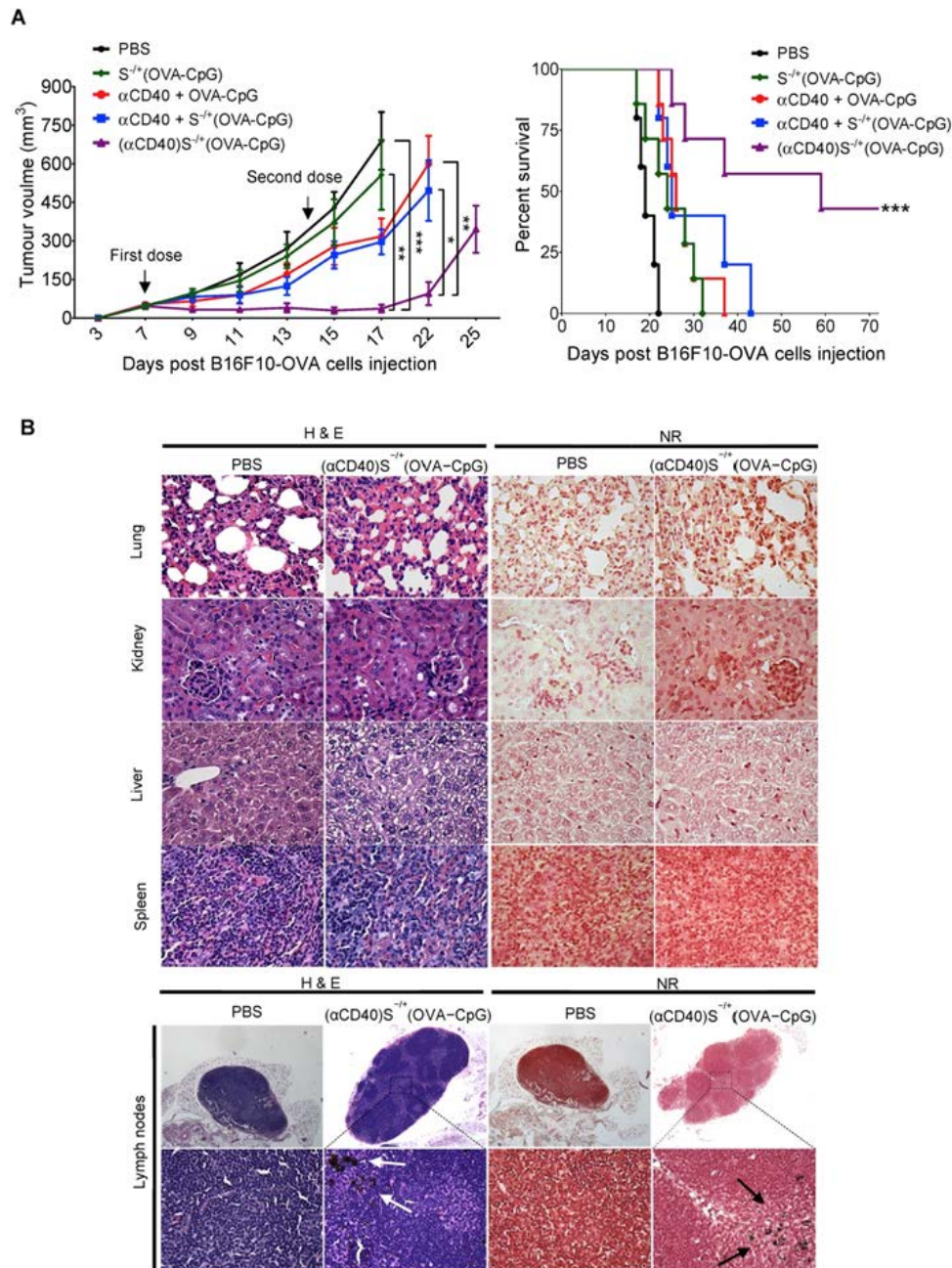


Figure 40: Assessment of anti-tumour response in subcutaneous tumour models. C57BL/6 mice ($n = 7$) were subcutaneously injected with 2.5×10^5 OVA-B16F10-Luc cells. On the 7th and 14th days post tumour cells injection, tumour-inoculated mice were immunized via footpad injection with the indicated treatments, each contained $6 \mu\text{g}$ OVA. (A) Tumour growth curve and mice survival. (Left) Tumour growth monitored by caliper measurement. Values are expressed as mean value \pm SEM. (Right) Tumour-inoculated mice survival. * $P < 0.05$, ** $P < 0.01$, *** $P < 0.001$. (B) Histological analysis. The main organs and lymph nodes excised from scarified subcutaneous tumour inoculated mice stained with haematoxylin and eosin (H & E) (left) or neutral red (NR) (right). Images were captured at $\times 40$ magnification. S^{-/+} appeared as dark black aggregates (arrows).

No changes in the histological features of the excised organs between the untreated and treated tumour bearing mice were observed indicating lack of organ toxicity (Fig. 40B). Dark black aggregates, which were absent in naïve mice, were detected in the popliteal lymph nodes from mice immunized with $(\alpha\text{CD40})\text{S}^{-/+}(\text{OVA-CpG})$, suggesting drainage of S^{-/+} into the popliteal lymph nodes.

Therapy studies were then performed in the more challenging pseudo-metastatic lung tumour model. The conjugates, containing $6 \mu\text{g}$ of both OVA and CpG, were administered to C57BL/6 mice previously intravenously inoculated with OVA-B16F10-Luc cells. Smaller bioluminescence signals and lung weights were observed in mice immunized with $(\alpha\text{CD40})\text{S}^{-/+}(\text{OVA-CpG})$ compared to S^{-/+}(OVA-CpG) treated mice (Fig. 41).

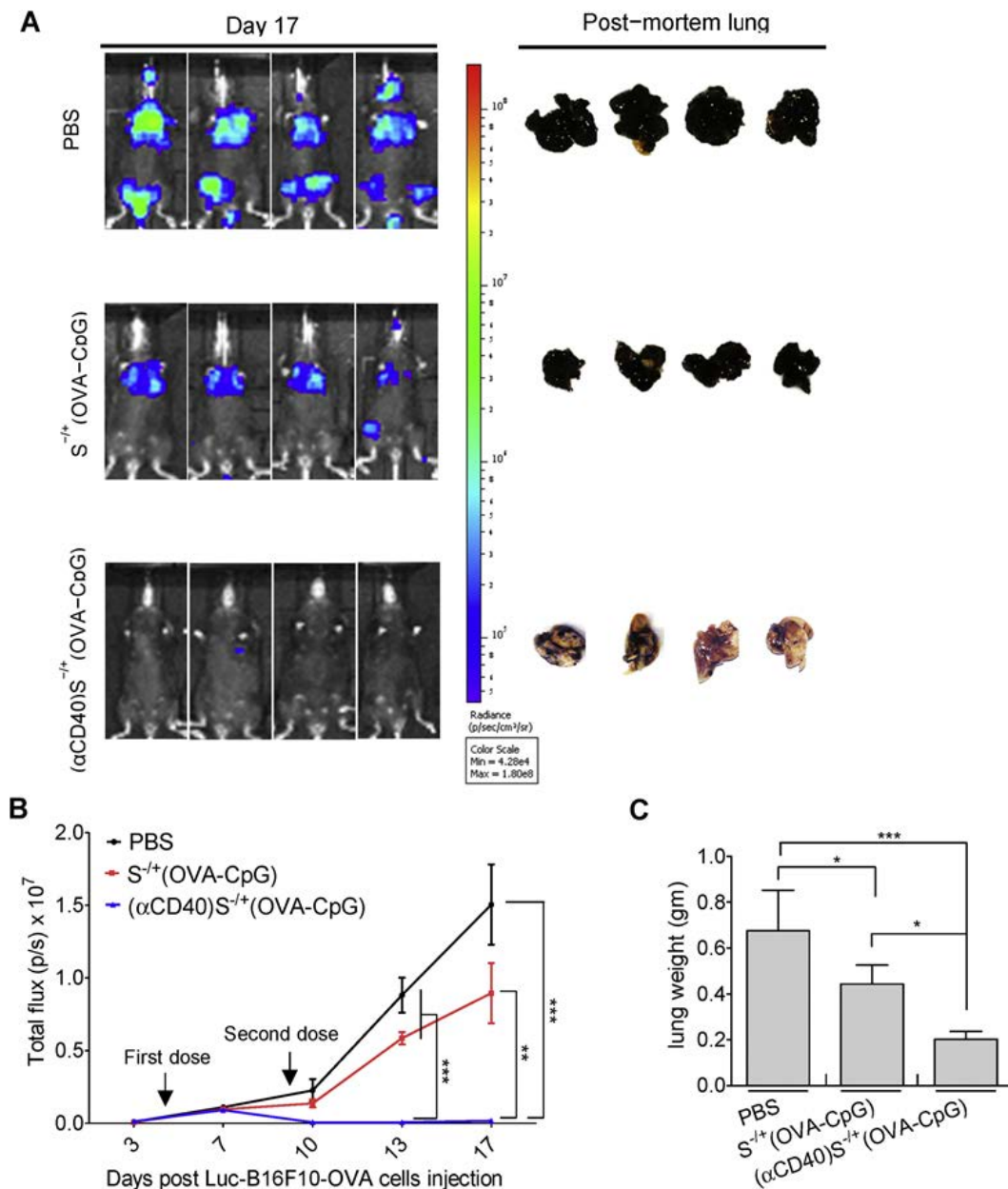


Figure 41: Assessment of anti-tumour response in lung pseudo-metastatic tumour models. C57BL/6 mice ($n = 6-8$) were intravenously injected with 2.5×10^5 OVA-B16F10-Luc cells. On the 4th and 9th days post tumour cells injection, tumour-inoculated mice were immunized via footpad injection with the indicated treatments, each contained $6 \mu\text{g}$ OVA. (A) Lung pseudo-metastatic tumour model. Tumour growth was monitored by whole body imaging. Representative images for in vivo bioluminescent imaging and the corresponding post-mortem lung photographs are shown. (B) Quantification of photon flux expressed as number of photons per second (p/s). Values are expressed as mean value \pm SEM. (C) The weights of the lung excised from scarified tumour inoculated mice. Values are expressed as mean value \pm S.D. * $P < 0.05$, ** $P < 0.01$, *** $P < 0.001$.

From the data [212] it has been concluded that vaccination with $(\alpha\text{CD40})\text{S}^{-/+}(\text{OVA-CpG})$ efficiently delayed the OVA-B16F10-Luc tumour growth in both solid and pseudo-metastatic tumour models, consistent with the immune enhancements observed in vitro and in vivo.

8. CNTs induce co-delivery systems vectors for antigens

One of the purposes of using delivery vectors for antigens is to improve the antigen uptake by the antigen presenting cells (APCs) in order to increase the intracellular antigen concentration, thus the density of antigen presented

by the APCs to T cells. It has been previously reported that polymeric spherical nanoparticles, e.g. PLGA nanoparticles, mainly utilize energy-dependent mechanisms of cellular uptake rather than energy-independent ones [248-250]. The reported findings that demonstrated the CNTs' ability to enter the cells via more than one route i.e. energy-dependent and/or passive routes, may suggest that CNTs can deliver higher amounts of antigens into the APCs compared to spherical nanoparticles. However, comparative studies need to be carried out to investigate the cellular uptake of CNTs versus the extensively studied spherical nanoparticles, e.g. PLGA nanoparticles and liposomes, by the APCs and the ensuing effects on the magnitude of immune response elicited

against incorporated antigen [216-218].

Covalent conjugation of OVA and CpG and their loading onto S-/+ improved OVA presentation in vitro by BM-DCs and efficiently elevated the magnitude of OVA-specific immune response in vivo. Additionally, the presence of α CD40 in S-/+ containing conjugated OVA-CpG led to i) more advanced augmentation of the OVA-specific immune response in vitro and in vivo, and ii) delayed growth of OVA-expressing B16F10 cells effectively in both subcutaneous and lung pseudo-metastatic tumour models, at reduced OVA and CpG doses.

It has been initially proposed [212] two distinct approaches for the concomitant delivery of the model antigen OVA and CpG using S-/+ to APCs. Mixing S-/+ with OVA and CpG was the first method, yielding (OVA)S-/(CpG); however, the loading of OVA and CpG onto each S-/+ was uncontrolled. In other words, the prepared (OVA)S-/(CpG) might possess lower OVA and CpG co-loading onto each S-/+ compared to S-/(OVA-CpG), and the formation of OVA or CpG only-conjugated S-/+ was also possible. Accordingly, the other approach was loading both agents in the form of the chemical conjugate, OVA-CpG, to ensure the co-incorporation of OVA and CpG onto the same S-/+ (S-/(OVA-CpG)). PAGE gel results confirmed that OVA contained in S-/(OVA-CpG) was in the CpG-conjugated form. (OVA)S-/(CpG) or S-/(OVA-CpG) elicited higher immune response potency in vitro and in vivo, compared to their control treatments, namely the mixture of unconjugated OVA and CpG or OVA-CpG, respectively. This was in agreement with the previously reported benefits of CNTs as a delivery vehicle for antigens [219, 221] or immunoadjuvants in vitro and in vivo [223, 224].

The co-delivery of antigen and CpG to APC has also been demonstrated using other particulate delivery systems. For instance, mice immunization with microparticles co-encapsulating OVA and CpG increased the anti-OVA antibodies [251] and CD8+ T cell responses [252, 253], and utilization of gold nanoclusters for the co-delivery of OVA-derived peptide and CpG augmented the production of anti-OVA antibodies in mice [254].

In a study by de Faria et al., OVA and CpG were co-incorporated onto MWNTs by mixing MWNTs with un-conjugated OVA and CpG, yielding a conjugate that induced higher immune response compared to mixture of unconjugated OVA and CpG (MWNT-free) in vivo [135]. It has been utilized the same approach to prepare (OVA)S-/(CpG), but additionally, it has been introduced in that study [212] a more robust approach for comparison, where a covalently conjugated OVA and CpG were loaded onto MWNTs yielding S-/(OVA-CpG). When, comparing the two MWNT based conjugates for OVA and CpG co-delivery, S-/(OVA-CpG) resulted in better OVA presentation by BM-DCs than (OVA)S-/(CpG). This could be attributed to the better capability of S-/(OVA-CpG), compared to (OVA)S-/(CpG), to co-internalize OVA and CpG into the same BM-DC. The enhanced OVA presentation might account for the higher cellular and humoral immune responses elicited by vaccination of C57BL/6 mice with S-/(OVA-CpG). Similar to our findings, but without

the use of a delivery system, previous studies have demonstrated that mice immunization with covalently conjugated OVA and CpG induced higher OVA-specific immune response compared to immunization with a mixture of unconjugated OVA and CpG [227, 240].

Schlosser et al. demonstrated that mixing PLGA polymer with OVA and CpG yielded microparticles that were described as OVA and CpG co-encapsulating microparticles, these microparticles induced higher CD8+ T cell response in vitro and in vivo in contrast to a mixture of OVA only-encapsulating microparticle and CpG only-encapsulating microparticle [255]. Similarly, Li et al. mixed lipid polymer with HER-2/neu derived peptide and CpG to yield liposomes that were referred to as antigen and CpG co-encapsulating liposomes, mice immunization with these liposomes induced higher immune response compared to a mixture of antigen-containing liposome and CpG-containing liposome [256]. The approach applied in these studies for antigen and CpG co-incorporation into a delivery system by mixing polymers with unconjugated antigen and CpG is similar, in its basic principle, to the one we followed for the synthesis of (OVA)S-/(CpG) but not S-/(OVA-CpG). These studies highlighted the importance of antigen and CpG co-delivery using a delivery system by comparing co-incorporated to separately incorporated antigen and CpG. However, the study [212] has been introduced a more advanced line of complexity by contrasting two methods for antigen and CpG concomitant delivery using a delivery vehicle as demonstrated by (OVA)S-/(CpG) versus S-/(OVA-CpG).

Previous studies reported the use of spherical-shaped delivery systems to improve antigen and α CD40 co-delivery. demonstrated that co-encapsulation of tetanus toxoid and α CD40 in liposomes augmented the antigen-specific antibody response in BALB/c mice, and [257]. reported an increase in CD8+ T cell response following mice immunization with α CD40-coated PLGA nanoparticles co-incorporating an oncoprotein and ligands for TLR2 and TLR3 [258]. Instead of harnessing the conventional spherical particulate delivery systems to co-deliver CpG and α CD40, it has been utilized an emerging cylindrical vector, namely the MWNTs, as a nano-carrier for both CpG and α CD40. In addition, the therapeutic outcome provided by the MWNT-delivered CpG and α CD40 was not only evaluated in a standard subcutaneous tumour model but also lung pseudo-metastatic tumour model.

The intensified strength of OVA specific-CTL response induced by vaccination of C57BL/6 mice with (α CD40) S-/(OVA-CpG) might be assigned to the better ability of this conjugate to induce DC maturation and to further fortify OVA presentation as observed in vitro. Stimulation of APC with α CD40 has been shown to upregulate MHC I and CD86 expression [259, 260]. Intracellular signaling induced by ligation of CD40 receptor with α CD40 requires CD40 receptor cross-linking that increases, accordingly, with the increase in the number of α CD40 interacting at the cell surface [261]. The observed better ability of (α CD40) S-/(OVA-CpG) than α CD40 + S-/(OVA-CpG) in upregulating MHC I and CD86

expression by BM-DCs could be attributed to the more efficient CD40 receptor cross-linking by the multiple, surface-bound, α CD40 contained in (α CD40) S-/(OVA-CpG) [262]. Expression of CD86 by APCs was increased following stimulation with α CD40-coated polymeric nanoparticles or silicon nanoparticles compared to free α CD40 [262, 263].

The fact that the MWNT-based conjugates were detected in the lymph nodes was in agreement with our previous study. Where, we were able to detect the presence of S-/+ and the processing of S-/+ conjugated OVA in the CD11c+ve DCs subsets in the popliteal lymph nodes [219]. These observations reflected the proficiency of MWNT as vaccine delivery vectors. Since efficient antitumour-immune response induction demands antigen trafficking through the lymphatic vessels and internalization by the lymph node-residing CD8+ DC, which is the only DC subset capable of inducing CD8+ T cell response in vivo [264].

Efficient eradication of B16-OVA or B16F10-OVA tumours in mice has been found to be associated with the cytolytic activity of CD8+ T cells demonstrated by OVA-specific CTL response [253, 258, 265]. The fact that lower OVA and CpG doses were required by (α CD40) S-/(OVA-CpG) than S-/(OVA-CpG) to induce strong anti-tumour response indicates the higher potency and better efficacy of the former conjugate in vivo. Collectively, the results shown in that study [212] in the chapter highlighted the exploitation of MWNTs as antigen and immunoadjuvants nanocarrier for the purpose of inducing potent anti-tumour immune response.

9. Future Perspective of CNTs as Vaccine Delivery Systems

As with all cancer vaccines their success, or failure, is dependent on finding the right combination of antigen, adjuvant and delivery vehicle. The future of CNTs as a delivery platform/adjuvant is dependent on their relative potency compared to other modalities while the future of the field itself is inextricably linked to the identification of novel antigens or vaccine regimes. In the immediate future, CNTs need to be comprehensively assessed against other vaccine formulations to establish where they belong on the 'spectrum of adjuvanticity'. These studies are seldom performed (or at least seldom published) on novel adjuvant candidates due to the fear of coming up short against current formulations and thus losing funding/interest. However, it has made assessing whether an adjuvant is clinically viable over an alternate, near impossible.

Whether the outcomes of these studies are positive or negative it should be noted CNTs have two distinct advantages over traditional adjuvants; the first is their mode of entry into cells. As previously reviewed CNTs have direct access to the cytosol through the proposed nano-needle mechanism. The implications of this in the context of vaccine adjuvants should not be understated. The ability to initiate a strong cytotoxic MHC class I restricted immune response to a soluble antigen has been seen as the Holy Grail for vaccine adjuvants. This is especially the case for cancer vaccines but also for vaccines against certain infectious agents [266, 267].

In addition, efficient delivery of payload to the cytosol may make other types of vaccines, specifically nucleic acid-based vaccine including DNA and recently mRNA vaccines, more viable. The nano-needle mechanism is poorly understood with many groups reporting differing outcomes following administration of CNTs depending on a multitude of factors such as surface chemistry, size and aspect ratios as previously discussed. The first step in the rational design of a CNT based delivery vehicle should be the systematic evaluation of physical traits and surface modifications in order to improve cytosolic delivery. It has been looked into some of the modifications of CNTs and has shown that relatively minor changes in structure can cause vast differences in immunogenicity though we have not been able to attribute this to improved cytosolic delivery [136]. Future work should continue and expand upon this.

The second key advantage of CNTs over traditional carriers is their large surface area. According to the current rationale for the use of CNTs, this enables the delivery of large amounts of antigen/adjuvant to APCs. Expanding on this theory, it has recently been shown that particulates can bind to antigen within the tumour environments following intratumoral inoculation [268]. For instance, Min et al. recently demonstrated that an injection of nanoparticle intratumorally, prior to radio ablation of the tumour, served to enhance the so called 'abscopal effect': the phenomenon whereby following the ablation of a tumour a systemic immune response is triggered against the released antigen/immune stimulants resulting in remission of distal tumours. One hypothesis is that the particles are retained within the tumour 'mopping up' antigen and immune active molecules. When the tumour is subsequently ablated the particles are released and are taken up by APCs in the tumour-draining lymph nodes [268]. The high surface area of the CNTs and the ability to form strong non-covalent associations with proteins specifically lends them to this purpose. Indeed, it has been shown that GO formulated with CpG can be used for photothermal ablation, though the assessment of the abscopal effect was not measured, there is clearly an immune component [269]. There have been some studies assessing the 'protein corona' following administration of CNT intravenously; it would be interesting to perform these studies following intra-tumoral administration to determine how much tumour antigen can be absorbed directly from the tumour tissue in comparison to other carriers [270, 271]. Supporting this general hypothesis, it has been shown that CNTs, when formulated in vitro with tumour cell lysate, can serve to protect from tumour challenge [272].

Another intra-tumoral approach is the concept of 'in situ' vaccination. Here an agent is injected into the tumour leading to activation of the immune system to antigens present on the tumour/in the microenvironment. This relatively simple concept has led to miraculous results preclinically, notably the use of CpG and anti-OX40 in combination is particularly potent [273]. It would be interesting to compare anti-OX40 to anti-CD40 antibody plus CpG in combination with CNT in a preclinical model to identify which approach is more efficient in eliciting anti-tumour immunity. It also would be in-

teresting to compare the efficacy of synthetic CNT vaccines to biological vaccines such as plant virus-based vaccines. Filamentous and spherical plant viruses have been explored as in situ vaccines [274, 275]. In contrast to plant viruses, which are complex biological entities, CNTs may provide a better-controllable synthetic platform to explore the relationship between morphology and immunogenicity. In addition, CNT vaccines allow different combinations of TLR agonists to be used, and thereby enables the dissection of the requirements for optimal formulation.

In more general terms, it is likely that all future cancer vaccine candidates will be trialed in combination with a checkpoint inhibitor at some stage during their clinical assessment. To date, two checkpoint inhibitors have been clinically approved and these are targeted against inhibitory molecules PD-1 and CTLA4 and their purported mechanism has been reviewed elsewhere [25]. However, new classes of stimulatory checkpoint molecules including agonistic anti-OX40 and anti-4-1-BBL antibodies are showing efficacy in preclinical trials [139]. This has led to the concept of an 'immune switch'; this is a biomaterial containing both an immune stimulatory antibody as well as an anti-inhibitory antibody [276]. In that study the authors show that the immune switch is more potent than either of the two antibodies when administered in their soluble form. Again, due to their high surface area and ease at forming non-covalent attachments to proteins, CNTs could be the preferred vehicle for this purpose [121]. Other than checkpoint blockade it could be argued that the generation of personalized vaccines becomes more feasible as DNA sequencing becomes faster and cheaper. The antigenic payload of personalized vaccines will likely be peptides or nucleic acid due to ease of synthesis and quality control. However, both of these modalities are typically poorly immunogenic and require a delivery platform and adjuvant. In a proof of concept study the group of Kuai et al. sequenced murine tumours to detect mutations and these neo peptides were synthesized and loaded on to lipid nano discs [277]. The resulting particles were shown to protect against tumour challenge. In this approach it could be envisioned that the adjuvant/delivery platform will be prepared in a ready to use 'off the shelf' format and simply mixed with individual tumour neo antigens as determined by high throughput sequencing. CNTs represent a candidate platform for this approach as they can be synthesised in bulk and stored for long durations with little degradation, furthermore they can be made positively charged or amine reactive for binding of nucleic acid or peptide respectively as previously discussed.

10. Conclusions

Use of CNTs can improve immune response. Vaccine delivery can be achieved by linking antigen to CNT and by inducing antibody response [278]. Tailoring the physical properties of MWNT-based vaccine delivery systems may increase their efficiency in inducing potent T cell immune responses against challenging infectious or cancer diseases. Although CNTs demonstrate practical applicability in all facets of science, be it biology, physics, medicine, nanotechnology, catalysis, or materials science, its long-term implications need to

be assessed from the perspective of human health to environmental risks. The long-term fate of CNTs released into the environment depends on the structural, morphological and synthetic treatments [278]. Methods of reducing toxicity in vivo and in vitro can be envisaged via functionalization of CNT. Proper assessment and in-depth study are essential to render nanotubes useful for diverse and environmentally benign applications.

It has been investigated the potential application of SWCNTs, graphene-based nanomaterials and its prototypes in TB and cancer chemotherapy using conventional DFT methods supported by molecular docking and MD simulation on the nature of interaction of therapeutic drug functionalized SWCNTs/graphene with the binding site of the protein. The functionalization of SWCNTs with therapeutic drugs using covalent and noncovalent schemes was adopted to investigate the drug binding with the nanotube and the stability of the conjugated complexes. DFT results supported by molecular docking and MD simulation help in contemplating the feasibility of SWCNT-based novel drug delivery in cancer and TB therapy.

The better understanding of tumour immunology has allowed development of cancer vaccines. However, tumour-induced immunosuppression has constituted a major hurdle to the capacity of these formulations to enhance the immune response. Attempts applied to augment anti-tumour immune response potency have included the delivery of the aforementioned vaccine formulations via nano-carriers. CNTs demonstrated characteristic cellular uptake properties that encouraged the exploitation of their nano-needle properties. Pre-clinical studies highlight that CNTs represent a competent cancer vaccine delivery system. Nevertheless, future studies are required to investigate the uniqueness that these CNTs possess as vaccine carrier over other vectors such as for example liposomes. In addition, despite the encouraging results reported in pre-clinical studies, clinical studies are hindered by the conflicting reports on CNTs biocompatibility and biodegradability. Finally, fortification of the vaccine formulations via the inclusion of multiple adjuvants, APCs targeting ligands and combining this approach with a checkpoint inhibitor, could dramatically reduce the required CNTs doses and encourage their clinical assessment.

OVA incorporation onto the MWNT in the form of CpG-conjugated OVA improved the CpG-mediated enhancements of OVA-specific immune response in vitro and in vivo. Furthermore, the utilization of MWNTs as vaccine delivery vector has intensified the CpG and α CD40-derived synergism that markedly retarded the OVA-B16F10 growth in the tested tumour models. The MWNT-delivered immune-based combinatorial therapeutic approach presented in this study could be exploited for potent anti-tumour immune response induction against challenging cancer diseases. Vaccine delivery can be achieved by linking antigen to CNT and by inducing antibody response [279]. In summary Use of CNTs can improve immune response.

References

1. Gottardi, R., Douradinha, B. (2013). Carbon nanotubes as a novel tool for vaccination against infectious diseases and cancer. *Journal of nanobiotechnology*, 11(1), 1-7.
2. Pondman, K. M., Sobik, M., Nayak, A., Tsolaki, A. G., Jäkel, A., et al. (2014). Complement activation by carbon nanotubes and its influence on the phagocytosis and cytokine response by macrophages. *Nanomedicine: nanotechnology, biology and medicine*, 10(6), 1287-1299.
3. He, H., Pham-Huy, L. A., Dramou, P., Xiao, D., Zuo, P., et al. (2013). Carbon nanotubes: applications in pharmacy and medicine. *BioMed research international*, 2013
4. Rosen, Y., Mattix, B., Rao, A., Alexis, F. (2011). Carbon nanotubes and infectious diseases. In *Nanomedicine in Health and Disease*, RJ Hunter, Ed, 249-267.
5. Pantarotto, D., Partidos, C. D., Hoebeke, J., Brown, F., Kramer, E. D., et al. (2003). Immunization with peptide-functionalized carbon nanotubes enhances virus-specific neutralizing antibody responses. *Chemistry biology*, 10(10), 961-966.
6. Salvador-Morales, C., Flahaut, E., Sim, E., Sloan, J., Green, M. L., et al. (2006). Complement activation and protein adsorption by carbon nanotubes. *Molecular immunology*, 43(3), 193-201.
7. Bianco, A., Hoebeke, J., Godefroy, S., Chaloin, O., Pantarotto, D., et al. (2005). Cationic carbon nanotubes bind to CpG oligodeoxynucleotides and enhance their immunostimulatory properties. *Journal of the American Chemical Society*, 127(1), 58-59.
8. Nahar, M., Dutta, T., Murugesan, S., Asthana, A., Mishra, D., et al. (2006). Functional polymeric nanoparticles: an efficient and promising tool for active delivery of bioactives. *Critical Reviews™ in Therapeutic Drug Carrier Systems*, 23(4).
9. McDevitt, M. R., Chattopadhyay, D., Kappel, B. J., Jaggi, J. S., Schiffman, S. R., et al. (2007). Tumor targeting with antibody-functionalized, radiolabeled carbon nanotubes. *Journal of Nuclear Medicine*, 48(7), 1180-1189.
10. Foldvari, M., Bagonluri, M. (2008). Carbon nanotubes as functional excipients for nanomedicines: II. Drug delivery and biocompatibility issues. *Nanomedicine: Nanotechnology, Biology and Medicine*, 4(3), 183-200.
11. Mac Manus, M., Lamborn, K., Khan, W., Varghese, A., Graef, L., et al. (1997). Radiotherapy-associated neutropenia and thrombocytopenia: analysis of risk factors and development of a predictive model. *Blood, The Journal of the American Society of Hematology*, 89(7), 2303-2310.
12. De Ruyscher, D., Dehing, C., Bremer, R. H., Bentzen, S. M., Koppe, F., et al. (2007). Maximal neutropenia during chemotherapy and radiotherapy is significantly associated with the development of acute radiation-induced dysphagia in lung cancer patients. *Annals of oncology*, 18(5), 909-916.
13. Peters III, W. A., Liu, P. Y., Barrett, R. J., Stock, R. J., Monk, B. J., et al. (2000). Concurrent chemotherapy and pelvic radiation therapy compared with pelvic radiation therapy alone as adjuvant therapy after radical surgery in high-risk early-stage cancer of the cervix. *Obstetrical Gynecological Survey*, 55(8), 491-492.
14. Crawford, J., Dale, D. C., Lyman, G. H. (2004). Chemotherapy-induced neutropenia: risks, consequences, and new directions for its management. *Cancer*, 100(2), 228-237.
15. Dunn, G. P., Bruce, A. T., Ikeda, H., Old, L. J., Schreiber, R. D. (2002). Cancer immunoediting: from immunosurveillance to tumor escape. *Nature immunology*, 3(11), 991-998.
16. I. Mellman, I., Coukos, G., Dranoff, G. (2011). Cancer immunotherapy comes of age. *Nature*, 480(7378), 480-489.
17. Parish, C. R. (2003). Cancer immunotherapy: the past, the present and the future. *Immunology and cell biology*, 81(2), 106-113.
18. Coulie, P. G., Van den Eynde, B. J., Van Der Bruggen, P., Boon, T. (2014). Tumour antigens recognized by T lymphocytes: at the core of cancer immunotherapy. *Nature Reviews Cancer*, 14(2), 135-146.
19. Stratton, M. R., Campbell, P. J., Futreal, P. A. (2009). The cancer genome. *Nature*, 458(7239), 719-724.
20. Schlom, J., Arlen, P. M., Gulley, J. L. (2007). Cancer vaccines: moving beyond current paradigms. *Clinical Cancer Research*, 13(13), 3776-3782.
21. Pagès, F., Berger, A., Camus, M., Sanchez-Cabo, F., Costes, A., R., et al. (2005). Effector memory T cells, early metastasis, and survival in colorectal cancer. *New England journal of medicine*, 353(25), 2654-2666. Z. Trajanoski, W.H. Fridman, J. Galon, Effector memory T cells, early metastasis, and survival in colorectal cancer, *N. Engl. J. Med.* 353 (2005) 2654-2666.
22. Palucka, K., Banchereau, J. (2012). Cancer immunotherapy via dendritic cells. *Nature Reviews Cancer*, 12(4), 265-277.
23. Finn, O. J. (2003). Cancer vaccines: between the idea and the reality. *Nature Reviews Immunology*, 3(8), 630-641.
24. . Zou, W. (2005). Immunosuppressive networks in the tumour environment and their therapeutic relevance. *Nature reviews cancer*, 5(4), 263-274.
25. Ribas, A., Wolchok, J. D. (2018). Cancer immunotherapy using checkpoint blockade. *Science*, 359(6382), 1350-1355.
26. Hirsch, A. (2010). The era of carbon allotropes. *Nature materials*, 9(11), 868-871.
27. Kroto, H. W., Heath, J. R., O'Brien, S. C., Curl, R. F., Smalley, R. E. (1985). C60: Buckminsterfullerene. *nature*, 318(6042), 162-163.
28. Novoselov, K. S., Geim, A. K., Morozov, S. V., Jiang, D. E., Zhang, Y., et al. (2004). Electric field effect in atomically thin carbon films. *science*, 306(5696), 666-669.
29. Iijima, S. (1991). Helical microtubules of graphitic carbon. *nature*, 354(6348), 56-58.
30. Thostenson, E. T., Ren, Z., Chou, T. W. (2001). Advances in the science and technology of carbon nanotubes and their composites: a review. *Composites science and technology*, 61(13), 1899-1912.
31. Xu, L., Liu, Y., Chen, Z., Li, W., Liu, Y., et al. (2013). Morphologically virus-like fullerene nanoparticles act as the dual-functional nanoadjuvant for HIV-1 vaccine. *Advanced materials*, 25(41), 5928-5936.
32. Trewyn, B. G., Nieweg, J. A., Zhao, Y., Lin, V. S. Y. (2008). Biocompatible mesoporous silica nanoparticles with

- different morphologies for animal cell membrane penetration. *Chemical Engineering Journal*, 137(1), 23-29.
33. Huang, X., Teng, X., Chen, D., Tang, F., He, J. (2010). The effect of the shape of mesoporous silica nanoparticles on cellular uptake and cell function. *Biomaterials*, 31(3), 438-448.
 34. Mei, K. C., Ghazaryan, A., Teoh, E. Z., Summers, H. D., Li, Y., et al. (2018). Protein-Corona-by-Design in 2D: A Reliable Platform to Decode Bio-Nano Interactions for the Next-Generation Quality-by-Design Nanomedicines. *Advanced Materials*, 30(40), 1802732.
 35. Rubio, N., Mei, K. C., Klippstein, R., Costa, P. M., Hodgins, N., et al. (2015). Solvent-free click-mechanochemistry for the preparation of cancer cell targeting graphene oxide. *ACS applied materials interfaces*, 7(34), 18920-18923.
 36. Mei, K. C., Guo, Y., Bai, J., Costa, P. M., Kafa, H., et al. (2015). Organic solvent-free, one-step engineering of graphene-based magnetic-responsive hybrids using design of experiment-driven mechanochemistry. *ACS applied materials interfaces*, 7(26), 14176-14181.
 37. Mei, K. C., Rubio, N., Costa, P. M., Kafa, H., Abbate, V., et al. (2015). Synthesis of double-clickable functionalised graphene oxide for biological applications. *Chemical Communications*, 51(81), 14981-14984.
 38. Yue, H., Wei, W., Gu, Z., Ni, D., Luo, N., et al. (2015). Exploration of graphene oxide as an intelligent platform for cancer vaccines. *Nanoscale*, 7(47), 19949-19957.
 39. Sinha, A., Cha, B. G., Choi, Y., Nguyen, T. L., Yoo, P. J., et al. (2017). Carbohydrate-functionalized rGO as an effective cancer vaccine for stimulating antigen-specific cytotoxic T cells and inhibiting tumor growth. *Chemistry of Materials*, 29(16), 6883-6892.
 40. Zhang, X., Hu, W., Li, J., Tao, L., Wei, Y. (2012). A comparative study of cellular uptake and cytotoxicity of multi-walled carbon nanotubes, graphene oxide, and nanodiamond. *Toxicology Research*, 1(1), 62-68.
 41. Singh, P., Campidelli, S., Giordani, S., Bonifazi, D., Bianco, A., et al. (2009). Organic functionalization and characterization of single-walled carbon nanotubes. *Chemical Society Reviews*, 38(8), 2214-2230.
 42. Tasis, D., Tagmatarchis, N., Bianco, A., Prato, M. (2006). Chemistry of carbon nanotubes. *Chemical reviews*, 106(3), 1105-1136.
 43. Liu, J., Rinzler, A. G., Dai, H., Hafner, J. H., Bradley, R. K., et al. (1998). Fullerene pipes. *Science*, 280(5367), 1253-1256.
 44. Ramanathan, T., Fisher, F. T., Ruoff, R. S., Brinson, L. C. (2005). Amino-functionalized carbon nanotubes for binding to polymers and biological systems. *Chemistry of Materials*, 17(6), 1290-1295.
 45. Zheng, M., Jagota, A., Semke, E. D., Diner, B. A., McLean, R. S., et al. (2003). DNA-assisted dispersion and separation of carbon nanotubes. *Nature materials*, 2(5), 338-342.
 46. Wang, X., Xia, T., Ntim, S. A., Ji, Z., George, S., et al. (2010). Quantitative techniques for assessing and controlling the dispersion and biological effects of multiwalled carbon nanotubes in mammalian tissue culture cells. *ACS nano*, 4(12), 7241-7252.
 47. Kafa, H., Wang, J. T. W., Rubio, N., Klippstein, R., Costa, P. M., et al. (2016). Translocation of LRP1 targeted carbon nanotubes of different diameters across the blood-brain barrier in vitro and in vivo. *Journal of Controlled Release*, 225, 217-229.
 48. Rubio, N., Hirvonen, L. M., Chong, E. Z., Wang, J. T. W., Bourgognon, M., et al. (2015). Multiphoton luminescence imaging of chemically functionalized multi-walled carbon nanotubes in cells and solid tumors. *Chemical Communications*, 51(45), 9366-9369.
 49. Summers, H. D., Rees, P., Wang, J. T., Al-Jamal, K. T. (2017). Spatially-resolved profiling of carbon nanotube uptake across cell lines. *Nanoscale*, 9(20), 6800-6807.
 50. Cartiera, M. S., Johnson, K. M., Rajendran, V., Caplan, M. J., Saltzman, W. M. (2009). The uptake and intracellular fate of PLGA nanoparticles in epithelial cells. *Biomaterials*, 30(14), 2790-2798.
 51. Mao, S., Germershaus, O., Fischer, D., Linn, T., Schnepf, R., Kissel, T. (2005). Uptake and transport of PEG-graft-trimethyl-chitosan copolymer-insulin nanocomplexes by epithelial cells. *Pharmaceutical research*, 22, 2058-2068.
 52. Shi Kam, N. W., Jessop, T. C., Wender, P. A., Dai, H. (2004). Nanotube molecular transporters: internalization of carbon nanotube-protein conjugates into mammalian cells. *Journal of the American chemical society*, 126(22), 6850-6851.
 53. Kam, N. W. S., Liu, Z., Dai, H. (2005). Functionalization of carbon nanotubes via cleavable disulfide bonds for efficient intracellular delivery of siRNA and potent gene silencing. *Journal of the American Chemical Society*, 127(36), 12492-12493.
 54. Cherukuri, P., Bachilo, S. M., Litovsky, S. H., Weisman, R. B. (2004). Near-infrared fluorescence microscopy of single-walled carbon nanotubes in phagocytic cells. *Journal of the American Chemical Society*, 126(48), 15638-15639.
 55. Pantarotto, D., Briand, J. P., Prato, M., Bianco, A. (2004). Translocation of bioactive peptides across cell membranes by carbon nanotubes. *Chemical communications*, (1), 16-17.
 56. Lopez, C. F., Nielsen, S. O., Moore, P. B., Klein, M. L. (2004). Understanding nature's design for a nanosyringe. *Proceedings of the National Academy of Sciences*, 101(13), 4431-4434.
 57. Kostarelos, K., Lacerda, L., Pastorin, G., Wu, W., Wieckowski, S., et al. (2007). Cellular uptake of functionalized carbon nanotubes is independent of functional group and cell type. *Nature nanotechnology*, 2(2), 108-113.
 58. Mu, Q., Broughton, D. L., Yan, B. (2009). Endosomal leakage and nuclear translocation of multiwalled carbon nanotubes: developing a model for cell uptake. *Nano letters*, 9(12), 4370-4375.
 59. Villadangos, J. A., Schnorrer, P. (2007). Intrinsic and cooperative antigen-presenting functions of dendritic-cell subsets in vivo. *Nature Reviews Immunology*, 7(7), 543-555.
 60. Tschopp, J., Schroder, K. (2010). NLRP3 inflammasome activation: the convergence of multiple signalling pathways on ROS production?. *Nature reviews immunology*, 10(3), 210-215.

61. He, Y., Hara, H., Núñez, G. (2016). Mechanism and regulation of NLRP3 inflammasome activation. *Trends in biochemical sciences*, 41(12), 1012-1021.
62. Cui, D., Tian, F., Ozkan, C. S., Wang, M., Gao, H. (2005). Effect of single wall carbon nanotubes on human HEK293 cells. *Toxicology letters*, 155(1), 73-85.
63. Rotoli, B. M., Bussolati, O., Bianchi, M. G., Barilli, A., Balasubramanian, C., et al. (2008). Non-functionalized multi-walled carbon nanotubes alter the paracellular permeability of human airway epithelial cells. *Toxicology letters*, 178(2), 95-102.
64. Hou, P. X., Liu, C., Cheng, H. M. (2008). Purification of carbon nanotubes. *carbon*, 46(15), 2003-2025.
65. Coccini, T., Roda, E., Sarigiannis, D. A., Mustarelli, P., Quartarone, E., Profumo, A., Manzo, L. (2010). Effects of water-soluble functionalized multi-walled carbon nanotubes examined by different cytotoxicity methods in human astrocyte D384 and lung A549 cells. *Toxicology*, 269(1), 41-53.
66. Vuković, G., Marinković, A., Obradović, M., Radmilović, V., Čolić, M., et al. (2009). Synthesis, characterization and cytotoxicity of surface amino-functionalized water-dispersible multi-walled carbon nanotubes. *Applied Surface Science*, 255(18), 8067-8075.
67. Zhang, L. W., Zeng, L., Barron, A. R., Monteiro-Riviere, N. A. (2007). Biological interactions of functionalized single-wall carbon nanotubes in human epidermal keratinocytes. *International Journal of Toxicology*, 26(2), 103-113.
68. Li, R., Wang, X., Ji, Z., Sun, B., Zhang, H., et al. (2013). Surface charge and cellular processing of covalently functionalized multiwall carbon nanotubes determine pulmonary toxicity. *ACS nano*, 7(3), 2352-2368.
69. Porter, A. E., Gass, M., Bendall, J. S., Muller, K., Goode, A., et al. (2009). Uptake of noncytotoxic acid-treated single-walled carbon nanotubes into the cytoplasm of human macrophage cells. *Acs Nano*, 3(6), 1485-1492.
70. Kagan, V. E., Tyurina, Y. Y., Tyurin, V. A., Konduru, N. V., Potapovich, A. I., et al. (2006). Direct and indirect effects of single walled carbon nanotubes on RAW 264.7 macrophages: role of iron. *Toxicology letters*, 165(1), 88-100.
71. Pulskamp, K., Diabaté, S., Krug, H. F. (2007). Carbon nanotubes show no sign of acute toxicity but induce intracellular reactive oxygen species in dependence on contaminants. *Toxicology letters*, 168(1), 58-74.
72. Palomaki, J., Valimaki, E., Sund, J., Vippola, M., Clausen, P. A., Jensen, K. A., ... Alenius, H. (2011). Long, needle-like carbon nanotubes and asbestos activate the NLRP3 inflammasome through a similar mechanism. *ACS nano*, 5(9), 6861-6870.
73. Wang, J., Sun, R. H., Zhang, N., Nie, H., Liu, J. H., Wang, J. N., ... Liu, Y. (2009). Multi-walled carbon nanotubes do not impair immune functions of dendritic cells. *Carbon*, 47(7), 1752-1760.
74. Dumortier, H., Lacotte, S., Pastorin, G., Marega, R., Wu, W., et al. (2006). Functionalized carbon nanotubes are non-cytotoxic and preserve the functionality of primary immune cells. *Nano letters*, 6(7), 1522-1528.
75. Pescatori, M., Bedognetti, D., Venturelli, E., Ménard-Moyon, C., Bernardini, C., et al. (2013). Functionalized carbon nanotubes as immunomodulator systems. *Biomaterials*, 34(18), 4395-4403.
76. Medepalli, K., Alphenaar, B., Raj, A., Sethu, P. (2011). Evaluation of the direct and indirect response of blood leukocytes to carbon nanotubes (CNTs). *Nanomedicine: Nanotechnology, Biology and Medicine*, 7(6), 983-991.
77. Yang, S. T., Guo, W., Lin, Y., Deng, X. Y., Wang, H. F., et al. (2007). Biodistribution of pristine single-walled carbon nanotubes in vivo. *The Journal of Physical Chemistry C*, 111(48), 17761-17764.
78. Al-Jamal, K. T., Nunes, A., Methven, L., Ali-Boucetta, H., Li, S., et al. (2012). Degree of chemical functionalization of carbon nanotubes determines tissue distribution and excretion profile. *Angewandte Chemie*, 124(26), 6495-6499.
79. Liu, Z., Davis, C., Cai, W., He, L., Chen, X., et al. (2008). Circulation and long-term fate of functionalized, biocompatible single-walled carbon nanotubes in mice probed by Raman spectroscopy. *Proceedings of the National Academy of Sciences*, 105(5), 1410-1415.
80. Schipper, M. L., Nakayama-Ratchford, N., Davis, C. R., Kam, N. W. S., Chu, P., Liu, Z., ... Gambhir, S. S. (2008). A pilot toxicology study of single-walled carbon nanotubes in a small sample of mice. *Nature nanotechnology*, 3(4), 216-221.
81. Guo, J., Zhang, X., Li, Q., Li, W. (2007). Biodistribution of functionalized multiwall carbon nanotubes in mice. *Nuclear medicine and biology*, 34(5), 579-583.
82. Meng, J., Yang, M., Jia, F., Xu, Z., Kong, H., Xu, H. (2011). Immune responses of BALB/c mice to subcutaneously injected multi-walled carbon nanotubes. *Nanotoxicology*, 5(4), 583-591.
83. Allen, B. L., Kichambare, P. D., Gou, P., Vlasova, I. I., Kapralov, A. A., et al. (2008). Biodegradation of single-walled carbon nanotubes through enzymatic catalysis. *Nano letters*, 8(11), 3899-3903.
84. Kagan, V. E., Konduru, N. V., Feng, W., Allen, B. L., Conroy, J., et al. (2010). Carbon nanotubes degraded by neutrophil myeloperoxidase induce less pulmonary inflammation. *Nature nanotechnology*, 5(5), 354-359.
85. Andón, F. T., Kapralov, A. A., Yanamala, N., Feng, W., Baygan, A., et al. (2013). Biodegradation of single-walled carbon nanotubes by eosinophil peroxidase. *Small*, 9(16), 2721-2729.
86. Shvedova, A. A., Kapralov, A. A., Feng, W. H., Kisin, E. R., Murray, A. R., et al. (2012). Impaired clearance and enhanced pulmonary inflammatory/fibrotic response to carbon nanotubes in myeloperoxidase-deficient mice. *PLoS one*, 7(3), e30923.
87. Nunes, A., Bussy, C., Gherardini, L., Meneghetti, M., Herroero, M. A., et al. (2012). In vivo degradation of functionalized carbon nanotubes after stereotactic administration in the brain cortex. *Nanomedicine*, 7(10), 1485-1494.
88. Alidori, S., Akhavein, N., Thorek, D. L., Behling, K., Romin, Y., et al. (2016). Targeted fibrillar nanocarbon RNAi treatment of acute kidney injury. *Science translational medicine*, 8(331), 331ra39-331ra39.
89. Geim, A. K., Novoselov, K. S. (2007). The rise of graphene. *Nature materials*, 6(3), 183-191.
90. Novoselov, K. S., Geim, A. K., Morozov, S. V., Jiang, D. E.,

- Zhang, Y., Dubonos, S. V., ... Firsov, A. A. (2004). Electric field effect in atomically thin carbon films. *science*, 306(5696), 666-669.
91. Feazell, R. P., Nakayama-Ratchford, N., Dai, H., Lippard, S. J. (2007). Soluble single-walled carbon nanotubes as longboat delivery systems for platinum (IV) anticancer drug design. *Journal of the American Chemical Society*, 129(27), 8438-8439.
 92. Dhar, S., Liu, Z., Thomale, J., Dai, H., Lippard, S. J. (2008). Targeted single-wall carbon nanotube-mediated Pt (IV) prodrug delivery using folate as a homing device. *Journal of the American Chemical Society*, 130(34), 11467-11476.
 93. Burger, K. N., Staffhorst, R. W., de Vijlder, H. C., Velinova, M. J., Bomans, P. H., et al. (2002). Nanocapsules: lipid-coated aggregates of cisplatin with high cytotoxicity.
 94. Hilder, T. A., Hill, J. M. (2007). Modelling the encapsulation of the anticancer drug cisplatin into carbon nanotubes. *Nanotechnology*, 18(27), 275704.
 95. Saikia, N., Deka, R. C. (2013). Ab initio study on the non-covalent adsorption of camptothecin anticancer drug onto graphene, defect modified graphene and graphene oxide. *Journal of computer-aided molecular design*, 27, 807-821.
 96. Ali-Boucetta, H., Al-Jamal, K. T., McCarthy, D., Prato, M., Bianco, A., Kostarelos, K. (2008). Multiwalled carbon nanotube-doxorubicin supramolecular complexes for cancer therapeutics. *Chemical Communications*, (4), 459-461.
 97. Liu, Z., Chen, K., Davis, C., Sherlock, S., Cao, Q., Chen, X., Dai, H. (2008). Drug delivery with carbon nanotubes for in vivo cancer treatment. *Cancer research*, 68(16), 6652-6660.
 98. De Temmerman, M. L., Rejman, J., Demeester, J., Irvine, D. J., Gander, B., et al. (2011). Particulate vaccines: on the quest for optimal delivery and immune response. *Drug discovery today*, 16(13-14), 569-582.
 99. Bachmann, M. F., Jennings, G. T. (2010). Vaccine delivery: a matter of size, geometry, kinetics and molecular patterns. *Nature Reviews Immunology*, 10(11), 787-796.
 100. Smith, D. M., Simon, J. K., Baker Jr, J. R. (2013). Applications of nanotechnology for immunology. *Nature Reviews Immunology*, 13(8), 592-605.
 101. Irvine, D. J., Swartz, M. A., Szeto, G. L. (2013). Engineering synthetic vaccines using cues from natural immunity. *Nature materials*, 12(11), 978-990.
 102. Krishnamachari, Y., Geary, S. M., Lemke, C. D., Salem, A. K. (2011). Nanoparticle delivery systems in cancer vaccines. *Pharmaceutical research*, 28, 215-236.
 103. Smyth, M. J., Ngiow, S. F., Ribas, A., Teng, M. W. (2016). Combination cancer immunotherapies tailored to the tumour microenvironment. *Nature reviews Clinical oncology*, 13(3), 143-158.
 104. Torchilin, V. P. (2005). Recent advances with liposomes as pharmaceutical carriers. *Nature reviews Drug discovery*, 4(2), 145-160.
 105. Whitmore, M. M., Li, S., Falo, L., Huang, L. (2001). Systemic administration of LPD prepared with CpG oligonucleotides inhibits the growth of established pulmonary metastases by stimulating innate and acquired antitumor immune responses. *Cancer Immunology, Immunotherapy*, 50, 503-514.
 106. Hamdy, S., Molavi, O., Ma, Z., Haddadi, A., Alshamsan, A., et al. (2008). Co-delivery of cancer-associated antigen and Toll-like receptor 4 ligand in PLGA nanoparticles induces potent CD8+ T cell-mediated anti-tumor immunity. *Vaccine*, 26(39), 5046-5057.
 107. Zeltins, A. (2013). Construction and characterization of virus-like particles: a review. *Molecular biotechnology*, 53(1), 92-107.
 108. Zhu, G., Lynn, G. M., Jacobson, O., Chen, K., Liu, Y., et al. (2017). Albumin/vaccine nanocomplexes that assemble in vivo for combination cancer immunotherapy. *Nature communications*, 8(1), 1954.
 109. Cha, B. G., Jeong, J. H., Kim, J. (2018). Extra-large pore mesoporous silica nanoparticles enabling co-delivery of high amounts of protein antigen and toll-like receptor 9 agonist for enhanced cancer vaccine efficacy. *ACS central science*, 4(4), 484-492.
 110. Mueller, M., Schlosser, E., Gander, B., Groettrup, M. (2011). Tumor eradication by immunotherapy with biodegradable PLGA microspheres—an alternative to incomplete Freund's adjuvant. *International journal of cancer*, 129(2), 407-416.
 111. Geary, S. M., Hu, Q., Joshi, V. B., Bowden, N. B., Salem, A. K. (2015). Diamino sulfide based polymer microparticles as cancer vaccine delivery systems. *Journal of controlled release*, 220, 682-690.
 112. Wakita, D., Chamoto, K., Zhang, Y., Narita, Y., Noguchi, D., et al. (2006). An indispensable role of type-1 IFNs for inducing CTL-mediated complete eradication of established tumor tissue by CpG-liposome co-encapsulated with model tumor antigen. *International immunology*, 18(3), 425-434.
 113. Ludewig, B., Barchiesi, F., Pericin, M., Zinkernagel, R. M., Hengartner, H., et al. (2000). In vivo antigen loading and activation of dendritic cells via a liposomal peptide vaccine mediates protective antiviral and anti-tumour immunity. *Vaccine*, 19(1), 23-32.
 114. Chen, W., Yan, W., Huang, L. (2008). A simple but effective cancer vaccine consisting of an antigen and a cationic lipid. *Cancer Immunology, Immunotherapy*, 57, 517-530.
 115. Shariat, S., Badiie, A., Jalali, S. A., Mansourian, M., Yazdani, M., et al. (2014). P5 HER2/neu-derived peptide conjugated to liposomes containing MPL adjuvant as an effective prophylactic vaccine formulation for breast cancer. *Cancer letters*, 355(1), 54-60.
 116. Zhang, Z., Tongchusak, S., Mizukami, Y., Kang, Y. J., Ioji, T., et al. (2011). Induction of anti-tumor cytotoxic T cell responses through PLGA-nanoparticle mediated antigen delivery. *Biomaterials*, 32(14), 3666-3678.
 117. Ahmed, K. K., Geary, S. M., Salem, A. K. (2016). Development and evaluation of biodegradable particles co-loaded with antigen and the Toll-like receptor agonist, pentaerythritol lipid A, as a cancer vaccine. *Journal of pharmaceutical sciences*, 105(3), 1173-1179.
 118. Rosalia, R. A., Cruz, L. J., van Duikeren, S., Tromp, A. T., Silva, A. L., et al. (2015). CD40-targeted dendritic cell delivery of PLGA-nanoparticle vaccines induce potent

- anti-tumor responses. *Biomaterials*, 40, 88-97.
119. Molino, N. M., Neek, M., Tucker, J. A., Nelson, E. L., Wang, S. W. (2016). Viral-mimicking protein nanoparticle vaccine for eliciting anti-tumor responses. *Biomaterials*, 86, 83-91.
 120. Mueller, M., Reichardt, W., Koerner, J., Groettrup, M. (2012). Coencapsulation of tumor lysate and CpG-ODN in PLGA-microspheres enables successful immunotherapy of prostate carcinoma in TRAMP mice. *Journal of controlled release*, 162(1), 159-166.
 121. Hassan, H. A., Diebold, S. S., Smyth, L. A., Walters, A. A., Lombardi, G., et al. (2019). Application of carbon nanotubes in cancer vaccines: Achievements, challenges and chances. *Journal of controlled release*, 297, 79-90.
 122. Sun, Z., Wang, W., Meng, J., Chen, S., Xu, H., et al. (2010). Multi-walled carbon nanotubes conjugated to tumor protein enhance the uptake of tumor antigens by human dendritic cells in vitro. *Cell research*, 20(10), 1170-1173.
 123. Meng, J., Meng, J., Duan, J., Kong, H., Li, L., et al. (2008). Carbon nanotubes conjugated to tumor lysate protein enhance the efficacy of an antitumor immunotherapy. *small*, 4(9), 1364-1370.
 124. Villa, C. H., Dao, T., Ahearn, I., Fehrenbacher, N., Casey, E., et al. (2011). Single-walled carbon nanotubes deliver peptide antigen into dendritic cells and enhance IgG responses to tumor-associated antigens. *ACS nano*, 5(7), 5300-5311.
 125. Diebold, S. S. (2008). Determination of T-cell fate by dendritic cells. *Immunology and cell biology*, 86(5), 389-397.
 126. Janeway Jr, C. A., Medzhitov, R. (2002). Innate immune recognition. *Annual review of immunology*, 20(1), 197-216.
 127. Palm, N. W., Medzhitov, R. (2009). Pattern recognition receptors and control of adaptive immunity. *Immunological reviews*, 227(1), 221-233.
 128. Gordon, S. (2002). Pattern recognition receptors: doubling up for the innate immune response. *Cell*, 111(7), 927-930.
 129. Krieg, A. M. (2008). Toll-like receptor 9 (TLR9) agonists in the treatment of cancer. *Oncogene*, 27(2), 161-167.
 130. Steinhagen, F., Kinjo, T., Bode, C., Klinman, D. M. (2011). TLR-based immune adjuvants. *Vaccine*, 29(17), 3341-3355.
 131. Klinman, D. M. (2004). Immunotherapeutic uses of CpG oligodeoxynucleotides. *Nature Reviews Immunology*, 4(4), 249-259.
 132. Zhao, D., Alizadeh, D., Zhang, L., Liu, W., Farrukh, O., Manuel, E., et al. (2011). Carbon nanotubes enhance CpG uptake and potentiate anti-glioma immunity. *Clinical Cancer Research*, 17(4), 771-782.
 133. Fan, H., Zhang, I., Chen, X., Zhang, L., Wang, H., et al. (2012). Intracerebral CpG immunotherapy with carbon nanotubes abrogates growth of subcutaneous melanomas in mice. *Clinical Cancer Research*, 18(20), 5628-5638.
 134. Ouyang, M., White, E. E., Ren, H., Guo, Q., Zhang, I., et al. (2016). Metronomic doses of temozolomide enhance the efficacy of carbon nanotube CpG immunotherapy in an invasive glioma model. *PloS one*, 11(2), e0148139.
 135. Faria, P. C. B. D., Santos, L. I. D., Coelho, J. P., Ribeiro, H. B., Pimenta, M. A., et al. (2014). Oxidized multiwalled carbon nanotubes as antigen delivery system to promote superior CD8+ T cell response and protection against cancer. *Nano letters*, 14(9), 5458-5470.
 136. Hassan, H. A., Smyth, L., Rubio, N., Ratnasothy, K., Wang, J. T. W., et al. (2016). Carbon nanotubes' surface chemistry determines their potency as vaccine nanocarriers in vitro and in vivo. *Journal of Controlled Release*, 225, 205-216.
 137. Hassan, H. A., Smyth, L., Wang, J. T. W., Costa, P. M., Ratnasothy, K., et al. (2016). Dual stimulation of antigen presenting cells using carbon nanotube-based vaccine delivery system for cancer immunotherapy. *Biomaterials*, 104, 310-322.
 138. van Kooten, C., Banchereau, J. (2000). CD40-CD40 ligand. *Journal of leukocyte biology*, 67(1), 2-17.
 139. Melero, I., Hervas-Stubbs, S., Glennie, M., Pardoll, D. M., Chen, L. (2007). Immunostimulatory monoclonal antibodies for cancer therapy. *Nature Reviews Cancer*, 7(2), 95-106.
 140. Chatterjee, B., Smed-Sørensen, A., Cohn, L., Chalouni, C., Vandlen, R., et al. (2012). Internalization and endosomal degradation of receptor-bound antigens regulate the efficiency of cross presentation by human dendritic cells. *Blood, The Journal of the American Society of Hematology*, 120(10), 2011-2020.
 141. Cohn, L., Chatterjee, B., Esselborn, F., Smed-Sørensen, A., Nakamura, N., et al. (2013). Antigen delivery to early endosomes eliminates the superiority of human blood BDCA3+ dendritic cells at cross presentation. *Journal of Experimental Medicine*, 210(5), 1049-1063.
 142. Kastenmüller, W., Kastenmüller, K., Kurts, C., Seder, R. A. (2014). Dendritic cell-targeted vaccines—hope or hype?. *Nature Reviews Immunology*, 14(10), 705-711.
 143. Smith, D. M., Simon, J. K., Baker Jr, J. R. (2013). Applications of nanotechnology for immunology. *Nature Reviews Immunology*, 13(8), 592-605.
 144. Bachmann, M. F., Jennings, G. T. (2010). Vaccine delivery: a matter of size, geometry, kinetics and molecular patterns. *Nature Reviews Immunology*, 10(11), 787-796.
 145. Irvine, D. J., Swartz, M. A., Szeto, G. L. (2013). Engineering synthetic vaccines using cues from natural immunity. *Nature materials*, 12(11), 978-990.
 146. Butts, C., Murray, N., Maksymiuk, A., Goss, G., Marshall, E., Soulières, D., ... Palmer, M. (2005). Randomized phase IIB trial of BLP25 liposome vaccine in stage IIIB and IV non-small-cell lung cancer. *Journal of Clinical Oncology*, 23(27), 6674-6681.
 147. Butts, C., Maksymiuk, A., Goss, G., Soulières, D., Marshall, E., Cormier, Y., ... Murray, N. (2011). Updated survival analysis in patients with stage IIIB or IV non-small-cell lung cancer receiving BLP25 liposome vaccine (L-BLP25): phase IIB randomized, multicenter, open-label trial. *Journal of cancer research and clinical oncology*, 137, 1337-1342.
 148. Martin, C. R., Kohli, P. (2003). The emerging field of nanotube biotechnology. *Nature Reviews Drug Discov-*

- ery, 2(1), 29-37.
149. Tasis, D., Tagmatarchis, N., Bianco, A., Prato, M. (2006). Chemistry of carbon nanotubes. *Chemical reviews*, 106(3), 1105-1136.
 150. Bianco, A., Kostarelos, K., Partidos, C. D., Prato, M. (2005). Biomedical applications of functionalised carbon nanotubes. *Chemical Communications*, (5), 571-577.
 151. Kam, N. W. S., Liu, Z., Dai, H. (2006). Carbon nanotubes as intracellular transporters for proteins and DNA: an investigation of the uptake mechanism and pathway. *Angewandte Chemie International Edition*, 45(4), 577-581.
 152. Kostarelos, K., Lacerda, L., Pastorin, G., Wu, W., Wiercowski, S., Luangsivilay, J., ... Bianco, A. (2007). Cellular uptake of functionalized carbon nanotubes is independent of functional group and cell type. *Nature nanotechnology*, 2(2), 108-113.
 153. Pantarotto, D., Partidos, C. D., Graff, R., Hoebeke, J., Briand, J. P., Prato, M., Bianco, A. (2003). Synthesis, structural characterization, and immunological properties of carbon nanotubes functionalized with peptides. *Journal of the American Chemical Society*, 125(20), 6160-6164.
 154. Pantarotto, D., Partidos, C. D., Hoebeke, J., Brown, F., Kramer, E. D., Briand, J. P., ... Bianco, A. (2003). Immunization with peptide-functionalized carbon nanotubes enhances virus-specific neutralizing antibody responses. *Chemistry biology*, 10(10), 961-966.
 155. in het Panhuis, M. (2003). Vaccine delivery by carbon nanotubes. *Chemistry biology*, 10(10), 897-898.
 156. Yandar, N., Pastorin, G., Prato, M., Bianco, A., Patarroyo, M. E., Lozano, J. M. (2008). Immunological profile of a Plasmodium vivax AMA-1 N-terminus peptide-carbon nanotube conjugate in an infected Plasmodium berghei mouse model. *Vaccine*, 26(46), 5864-5873.
 157. Zeinali, M., Jammalan, M., Ardestani, S. K., Mosaveri, N. (2009). Immunological and cytotoxicological characterization of tuberculin purified protein derivative (PPD) conjugated to single-walled carbon nanotubes. *Immunology letters*, 126(1-2), 48-53.
 158. Meng, J., Meng, J., Duan, J., Kong, H., Li, L., Wang, C., ... Yang, X. D. (2008). Carbon nanotubes conjugated to tumor lysate protein enhance the efficacy of an antitumor immunotherapy. *small*, 4(9), 1364-1370.
 159. Sun, Z., Wang, W., Meng, J., Chen, S., Xu, H., et al. (2010). Multi-walled carbon nanotubes conjugated to tumor protein enhance the uptake of tumor antigens by human dendritic cells in vitro. *Cell research*, 20(10), 1170-1173.
 160. Villa, C. H., Dao, T., Ahearn, I., Fehrenbacher, N., Casey, E., et al. (2011). Single-walled carbon nanotubes deliver peptide antigen into dendritic cells and enhance IgG responses to tumor-associated antigens. *ACS nano*, 5(7), 5300-5311.
 161. Bianco, A., Hoebeke, J., Godefroy, S., Chaloin, O., Pantarotto, D., et al. (2005). Cationic carbon nanotubes bind to CpG oligodeoxynucleotides and enhance their immunostimulatory properties. *Journal of the American Chemical Society*, 127(1), 58-59.
 162. Zhao, D., Alizadeh, D., Zhang, L., Liu, W., Farrukh, O., Manuel, E., et al. (2011). Carbon nanotubes enhance CpG uptake and potentiate antiglioma immunity. *Clinical Cancer Research*, 17(4), 771-782.
 163. Liu, Y., Xu, Y., Tian, Y., Chen, C., Wang, C., Jiang, X. (2014). Functional nanomaterials can optimize the efficacy of vaccines. *Small*, 10(22), 4505-4520.
 164. Fadel, T. R., Fahmy, T. M. (2014). Immunotherapy applications of carbon nanotubes: from design to safe applications. *Trends in Biotechnology*, 32(4), 198-209.
 165. Parra, J., Abad-Somovilla, A., Mercader, J. V., Taton, T. A., Abad-Fuentes, A. (2013). Carbon nanotube-protein carriers enhance size-dependent self-adjunct antibody response to haptens. *Journal of Controlled Release*, 170(2), 242-251.
 166. Hassan, H. A., Smyth, L., Rubio, N., Ratnasothy, K., Wang, J. T. W., et al. (2016). Carbon nanotubes' surface chemistry determines their potency as vaccine nanocarriers in vitro and in vivo. *Journal of Controlled Release*, 225, 205-216.
 167. Wang, J., Sun, R. H., Zhang, N., Nie, H., Liu, J. H., et al. (2009). Multi-walled carbon nanotubes do not impair immune functions of dendritic cells. *Carbon*, 47(7), 1752-1760.
 168. Tkach, A. V., Shurin, G. V., Shurin, M. R., Kisin, E. R., Murray, A. R., et al. (2011). Direct effects of carbon nanotubes on dendritic cells induce immune suppression upon pulmonary exposure. *ACS nano*, 5(7), 5755-5762.
 169. Fadel, T. R., Sharp, F. A., Vudattu, N., Ragheb, R., Garyu, J., et al. (2014). A carbon nanotube-polymer composite for T-cell therapy. *Nature nanotechnology*, 9(8), 639-647.
 170. Fadel, T. R., Li, N., Shah, S., Look, M., Pfefferle, L. D., et al. (2013). Adsorption of multimeric T cell antigens on carbon nanotubes: effect on protein structure and antigen-specific T cell stimulation. *Small*, 9(5), 666-672.
 171. Calvaresi, M., Zerbetto, F. (2013). The devil and holy water: protein and carbon nanotube hybrids. *Accounts of chemical research*, 46(11), 2454-2463.
 172. Li, R., Wang, X., Ji, Z., Sun, B., Zhang, H., et al. (2013). Surface charge and cellular processing of covalently functionalized multiwall carbon nanotubes determine pulmonary toxicity. *ACS nano*, 7(3), 2352-2368.
 173. Herrero, M. A., Toma, F. M., Al-Jamal, K. T., Kostarelos, K., Bianco, A., et al. (2009). Synthesis and characterization of a carbon nanotube-dendron series for efficient siRNA delivery. *Journal of the American Chemical Society*, 131(28), 9843-9848.
 174. Al-Jamal, K. T., Toma, F. M., Yilmazer, A., Ali-Boucetta, H., Nunes, A., et al. (2010). Enhanced cellular internalization and gene silencing with a series of cationic dendron-multiwalled carbon nanotube: siRNA complexes. *The FASEB Journal*, 24(11), 4354-4365.
 175. Thiele, L., Rothen-Rutishauser, B., Jilek, S., Wunderli-Allenspach, H., Merkle, H. P., et al. (2001). Evaluation of particle uptake in human blood monocyte-derived cells in vitro. Does phagocytosis activity of dendritic cells measure up with macrophages. *Journal of Controlled Release*, 76(1-2), 59-71.
 176. Foged, C., Brodin, B., Frokjaer, S., Sundblad, A. (2005). Particle size and surface charge affect particle uptake by

- human dendritic cells in an in vitro model. *International journal of pharmaceutics*, 298(2), 315-322.
177. Hu, Y., Ehrich, M., Fuhrman, K., Zhang, C. (2014). In vitro performance of lipid-PLGA hybrid nanoparticles as an antigen delivery system: lipid composition matters. *Nanoscale research letters*, 9, 1-10.
 178. Thomas, C., Gupta, V., Ahsan, F. (2009). Influence of surface charge of PLGA particles of recombinant hepatitis B surface antigen in enhancing systemic and mucosal immune responses. *International journal of pharmaceutics*, 379(1), 41-50.
 179. Sayın, B., Somavarapu, S., Li, X. W., Thanou, M., Sesaradic, D., et al. (2008). Mono-N-carboxymethyl chitosan (MCC) and N-trimethyl chitosan (TMC) nanoparticles for non-invasive vaccine delivery. *International journal of pharmaceutics*, 363(1-2), 139-148.
 180. Fromen, C. A., Robbins, G. R., Shen, T. W., Kai, M. P., Ting, J. P., DeSimone, J. M. (2015). Controlled analysis of nanoparticle charge on mucosal and systemic antibody responses following pulmonary immunization. *Proceedings of the National Academy of Sciences*, 112(2), 488-493.
 181. Li, X., Sloat, B. R., Yanasarn, N., Cui, Z. (2011). Relationship between the size of nanoparticles and their adjuvant activity: data from a study with an improved experimental design. *European Journal of Pharmaceutics and Biopharmaceutics*, 78(1), 107-116.
 182. Fifis, T., Gamvrellis, A., Crimeen-Irwin, B., Pietersz, G. A., Li, J., et al. (2004). Size-dependent immunogenicity: therapeutic and protective properties of nano-vaccines against tumors. *The Journal of Immunology*, 173(5), 3148-3154.
 183. Silva, A. L., Rosalia, R. A., Varypataki, E., Sibuea, S., Ossendorp, F., et al. (2015). Poly-(lactic-co-glycolic acid)-based particulate vaccines: particle uptake by dendritic cells is a key parameter for immune activation. *Vaccine*, 33(7), 847-854.
 184. Pastorin, G., Wu, W., Wieckowski, S., Briand, J. P., Kostarelos, K., et al. (2006). Double functionalization of carbon nanotubes for multimodal drug delivery. *Chemical communications*, (11), 1182-1184.
 185. Tagmatarchis, N., Prato, M. (2004). Functionalization of carbon nanotubes via 1, 3-dipolar cycloadditions. *Journal of materials chemistry*, 14(4), 437-439.
 186. Musso, S., Porro, S., Vinante, M., Vanzetti, L., Ploeger, R., Giorcelli, M., et al. (2007). Modification of MWNTs obtained by thermal-CVD. *Diamond and related materials*, 16(4-7), 1183-1187.
 187. Kuznetsova, A., Mawhinney, D. B., Naumenko, V., Yates Jr, J. T., et al. (2000). Enhancement of adsorption inside of single-walled nanotubes: opening the entry ports. *Chemical Physics Letters*, 321(3-4), 292-296.
 188. Datsyuk, V., Kalyva, M., Papagelis, K., Parthenios, J., Tasis, D., et al. (2008). Chemical oxidation of multiwalled carbon nanotubes. *carbon*, 46(6), 833-840.
 189. Lin, Z., Le, T., Song, X., Yao, Y., Li, Z., et al. (2013). Preparation of water-based carbon nanotube inks and application in the inkjet printing of carbon nanotube gas sensors. *Journal of Electronic Packaging*, 135(1), 011001.
 190. Huang, W., Lin, Y., Taylor, S., Gaillard, J., Rao, A. M., et al. (2002). Sonication-assisted functionalization and solubilization of carbon nanotubes. *Nano Letters*, 2(3), 231-234.
 191. Ramanathan, T., Fisher, F. T., Ruoff, R. S., Brinson, L. C. (2005). Amino-functionalized carbon nanotubes for binding to polymers and biological systems. *Chemistry of Materials*, 17(6), 1290-1295.
 192. Samori, C., Sainz, R., Ménard-Moyon, C., Toma, F. M., Venturelli, E., et al. (2010). Potentiometric titration as a straightforward method to assess the number of functional groups on shortened carbon nanotubes. *Carbon*, 48(9), 2447-2454.
 193. Lehman, J. H., Terrones, M., Mansfield, E., Hurst, K. E., Meunier, V. (2011). Evaluating the characteristics of multiwall carbon nanotubes. *Carbon*, 49(8), 2581-2602.
 194. Venturelli, E., Fabbro, C., Chaloin, O., Ménard-Moyon, C., Smulski, C. R., et al. (2011). Antibody covalent immobilization on carbon nanotubes and assessment of antigen binding. *Small*, 7(15), 2179-2187.
 195. Traut, R. R., Bollen, A., Sun, T. T., Hershey, J. W., Sundberg, J., et al. (1973). Methyl 4-mercaptobutyrimidate as a cleavable crosslinking reagent and its application to the Escherichia coli 30S ribosome. *Biochemistry*, 12(17), 3266-3273.
 196. Jue, R., Lambert, J. M., Pierce, L. R., Traut, R. R. (1978). Addition of sulfhydryl groups of Escherichia coli ribosomes by protein modification with 2-iminothiolane (methyl 4-mercaptobutyrimidate). *Biochemistry*, 17(25), 5399-5406.
 197. Ellman, G. L. (1959). Tissue sulfhydryl groups. *Archives of biochemistry and biophysics*, 82(1), 70-77.
 198. Inaba, K., Inaba, M., Romani, N., Aya, H., Deguchi, M., et al. (1992). Generation of large numbers of dendritic cells from mouse bone marrow cultures supplemented with granulocyte/macrophage colony-stimulating factor. *The Journal of experimental medicine*, 176(6), 1693-1702.
 199. Kurts, C. (2008). CD11c: not merely a murine DC marker, but also a useful vaccination target. *European journal of immunology*, 38(8), 2072-2075.
 200. Marangon, I., Boggetto, N., Ménard-Moyon, C., Venturelli, E., Béoutis, M. L., et al. (2012). Intercellular carbon nanotube translocation assessed by flow cytometry imaging. *Nano Letters*, 12(9), 4830-4837.
 201. Marangon, I., Boggetto, N., Ménard-Moyon, C., Luciani, N., Wilhelm, C., Bianco, A., Gazeau, F. (2013). Localization and relative quantification of carbon nanotubes in cells with multispectral imaging flow cytometry. *JoVE (Journal of Visualized Experiments)*, (82), e50566.
 202. Summers, H. D., Rees, P., Holton, M. D., Rowan Brown, M., Chappell, S. C., Smith, P. J., Errington, R. J. (2011). Statistical analysis of nanoparticle dosing in a dynamic cellular system. *Nature nanotechnology*, 6(3), 170-174.
 203. Ali-Boucetta, H., Al-Jamal, K. T., Kostarelos, K. (2011). Cytotoxic assessment of carbon nanotube interaction with cell cultures. *Biomedical Nanotechnology: Methods and Protocols*, 299-312.
 204. Yoshida, M., Babensee, J. E. (2004). Poly (lactic-co-glycolic acid) enhances maturation of human monocyte-

- derived dendritic cells. *Journal of Biomedical Materials Research Part A: An Official Journal of The Society for Biomaterials, The Japanese Society for Biomaterials, and The Australian Society for Biomaterials and the Korean Society for Biomaterials*, 71(1), 45-54.
205. Sapoznikov, A., Fischer, J. A., Zaft, T., Krauthgamer, R., Dzionek, A., et al. (2007). Organ-dependent in vivo priming of naive CD4+, but not CD8+, T cells by plasmacytoid dendritic cells. *The Journal of experimental medicine*, 204(8), 1923-1933.
206. Kreutz, M., Giquel, B., Hu, Q., Abuknesha, R., Uematsu, S., et al. (2012). Antibody-antigen-adjuvant conjugates enable co-delivery of antigen and adjuvant to dendritic cells in cis but only have partial targeting specificity. *PLoS one*, 7(7), e40208.
207. Santambrogio, L., Sato, A. K., Carven, G. J., Belyanskaya, S. L., Strominger, J. L., et al (1999). Extracellular antigen processing and presentation by immature dendritic cells. *Proceedings of the National Academy of Sciences*, 96(26), 15056-15061.
208. Iannazzo, D., Pistone, A., Galvagno, S., Ferro, S., De Luca, L., Monforte, A. M., ... Pannecouque, C. (2015). Synthesis and anti-HIV activity of carboxylated and drug-conjugated multi-walled carbon nanotubes. *Carbon*, 82, 548-561.
209. Ackerman, A. L., Cresswell, P. (2004). Cellular mechanisms governing cross-presentation of exogenous antigens. *Nature immunology*, 5(7), 678-684.
210. Villadangos, J. A., Schnorrer, P. (2007). Intrinsic and cooperative antigen-presenting functions of dendritic-cell subsets in vivo. *Nature Reviews Immunology*, 7(7), 543-555.
211. Vyas, J. M., Van der Veen, A. G., Ploegh, H. L. (2008). The known unknowns of antigen processing and presentation. *Nature Reviews Immunology*, 8(8), 607-618.
212. Hassan, H. A., Smyth, L., Wang, J. T. W., Costa, P. M., Ratnasothy, K., et al. (2016). Dual stimulation of antigen presenting cells using carbon nanotube-based vaccine delivery system for cancer immunotherapy. *Biomaterials*, 104, 310-322.
213. Palucka, K., Banchereau, J. (2012). Cancer immunotherapy via dendritic cells. *Nature Reviews Cancer*, 12(4), 265-277.
214. Quail, D. F., Joyce, J. A. (2013). Microenvironmental regulation of tumor progression and metastasis. *Nature medicine*, 19(11), 1423-1437.
215. Smyth, M. J., Ngiow, S. F., Ribas, A., Teng, M. W. (2016). Combination cancer immunotherapies tailored to the tumour microenvironment. *Nature reviews Clinical oncology*, 13(3), 143-158.
216. Kam, N. W. S., Liu, Z., Dai, H. (2006). Carbon nanotubes as intracellular transporters for proteins and DNA: an investigation of the uptake mechanism and pathway. *Angewandte Chemie International Edition*, 45(4), 577-581.
217. Bianco, A., Kostarelos, K., Partidos, C. D., Prato, M. (2005). Biomedical applications of functionalised carbon nanotubes. *Chemical Communications*, (5), 571-577.
218. Kostarelos, K., Lacerda, L., Pastorin, G., Wu, W., Wiekowski, S., Luangsivilay, J., ... Bianco, A. (2007). Cellular uptake of functionalized carbon nanotubes is independent of functional group and cell type. *Nature nanotechnology*, 2(2), 108-113.
219. Hassan, H. A., Smyth, L., Rubio, N., Ratnasothy, K., Wang, J. T. W., et al. (2016). Carbon nanotubes' surface chemistry determines their potency as vaccine nanocarriers in vitro and in vivo. *Journal of Controlled Release*, 225, 205-216.
220. Sun, Z., Wang, W., Meng, J., Chen, S., Xu, H., Yang, X. D. (2010). Multi-walled carbon nanotubes conjugated to tumor protein enhance the uptake of tumor antigens by human dendritic cells in vitro. *Cell research*, 20(10), 1170-1173.
221. Meng, J., Meng, J., Duan, J., Kong, H., Li, L., et al. (2008). Carbon nanotubes conjugated to tumor lysate protein enhance the efficacy of an antitumor immunotherapy. *small*, 4(9), 1364-1370.
222. Bianco, A., Hoebeke, J., Godefroy, S., Chaloin, O., Pantarotto, D., Briand, J. P., ... Partidos, C. D. (2005). Cationic carbon nanotubes bind to CpG oligodeoxynucleotides and enhance their immunostimulatory properties. *Journal of the American Chemical Society*, 127(1), 58-59.
223. Zhao, D., Alizadeh, D., Zhang, L., Liu, W., Farrukh, O., Manuel, E., ... Badie, B. (2011). Carbon nanotubes enhance CpG uptake and potentiate antiglioma immunity. *Clinical Cancer Research*, 17(4), 771-782.
224. Fan, H., Zhang, I., Chen, X., Zhang, L., Wang, H., et al. (2012). Intracerebral CpG immunotherapy with carbon nanotubes abrogates growth of subcutaneous melanomas in mice. *Clinical Cancer Research*, 18(20), 5628-5638.
225. Hennessy, E. J., Parker, A. E., O'neill, L. A. (2010). Targeting Toll-like receptors: emerging therapeutics?. *Nature reviews Drug discovery*, 9(4), 293-307.
226. Krieg, A. M. (2008). Toll-like receptor 9 (TLR9) agonists in the treatment of cancer. *Oncogene*, 27(2), 161-167.
227. Yarovinsky, F., Kanzler, H., Hieny, S., Coffman, R. L., Sher, A. (2006). Toll-like receptor recognition regulates immunodominance in an antimicrobial CD4+ T cell response. *Immunity*, 25(4), 655-664.
228. Wilson, N. S., Behrens, G. M., Lundie, R. J., Smith, C. M., Waithman, J., et al. (2006). Systemic activation of dendritic cells by Toll-like receptor ligands or malaria infection impairs cross-presentation and antiviral immunity. *Nature immunology*, 7(2), 165-172.
229. Blander, J. M., Medzhitov, R. (2006). Toll-dependent selection of microbial antigens for presentation by dendritic cells. *Nature*, 440(7085), 808-812.
230. van Kooten, C., Banchereau, J. (2000). CD40-CD40 ligand. *Journal of leukocyte biology*, 67(1), 2-17.
231. Quezada, S. A., Jarvinen, L. Z., Lind, E. F., Noelle, R. J. (2004). CD40/CD154 interactions at the interface of tolerance and immunity. *Annu. Rev. Immunol.*, 22, 307-328.
232. Chatterjee, B., Smed-Sørensen, A., Cohn, L., Chalouni, C., Vandlen, R., et al. (2012). Internalization and endosomal degradation of receptor-bound antigens regulate the efficiency of cross presentation by human dendritic cells. *Blood*, *The Journal of the American Society of He-*

- matology, 120(10), 2011-2020.
233. Cohn, L., Chatterjee, B., Esselborn, F., Smed-Sørensen, A., Nakamura, N., et al. (2013). Antigen delivery to early endosomes eliminates the superiority of human blood BDCA3+ dendritic cells at cross presentation. *Journal of Experimental Medicine*, 210(5), 1049-1063.
 234. Burgdorf, S., Kautz, A., Böhnert, V., Knolle, P. A., Kurts, C. (2007). Distinct pathways of antigen uptake and intracellular routing in CD4 and CD8 T cell activation. *science*, 316(5824), 612-616.
 235. Kastenmüller, W., Kastenmüller, K., Kurts, C., Seder, R. A. (2014). Dendritic cell-targeted vaccines—hope or hype?. *Nature Reviews Immunology*, 14(10), 705-711.
 236. Schoenberger, S. P., Toes, R. E., Van Der Voort, E. I., Offringa, R., Melief, C. J. (1998). T-cell help for cytotoxic T lymphocytes is mediated by CD40-CD40L interactions. *Nature*, 393(6684), 480-483.
 237. Bennett, S. R., Carbone, F. R., Karamalis, F., Flavell, R. A., Miller, J. F., Heath, W. R. (1998). Help for cytotoxic-T-cell responses is mediated by CD40 signalling. *Nature*, 393(6684), 478-480.
 238. Bennett, S. R., Carbone, F. R., Karamalis, F., Miller, J. F., Heath, W. R. (1997). Induction of a CD8+ cytotoxic T lymphocyte response by cross-priming requires cognate CD4+ T cell help. *The Journal of experimental medicine*, 186(1), 65-70.
 239. Kreutz, M., Giquel, B., Hu, Q., Abuknesha, R., Uematsu, S., et al. (2012). Antibody-antigen-adjuvant conjugates enable co-delivery of antigen and adjuvant to dendritic cells in cis but only have partial targeting specificity. *PLoS one*, 7(7), e40208.
 240. Cho, H. J., Takabayashi, K., Cheng, P. M., Nguyen, M. D., Corr, M., et al. (2000). Immunostimulatory DNA-based vaccines induce cytotoxic lymphocyte activity by a T-helper cell-independent mechanism. *Nature biotechnology*, 18(5), 509-514.
 241. Calvaresi, M., Zerbetto, F. (2013). The devil and holy water: protein and carbon nanotube hybrids. *Accounts of chemical research*, 46(11), 2454-2463.
 242. Zheng, M., Jagota, A., Semke, E. D., Diner, B. A., McLean, R. S., et al. (2003). DNA-assisted dispersion and separation of carbon nanotubes. *Nature materials*, 2(5), 338-342.
 243. Lehman, J. H., Terrones, M., Mansfield, E., Hurst, K. E., Meunier, V. (2011). Evaluating the characteristics of multiwall carbon nanotubes. *Carbon*, 49(8), 2581-2602.
 244. Cataldo, F. (2002). A study on the thermal stability to 1000 C of various carbon allotropes and carbonaceous matter both under nitrogen and in air. *Fullerenes, nanotubes and Carbon nanostructures*, 10(4), 293-311.
 245. Mahajan, A., Kingon, A., Kukovec, A., Konya, Z., Vilarinho, P. M. (2013). Studies on the thermal decomposition of multiwall carbon nanotubes under different atmospheres. *Materials Letters*, 90, 165-168.
 246. Schmidt, V., Giacomelli, C., Soldi, V. (2005). Thermal stability of films formed by soy protein isolate-sodium dodecyl sulfate. *Polymer degradation and stability*, 87(1), 25-31.
 247. Parente-Pereira, A. C., Wilkie, S., van der Stegen, S. J., Davies, D. M., Maher, J. (2014). Use of retroviral-mediated gene transfer to deliver and test function of chimeric antigen receptors in human T-cells. *Journal of Biological Methods*, 1(2), e7-e7.
 248. Cartiera, M. S., Johnson, K. M., Rajendran, V., Caplan, M. J., Saltzman, W. M. (2009). The uptake and intracellular fate of PLGA nanoparticles in epithelial cells. *Biomaterials*, 30(14), 2790-2798.
 249. Mao, S., Germershaus, O., Fischer, D., Linn, T., Schnepf, R., Kissel, T. (2005). Uptake and transport of PEG-graft-trimethyl-chitosan copolymer-insulin nanocomplexes by epithelial cells. *Pharmaceutical research*, 22, 2058-2068.
 250. He, C., Hu, Y., Yin, L., Tang, C., Yin, C. (2010). Effects of particle size and surface charge on cellular uptake and biodistribution of polymeric nanoparticles. *Biomaterials*, 31(13), 3657-3666.
 251. Zhang, X. Q., Dahle, C. E., Baman, N. K., Rich, N., Weiner, G. J., Salem, A. K. (2007). Potent antigen-specific immune responses stimulated by codelivery of CpG ODN and antigens in degradable microparticles. *Journal of Immunotherapy*, 30(5), 469-478.
 252. Beaudette, T. T., Bachelder, E. M., Cohen, J. A., Obermeyer, A. C., et al. (2009). In vivo studies on the effect of co-encapsulation of CpG DNA and antigen in acid-degradable microparticle vaccines. *Molecular pharmaceutics*, 6(4), 1160-1169.
 253. Heit, A., Schmitz, F., Haas, T., Busch, D. H., Wagner, H. (2007). Antigen co-encapsulated with adjuvants efficiently drive protective T cell immunity. *European journal of immunology*, 37(8), 2063-2074.
 254. Tao, Y., Zhang, Y., Ju, E., Ren, H., Ren, J. (2015). Gold nanocluster-based vaccines for dual-delivery of antigens and immunostimulatory oligonucleotides. *Nanoscale*, 7(29), 12419-12426.
 255. Schlosser, E., Mueller, M., Fischer, S., Basta, S., Busch, D. H., et al. (2008). TLR ligands and antigen need to be coencapsulated into the same biodegradable microsphere for the generation of potent cytotoxic T lymphocyte responses. *Vaccine*, 26(13), 1626-1637.
 256. Li, W. M., Dragowska, W. H., Bally, M. B., Schutze-Redelmeier, M. P. (2003). Effective induction of CD8+ T-cell response using CpG oligodeoxynucleotides and HER-2/neu-derived peptide co-encapsulated in liposomes. *Vaccine*, 21(23), 3319-3329.
 257. Hatzifoti, C., Bacon, A., Marriott, H., Laing, P., Heath, A. W. (2008). Liposomal co-entrapment of CD40mAb induces enhanced IgG responses against bacterial polysaccharide and protein. *PLoS One*, 3(6), e2368.
 258. Rosalia, R. A., Cruz, L. J., van Duikeren, S., Tromp, A. T., Silva, A. L., et al. (2015). CD40-targeted dendritic cell delivery of PLGA-nanoparticle vaccines induce potent anti-tumor responses. *Biomaterials*, 40, 88-97.
 259. Khanna, R., Cooper, L., Kienzle, N., Moss, D. J., Burrows, S. R., Khanna, K. K. (1997). Engagement of CD40 antigen with soluble CD40 ligand up-regulates peptide transporter expression and restores endogenous processing function in Burkitt's lymphoma cells. *Journal of immunology (Baltimore, Md.: 1950)*, 159(12), 5782-5785.
 260. Cella, M., Scheidegger, D., Palmer-Lehmann, K., Lane,

- P, Lanzavecchia, A., et al. (1996). Ligation of CD40 on dendritic cells triggers production of high levels of interleukin-12 and enhances T cell stimulatory capacity: T_H help via APC activation. *The Journal of experimental medicine*, 184(2), 747-752.
261. Haswell, L. E., Glennie, M. J., Al-Shamkhani, A. (2001). Analysis of the oligomeric requirement for signaling by CD40 using soluble multimeric forms of its ligand, CD154. *European journal of immunology*, 31(10), 3094-3100.
262. Broos, S., Sandin, L. C., Apel, J., Tötterman, T. H., Akagi, T., et al. (2012). Synergistic augmentation of CD40-mediated activation of antigen-presenting cells by amphiphilic poly (γ -glutamic acid) nanoparticles. *Biomaterials*, 33(26), 6230-6239.
263. Gu, L., Ruff, L. E., Qin, Z., Corr, M., Hedrick, S. M., Sailor, M. J. (2012). Multivalent porous silicon nanoparticles enhance the immune activation potency of agonistic CD40 antibody. *Advanced materials*, 24(29), 3981-3987.
264. Bachmann, M. F., Jennings, G. T. (2010). Vaccine delivery: a matter of size, geometry, kinetics and molecular patterns. *Nature Reviews Immunology*, 10(11), 787-796.
265. Fadel, T. R., Sharp, F. A., Vudattu, N., Ragheb, R., Garyu, J., et al. (2014). A carbon nanotube-polymer composite for T-cell therapy. *Nature nanotechnology*, 9(8), 639-647.
266. Wen, J., Elong Ngonu, A., Regla-Nava, J. A., Kim, K., Gorman, M. J., et al. (2017). Dengue virus-reactive CD8⁺ T cells mediate cross-protection against subsequent Zika virus challenge. *Nature communications*, 8(1), 1459.
267. Van Braeckel-Budimir, N., Harty, J. T. (2014). CD8 T-cell-mediated protection against liver-stage malaria: lessons from a mouse model. *Frontiers in microbiology*, 5, 272.
268. Min, Y., Roche, K. C., Tian, S., Eblan, M. J., McKinnon, K. P., Caster, J. M., et al. (2017). Antigen-capturing nanoparticles improve the abscopal effect and cancer immunotherapy. *Nature nanotechnology*, 12(9), 877-882.
269. Tao, Y., Ju, E., Ren, J., Qu, X. (2014). Immunostimulatory oligonucleotides-loaded cationic graphene oxide with photothermally enhanced immunogenicity for photothermal/immune cancer therapy. *Biomaterials*, 35(37), 9963-9971.
270. Cai, X., Ramalingam, R., San Wong, H., Cheng, J., Ajuh, P., et al. (2013). Characterization of carbon nanotube protein corona by using quantitative proteomics. *Nano-medicine: Nanotechnology, biology and medicine*, 9(5), 583-593.
271. De Paoli, S. H., Diduch, L. L., Tegegn, T. Z., Orecna, M., Strader, M. B., et al. (2014). The effect of protein corona composition on the interaction of carbon nanotubes with human blood platelets. *Biomaterials*, 35(24), 6182-6194.
272. Meng, J., Meng, J., Duan, J., Kong, H., Li, L., Wang, C., et al. (2008). Carbon nanotubes conjugated to tumor lysate protein enhance the efficacy of an antitumor immunotherapy. *small*, 4(9), 1364-1370.
273. Sagiv-Barfi, I., Czerwinski, D. K., Levy, S., Alam, I. S., Mayer, A. T., et al. (2018). Eradication of spontaneous malignancy by local immunotherapy. *Science translational medicine*, 10(426), eaan4488.
274. Lizotte, P. H., Wen, A. M., Sheen, M. R., Fields, J., Rojanasopondist, P., et al. (2016). In situ vaccination with cowpea mosaic virus nanoparticles suppresses metastatic cancer. *Nature nanotechnology*, 11(3), 295-303.
275. Murray, A. A., Wang, C., Fiering, S., Steinmetz, N. F. (2018). In situ vaccination with cowpea vs tobacco mosaic virus against melanoma. *Molecular pharmaceuticals*, 15(9), 3700-3716.
276. Kosmides, A. K., Sidhom, J. W., Fraser, A., Bessell, C. A., Schneck, J. P. (2017). Dual targeting nanoparticle stimulates the immune system to inhibit tumor growth. *ACS nano*, 11(6), 5417-5429.
277. Kuai, R., Ochyl, L. J., Bahjat, K. S., Schwendeman, A., Moon, J. J. (2017). Designer vaccine nanodiscs for personalized cancer immunotherapy. *Nature materials*, 16(4), 489-496.
278. Helland, A., Wick, P., Koehler, A., Schmid, K., Som, C. (2007). Reviewing the environmental and human health knowledge base of carbon nanotubes. *Environmental health perspectives*, 115(8), 1125-1131.
279. Pantarotto, D., Singh, R., McCarthy, D., Erhardt, M., Briand, J. P., et al. (2004). Functionalized carbon nanotubes for plasmid DNA gene delivery. *Angewandte Chemie International Edition*, 43(39), 5242-5246.